Progress in Nuclear Magnetic Resonance Spectroscopy 132–133 (2022) 113–139

Contents lists available at ScienceDirect

Progress in Nuclear Magnetic Resonance Spectroscopy

journal homepage: www.elsevier.com/locate/pnmrs

Solvent paramagnetic relaxation enhancement as a versatile method for studying structure and dynamics of biomolecular systems

Aneta J. Lenard [a], Frans A.A. Mulder [b,c], Tobias Madl [a,d,*]

[a] Gottfried Schatz Research Center for Cell Signaling, Metabolism and Ageing, Molecular Biology and Biochemistry, Research Unit Integrative Structural Biology, Medical University of Graz, 8010 Graz, Austria
[b] Interdisciplinary Nanoscience Center and Department of Chemistry, University of Aarhus, DK-8000 Aarhus, Denmark
[c] Institute of Biochemistry, Johannes Kepler Universität Linz, 4040 Linz, Austria
[d] BioTechMed-Graz, 8010 Graz, Austria

Edited by David Neuhaus and Gareth Morris

ARTICLE INFO

Article history:
Received 12 February 2022
Accepted 15 September 2022
Available online 21 September 2022

Keywords:
Solvent paramagnetic relaxation enhancement (sPRE)
Nuclear magnetic resonance (NMR) spectroscopy
Paramagnetic co-solutes
Structural biology
Solvent accessibility

ABSTRACT

Solvent paramagnetic relaxation enhancement (sPRE) is a versatile nuclear magnetic resonance (NMR)-based method that allows characterization of the structure and dynamics of biomolecular systems through providing quantitative experimental information on solvent accessibility of NMR-active nuclei. Addition of soluble paramagnetic probes to the solution of a biomolecule leads to paramagnetic relaxation enhancement in a concentration-dependent manner. Here we review recent progress in the sPRE-based characterization of structural and dynamic properties of biomolecules and their complexes, and aim to deliver a comprehensive illustration of a growing number of applications of the method to various biological systems. We discuss the physical principles of sPRE measurements and provide an overview of available co-solute paramagnetic probes. We then explore how sPRE, in combination with complementary biophysical techniques, can further advance biomolecular structure determination, identification of interaction surfaces within protein complexes, and probing of conformational changes and low-population transient states, as well as deliver insights into weak, nonspecific, and transient interactions between proteins and co-solutes. In addition, we present examples of how the incorporation of solvent paramagnetic probes can improve the sensitivity of NMR experiments and discuss the prospects of applying sPRE to NMR metabolomics, drug discovery, and the study of intrinsically disordered proteins.

Contents

Abbreviations: CASP, Critical Assessment of Protein Structure; CPMG, Carr-Purcell-Meiboom-Gill; Cryo-EM, cryo-electron microscopy; CSP, chemical shift perturbation; DMPC, dimyristoylphosphatodylcholine; DPC, dodecylphosphocholine; DTBN, di-*tert*-butyl aminoxyl; EPR, electron paramagnetic resonance; Gd(DTPA-BMA), diethylenetriamine pentaacetic acid-bismethylamide gadolinium chelate; Gd(TTHA-TMA), triethylenetetramine hexaacetate-trimethylamide gadolinium chelate; HADDOCK, high ambiguity driven docking; IDPs, intrinsically disordered proteins; IDRs, intrinsically disordered regions; LLPS, liquid–liquid phase separation; MD, molecular dynamics; MS, mass spectrometry; MRI, magnetic resonance imaging; NMR, nuclear magnetic resonance; NOE, nuclear Overhauser effect; PCSs, pseudo-chemical shifts; PTMs, post-translational modifications; RDC, residual dipolar coupling; RMSD, root mean-square deviation; RMSF, root-mean-square fluctuation; SAXS/SANS, small-angle X-ray/neutron scattering; SBM, Solomon, Bloembergen, Morgan theory; SDS, sodium dodecylsulfate; smFRET, single-molecule Förster resonance energy transfer; SOP, standard operating procedure; (s)PRE, (solvent) paramagnetic relaxation enhancement; TEMPOL, 4-hydroxy-2,2,6,6-tetramethylpiperidin-1-oxyl; TROSY, transverse relaxation optimized spectroscopy.

* Corresponding author at: Research Unit Integrative Structural Biology, Molecular Biology and Biochemistry, Medical University of Graz, Neue Stiftingtalstraße 6/VI, 8010 Graz, Austria.

E-mail addresses: aneta.lenard@medunigraz.at (A.J. Lenard), frans.mulder@jku.at (F.A.A. Mulder), tobias.madl@medunigraz.at (T. Madl).

https://doi.org/10.1016/j.pnmrs.2022.09.001
0079-6565/

1. Introduction

Life is orchestrated via an intricate molecular communication between proteins and other biomolecules, in and between cells. To better comprehend how information is conveyed between molecules, as well as the molecular mechanisms underlying the onset of many diseases, we need first to develop methods to characterize structural and dynamic properties of proteins and changes resulting from the formation of protein complexes [1,2]. X-ray crystallography, cryo-electron microscopy (cryo-EM) and NMR spectroscopy are the most frequently employed methods for solving high-resolution biomolecular structures at atomic resolution, with the former accounting for the vast majority of protein structures deposited in the Protein Data Bank [3,4]. While the disadvantages of X-ray crystallography lie in the fact that crystallization may not be possible, and artificial conformations of flexible biomolecules may arise from crystal packing, protein structure determination by means of NMR spectroscopy is usually limited to smaller structures, due to the unfavourable NMR properties (linewidths and spectral crowding) for biosystems with an aggregate molecular mass exceeding 50 kDa.

Solution NMR spectroscopy can provide detailed insights into the conformational dynamics of biomolecules and their complexes at an atomic level over a wide range of time scales (ranging from picoseconds to days). NMR has been successfully applied to investigate complex biological systems ranging from intrinsically disordered proteins (IDPs) to large biomolecular complexes [2,5–8]. Examining biomolecular dynamics and probing structural parameters of macromolecular complexes by means of conventional solution NMR analysis can be demanding, due to severe spectral overlap and adverse relaxation properties leading to extensive resonance line broadening effects. These limitations have been addressed by substantial developments in NMR instrumentation and electronics, as well as in the tools used for data interpretation and structural modeling [9–16]. Additional advances stem from the exploitation of transverse relaxation optimized spectroscopy (TROSY), combined with deuteration and/or methyl-labeling schemes, developments of segmental isotopic labeling and heteronuclear direct-detection experiments [17–25]. This resulted in the steady growth in the number of NMR spectroscopic studies of complex biomolecular systems and processes [5,20,26]. Fast NMR data acquisition methods, nonuniform sampling and processing, pure shift NMR, and pressure-jump NMR experiments will be increasingly widely adopted, continuously expanding applications of NMR spectroscopy in biomolecular sciences [27–32].

NMR spectroscopy is increasingly being combined with complementary structural biology and biophysical methods in an integrative approach. This includes, but is not limited to, small-angle X-ray/neutron scattering (SAXS/SANS), cryo-electron microscopy and tomography, electron paramagnetic resonance (EPR) spectroscopy, mass spectrometry (MS), single-molecule Förster resonance energy transfer (smFRET), and molecular dynamics (MD) simulations, further facilitating studies of biomolecular structure and dynamics [2,4,33–38].

At this point, recent advances in machine learning are also worth mentioning. The deep neural network algorithm AlphaFold2 developed by DeepMind [39–41] has demonstrated astounding accuracy in predicting the three-dimensional structures of single protein chains with *a priori* unknown fold from their amino acid sequences, and has significantly outperformed other protein structure modeling methods in the 14th edition of the Critical Assessment of Protein Structure (CASP) [42,43]. AlphaFold2 currently provides full-chain structure prediction models for 98.5 % of human proteins (which are publicly available under https://alphafold.ebi.ac.uk/), and DeepMind has announced the expansion of the structure prediction database to the proteomes of other organisms. Furthermore, the recently presented AlphaFold-Multimer system allows for the accurate structure prediction of protein complexes, as well as homomeric and heteromeric protein interfaces [44]. In addition, Hekkelman *et al.* have released an AlphaFill algorithm that further enriches AlphaFold2 prediction models with otherwise missing small molecule ligands and co-factors [45]. The organization of AlphaFold2-collected data into an easily accessible open database (together with open-source code) offers novel possibilities for structural biologists as well as non-experts. These possibilities include, but are not limited to, especially in combination with experimental methods, i) cross-validation of experimentally-derived models of biomolecular structures; ii) refinement of structural models of proteins and their complexes during integrative modeling and protein design; and iii) advancing structure-based drug design by accelerating biomolecular modeling and docking [46]. Moreover, development of the

machine-learning based method ARTINA for automatic protein resonance assignment and structure calculation from raw NMR spectra, enables automated analysis of NMR data within hours after recording the measurements [47].

A classical structure determination approach for proteins and their complexes in solution by means of NMR spectroscopy is based on measuring nuclear Overhauser effects (NOEs), nuclear relaxation rates, hydrogen exchange rates, scalar couplings (J-couplings), residual dipolar couplings (RDCs), and paramagnetic data such as pseudocontact chemical shifts (PCSs) and paramagnetic relaxation enhancements (PREs), and the mapping of chemical shift perturbations (CSPs) [2,48–56]. However, these methods may require extensive sample modifications, such as the addition of external alignment media in the case of RDCs, or the incorporation of a covalently-attached tag for PCS and PRE data collection [57,58].

As an alternative or complement, paramagnetic relaxation enhancements can be obtained in the presence of paramagnetic soluble probes in solution (known as solvent PREs, co-solute PREs, sPREs) [59,60]. The strength of this method, as compared to techniques that involve covalently attached paramagnetic probes, lies in its simple sample preparation protocol, in which freely diffusing small, soluble paramagnetic probes (also known as paramagnetic agents, co-solute probes/agents) such as ions, organic radicals, or lanthanide metal chelates are added to the solution of a sample under investigation without the need for any chemical modifications. The addition of paramagnetic probes leads to concentration-dependent effects that depend on the intrinsic properties of the paramagnetic molecule, the studied biomolecule, and on the nature of interaction between the two. Such sPRE analysis provides information on long-range distances and dynamics in biomolecules and the data obtained can be used to aid calculations of biomolecular conformational ensembles. We focus exclusively on solution-state NMR in the following; interested readers can find prominent examples of the application of sPRE to solid-state NMR studies described elsewhere [61–63].

In this review, we provide an in-depth overview of solvent PREs and their roles in shedding light on the structural and dynamic properties of complex biomolecular systems. We begin by introducing the physical principles of sPRE, along with a summary of the available co-solute paramagnetic probes and the current state-of-the-art NMR toolbox. Subsequently, we highlight recent applications of sPRE in structural, dynamic, and functional studies on a variety of biomolecular systems, with the majority of the examples presented concerning proteins.

2. Theory

2.1. Solvent paramagnetic-relaxation enhancement

In the presence of the magnetic moments of unpaired electron spins, a nucleus will experience a variety of paramagnetic effects including pseudocontact shifts, paramagnetic relaxation enhancement, and residual dipolar couplings (via induction of partial orientation of molecules in a high magnetic field). Much of the theory used to describe these effects was developed in the context of studies of the relaxation of bulk water containing paramagnetic solutes (proteins, metal complexes, small molecule radicals, etc.), but it is equally applicable to analysing the relaxation of nuclei in diamagnetic biomolecules during solvent PRE experiments. In these cases the effects originate from an added paramagnetic probe, and are determined by its magnetic susceptibility tensor (χ) and by the nature of the interaction between the paramagnetic probe and the diamagnetic co-solute biomolecule (in this section we will call it "target") [53,64–67]. The asphericity of the magnetic susceptibility tensor reflects changes in the electron magnetic moment with varying orientations of the probe-target vector (*i.e.* anisotropic component ($\Delta\chi \neq 0$) – variation of the electron magnetic moment with orientation; isotropic component ($\Delta\chi \approx 0$) – no observable orientation dependence) [53,55,68]. A paramagnetic probe with a vanishing $\Delta\chi$ still gives rise to PREs but it will not induce PCSs and RDCs.

The paramagnetic probe and the co-solute diamagnetic biomolecular target can either form a transient, nonspecific, yet rotationally correlated complex, or alternatively the two molecules can freely diffuse in the solution without associating with one another [69,70]. These two situations require different models for quantitative analysis of the sPRE; while the former is best described by an inner-sphere relaxation model [66], the latter obeys an outer-sphere relaxation model [71,72]. In general, sPREs of biomolecules and biomolecular complexes appear to be better described by the inner-sphere model, whereas the outer-sphere model is more applicable for sPRE interactions with small molecules [59,69]. It has been reported that predictions based on the outer-sphere model analysis can deviate from the experimental data because of inherent approximations in treating molecules as rigid and spherical, as well as from failure to account for electrostatic interactions in the model [59,69].

To provide a minimum of theory to understand the following application sections, we briefly summarize here several important relaxation mechanisms and their relation to the dynamics of the system. For a detailed and extensive treatment, the interested reader is referred to a recent volume edited by Parigi, Luchinat and Ravera [81], where Chapter 1 contains a comprehensive theoretical description for a system in which the relaxation of nuclei in a target solute biomolecule (*eg.* a protein) are affected by unpaired electrons present in a probe in the same isotropic solution. If the relaxation rates in the diamagnetic state are given by R_i^{dia}, where (i = 1) corresponds to longitudinal and (i = 2) to the transverse relaxation rates, then additional contributions $\Gamma_i = R_i^{para} - R_i^{dia}$ are caused by time-dependent magnetic contributions to the intermolecular interaction energies.

As the Fermi contact term is rarely a significant source of relaxation in practice, the PRE predominantly comes about due to two mechanisms that are dipolar in origin: the modulation of the nuclear-electron (*i.e.* hyperfine) interaction - as described by Solomon, Bloembergen and Morgan (SBM) [82,83] - and the Curie spin relaxation contribution [84]. The stochastic fluctuations with time that drive relaxation then come about by the modulation (*i.e.* changes in magnitude) of the specific interactions. As the fluctuations in the intermolecular interaction energy rely on variation in (*i*) the presence; (*ii*) the distance; or (*iii*) the orientation of the interaction with respect to the magnetic field, there are four time constants that are important: (a) τ_M, the lifetime of the intermolecular complex between the target and the probe, over which the magnitude of the interaction changes (note that τ_M^{-1} is the exchange rate constant); (b) T_{je}, the electron spin relaxation times (j = 1 or j = 2, respectively, for longitudinal and transverse relaxation), as the electron spin orientation changes – N.B. this term is irrelevant for Curie relaxation; (c) the effective translational diffusion constant D characterising the relative movement of the two molecules due to Brownian diffusion; (d) τ_r, the rotational correlation time describing the collective rotational motion of the target-probe complex during the time that they are associated, over which the orientation of the inter-spin vector changes.

To develop further, we must consider that the nuclear spins may exist in two magnetic environments, either in the absence or the presence of the paramagnetic probe, respectively. Defining the relative relaxation rates Γ_i as the additional relaxation (PRE) due to the probe, then, given a chemical shift difference $\Delta\omega_p$ of a

target nucleus between the two milieux, we obtain the Swift-Connick relations [85]:

$$\Gamma_1 = \frac{f_M}{\frac{1}{R_1^{para}} + \tau_M} \tag{1}$$

$$\Gamma_2 = \frac{f_M}{\tau_M} \frac{\left(R_2^{para}\right)^2 + R_2^{para}\tau_M^{-1} + (\Delta\omega_M)^2}{\left(R_2^{para} + \tau_M^{-1}\right)^2 + (\Delta\omega_M)^2} \tag{2}$$

$$\Delta\omega_p = \frac{f_M}{\tau_M^2} \frac{\Delta\omega_M}{\left(R_2^{para} + \tau_M^{-1}\right)^2 + (\Delta\omega_M)^2} \tag{3}$$

Here f_M is the mole fraction of the target nuclei in the bound state and $\Delta\omega_M$ is the difference between the chemical shift of the target nucleus in the presence and absence of the paramagnetic probe. The chemical exchange rate effectively limits the propagation of the effect from the paramagnetic site to the protons of the diamagnetic target. Importantly, for relatively low concentrations of the PRE probe, the magnitudes of the paramagnetic relaxation enhancements vary linearly with the concentration of the paramagnetic center, and hence they can be approximated by a simple product of the concentration (in mM) and the relaxivity (the amount of relaxation caused by 1 mM of the probe). Such usage is common in the field of contrast agents. One has to keep in mind, however, that the relaxivity is often field-dependent.

The extent to which the PRE is affected by these mechanisms depends on an effective correlation time τ_c according to Equation (4):

$$\frac{1}{\tau_{c1}} = \frac{1}{T_{1e}} + \frac{1}{\tau_r} + \frac{1}{\tau_M} \quad , \quad \frac{1}{\tau_{c2}} = \frac{1}{T_{2e}} + \frac{1}{\tau_r} + \frac{1}{\tau_M}, \tag{4}$$

which shows that the mechanism with the shortest correlation time will tend to dominate the relaxation. In cases when longitudinal and transverse electron relaxation times are equal (T_{1e} = T_{2e} (=T_e)), or when both T_{1e} and T_{2e} are much longer than the rotational correlation time τ_r or the lifetime of the intermolecular complex τ_M, a single correlation time $\tau_c = \tau_{c1}$ can be used to calculate PRE values [68,81]. Although exact numbers for each of these correlation times are not available for biomolecules, there have been ample investigations done for small molecules. If we focus on the situation of sPRE caused by Gd(III) chelates - such as contrast agents - and aminoxyl (*e.g.* TEMPO) derivatives, then the long electron spin relaxation typically causes the nuclear relaxation to report on translational and rotational diffusion. In this regime, the SBM contribution also strongly predominates over the Curie contribution [59,86], because in such cases only the average magnetic moment of the electron, rather than the instantaneous moment, is the source of relaxation. Only in situations where electron spin relaxation is very much faster than molecular rotation will the Curie relaxation component become significant, in which case the Curie effective correlation time can be modulated by reorientation and chemical exchange only [86]. In situations where electron relaxation has a significant contribution to the definition of the effective correlation time, one should take into account its dependence on the applied magnetic field.

In cases in which the target only spends a small fraction of its time bound to the paramagnetic probe, the Swift-Connick relations [85], Equations (1)–(3), can be used to account for this dynamic equilibrium. The electron and nuclear spin form a common entity, such as a complex in which the two molecules rotate jointly in solution for as long as they remain associated. In this case the inner-sphere relaxation regime applies [66], and the paramagnetic relaxation rate Γ_1 for the nucleus can be calculated from Equation (5):

$$\Gamma_1 = \frac{2}{15}\left(\frac{\mu_0}{4\pi}\right)^2 \frac{\gamma_I^2 \left(g_J \mu_B\right)^2 J(J+1)}{r^6} \left(\frac{3\tau_{1c}}{1+\omega_I^2\tau_{1c}^2} + \frac{7\tau_{2c}}{1+\omega_S^2\tau_{2c}^2}\right), \tag{5}$$

and the relaxation rate Γ_2 from:

$$\Gamma_2 = \frac{1}{15}\left(\frac{\mu_0}{4\pi}\right)^2 \frac{\gamma_I^2 \left(g_J \mu_B\right)^2 J(J+1)}{r^6} \left(4\tau_{1c} + \frac{3\tau_{1c}}{1+\omega_I^2\tau_{1c}^2} + \frac{13\tau_{2c}}{1+\omega_S^2\tau_{2c}^2}\right), \tag{6}$$

where μ_0 is the magnetic permeability of vacuum, γ_I denotes the magnetogyric ratio of the nuclear spin of interest, g_J designates the Landé factor, μ_B is the Bohr magneton, J denotes the total angular momentum of the paramagnetic probe (*e.g.* J = 1/2 for aminoxyl radicals), r stands for the distance between the nucleus and the paramagnetic centre (considered in more detail below), τ_{jc} is the effective correlation time defined by Equation (4), and ω_I and ω_S are the nuclear and electron Larmor frequencies, respectively, with $\omega_S \gg \omega_I$.

When the paramagnetic probe and the biomolecular target do not physically associate, the outer-sphere model should be considered, in which purely diffusive effects of the probe will depend on its molar concentration *[S]* and a steric accessibility factor *P* for the nuclear spin [66,71,87]. In this model, the overall PRE rates can be calculated as follows:

$$\Gamma_1 = \left(\frac{32\pi}{405}\right)\gamma_I^2\gamma_S^2\hbar^2 J(J+1)\frac{N_A P[S]}{1000bD}\{3j_1(\omega_I) + 7j_2(\omega_S)\} \tag{7}$$

$$\Gamma_2 = \left(\frac{16\pi}{405}\right)\gamma_I^2\gamma_S^2\hbar^2 J(J+1)\frac{N_A P[S]}{1000bD}\{4 + 3j_1(\omega_I) + 13j_2(\omega_S)\} \tag{8}$$

where $\hbar$ is Planck's constant divided by 2π, and the spectral density $j_k(\omega)$ is defined as:

$$j_k(\omega) = Re\left\{\frac{1+\frac{1}{4}\left[i\omega\tau + \left(\frac{\tau}{T_{jS}}\right)\right]^{1/2}}{1+\left[i\omega\tau + \left(\frac{\tau}{T_{jS}}\right)\right]^{1/2} + \frac{4}{9}\left[i\omega\tau + \left(\frac{\tau}{T_{jS}}\right)\right] + \frac{1}{9}\left[i\omega\tau + \left(\frac{\tau}{T_{jS}}\right)\right]^{3/2}}\right\}. \tag{9}$$

Here, N_A is Avogadro's number, T_{jS} denotes the electron spin relaxation time, b stands for the closest attainable distance between the electron and nuclear spins, D designates the relative translational diffusion constant between the electron and the nucleus, $\tau = b^2/D$ is the translational diffusion correlation time, and *Re* denotes the real part of the spectral density function $j_k(\omega)$. Note that the PRE here is directly proportional to concentration, whereas in the case of inner-sphere relaxation, the concentration dependence results from the linear increase in the mole fraction of probe nuclei in bound states, Equations (1)–(2).

The dipole–dipole interaction between electrons and a nucleus will lead to an increase in nuclear relaxation rate. As the spectral linewidth is proportional to the transverse relaxation rate, resonances of nuclei in the vicinity of the paramagnetic centre will broaden, while the sPREs on the longitudinal relaxation rate result in a faster recovery of the magnetization. In general, Equations (5) and (6) can be approximated by the following formula, emphasising the r^{-6} dependence of sPRE effects:

$$\Gamma_j = \frac{\alpha_j}{r^6}, \tag{10}$$

where j = 1 stands for longitudinal relaxation, j = 2 for transverse, and α_j encompasses all terms present in Equations (5) and (6) [59,70].

Under conditions approximating to the inner-sphere relaxation model, sPREs can be determined by integration over the entire solvent volume [59,70]. The volume integration can be obtained by performing a back-calculation (prediction) of the sPRE value for a given nucleus by using numerical integration over a grid with a defined spacing. For a few special cases, the sPRE can be obtained analytically. One such example is the sPRE of spins in a system with, to a first approximation, a planar surface, such as a large

spherical micelle. The volume integration after the transformation to spherical coordinates yields [88]:

$$\int_{\phi(V)} \frac{1}{r^{-6}} d^3r = \int_{\bar{r}=d+r_{para}}^{\infty} \int_{\theta=0}^{\pi} \int_{\phi=0}^{2\pi} \frac{1}{r^4} \sin\theta dr d\theta d\phi = \frac{4\pi}{3(d+r_{para})^3}, \quad (11)$$

where ϕ and θ are the angles in the spherical coordinate system, r stands for the distance between the nucleus and the paramagnetic centre, d corresponds to the immersion depth of the nucleus, for example in the micelle, and r_{para} represents the hydrodynamic radius of the paramagnetic compound.

In the case of outer-sphere relaxation, the dipole–dipole interaction fluctuates due to translational diffusion and electron spin relaxation, and the sPRE is independent of molecular tumbling [89]. Conversely, inner-sphere relaxation shows a high sensitivity to the rotational correlation time [89]. The choice of relaxation model is an important step in sPRE data analysis. When designing sPRE experiments, system-specific characteristics ought to be considered, such as the nature of the probe – target interaction, the relative timescales of electronic relaxation, exchange, and rotation, and the size of the system of interest.

These equations lead to some important points relevant to interpreting sPRE effects and designing studies. Although Equation (10) indicates that sPRE will decrease rapidly with increasing distance r, larger distances (>15 Å) than those for the commonly used ^{1}H-^{1}H NOE analysis can still be determined [59,90] due to the fact that the magnetogyric ratio of the electron is 658.2 times larger than that of the proton [81]. It further follows that solvent-exposed residues will experience stronger PREs than those buried in the protein core, as long as the probe molecule does not enter or bind to the protein. According to Equations (5)–(8), probes possessing larger spin angular momentum will give rise to stronger PRE effects. For example, for a given distance r Gd^{3+} (J = 7/2) induces a stronger PRE than would aminoxyl radicals (J = 1/2). Furthermore, in the case when the sPRE scales linearly with the concentration of the paramagnetic probe (as in Equations (7)–(8)) larger distances can be determined by using higher concentrations of the paramagnetic agent, limited primarily by probe solubility.

2.2. The modulation of sPRE by internal dynamics

On the pico- to nanosecond time scale, physicochemical processes such as bond vibration and libration, side chain rotamer interconversion, and backbone torsion angle changes can all occur [92,93]. The importance of these rapid motions has been noted for a variety of biochemical processes and properties such as enzyme function [94], ligand recognition [95], conformational entropy [96,97] and allosteric transmission [98]. The impact of fast dynamics on the PRE is described by Solomon-Bloembergen theory and the model-free approach [82,83,99–102]. Fast internal motions are described by specifying the correlation time for the internal motion τ_i and the square of the generalized order parameter S^2 for bond vectors, which provides local radial and angular information on internal motions. In the model-free formalism, assuming no coupling between the internal motions and the overall tumbling of the molecule, the correlation function $C_I(t)$ for the internal motion of the interaction vector within the molecular frame may be approximated using the following equation:

$$C_I(t) = S^2 + \left(1 - S^2\right) \exp\left(-\frac{t}{\tau_i}\right). \quad (12)$$

The order parameter S^2 can be defined both for fixed-length interaction vectors, such as ^{15}N-^{1}H and ^{13}C-^{1}H bond vectors, and for variable length vectors, *e.g.* a ^{1}H-^{1}H dipolar interaction vector [103–105]. In the case of transition metal ions, the electron relaxation originates from the zero-field splitting tensor, and thus depends on very short lifetimes between collisions with solvent molecules, τ_v [99,106]. With the assumptions that the effective electron relaxation rate τ_s^{-1} is independent of the correlation times for the overall and internal motions, and that $\tau_i \gg \tau_t$, the incorporation of $C_I(t)$ into the correlation function for PRE and its subsequent transformation yields the spectral density function [99]:

$$J_{SBMF}(\omega) = \langle r^{-6} \rangle \left(\frac{S^2 \tau_c}{1+\omega^2 \tau_c^2} + \frac{(1-S^2)\tau_t}{1+\omega^2 \tau_t^2} \right), \quad (13)$$

where the subscript SBMF refers to the SBM theory in the model-free formalism, τ_c is the correlation time defined as $(\tau_r^{-1} + \tau_s^{-1})^{-1}$ with τ_r being the rotational correlation time of the molecule, and τ_t represents the total correlation time defined as $(\tau_r^{-1} + \tau_s^{-1} + \tau_i^{-1})^{-1}$. The PRE rates in the Solomon-Bloembergen theory can be represented in its general form as:

$$\Gamma_j = \langle r^{-6} \rangle f_{SB,j}(\tau_c), \ (j = 1 \text{ or } 2) \quad (14)$$

where $f_{SB,j}(\tau_c)$ corresponds to the α_j constant from Eq. (10) expressed as a function of τ_c. After the incorporation of the model-free formalism accounting for the internal fast motions, this equation becomes:

$$\Gamma_j = \langle r^{-6} \rangle f_{SB,j}(\tau_c) + \left(1 - S^2\right) \langle r^{-6} \rangle f_{SB,j}(\tau_I). \quad (15)$$

The formulas (Eq. (14)–(15)) should only be used for systems that tumble isotropically. For nonglobular systems, with significantly anisotropic diffusion, the additional PRE dependence on the angles between the principal axes of the diffusion tensor and the electron-nucleus interaction vector should be included [99].

Fast internal motions imply different effects on the ^{1}H-Γ_1 and ^{1}H-Γ_2 PRE rates [99,102]. The contribution of the internal motion correlation time τ_i can be determined from the second term of Equation (15). Owing to differences in the internal dynamics of individual ^{1}H nuclei in the biomolecule, the τ_i can take a wide range of values. On the other hand, the variation in the values of the order parameters S^2 for the PRE interaction vectors is rather limited due to the larger distances involved in the PRE. For lower values of the order parameter S^2 (<0.5), indicating flexibility at this residue site, it can be shown that the ^{1}H-Γ_1 rate is strongly dependent on τ_i (especially for $\tau_i < 1/\omega_H$). In contrast, the ^{1}H-Γ_2 rate exhibits much less sensitivity to variation in τ_i. Additionally, ^{1}H-Γ_1 rates are sensitive to cross-correlation effects and exchange with water (for amide protons), which further complicates detected ^{1}H-Γ_1 rates [99,103]. Moreover, it has been shown that ^{1}H$_N$-Γ_1 backbone amides rates display a significant magnetic field dependence, and the comparison of ^{1}H$_N$-Γ_1 recorded at different fields can indicate the presence of dynamics of the PRE vectors occurring on the pico- to nanosecond timescale, whereas ^{1}H$_N$-Γ_2 rates are negligibly dependent on the magnetic field [103].

While fast internal motions affect the autocorrelation function, the effects of slower dynamics (in the 10^{-6}–10^{-1} s time-scale range) on PRE are more relevant for the detection of kinetic exchange processes in biomolecules, such as biomolecular complex association and dissociation, oligomerization, aggregation, exchange between protonated and deprotonated states, and conformational switches [1,2,8,93,107]. The effects of slower dynamics on the NMR observables can be described using the McConnell equations [108], which can be written in matrix form for transverse magnetization as:

$$\frac{d}{dt} m = -(\boldsymbol{R} + \boldsymbol{K} - i\boldsymbol{W})m, \quad (16)$$

in which m is a vector containing the complex transverse magnetizations ($M_x + iM_y$) of the exchanging states, $\boldsymbol{R}$ represents a relaxation matrix, $\boldsymbol{K}$ stands for a kinetic matrix describing the interconversion between states, and $\boldsymbol{W}$ is a chemical shift matrix.

This equation takes into consideration the effects of different frequencies, exchange rates and relaxation rates during chemical shift evolution. The McConnell equations can be solved to provide a time-dependent exponential decay of the magnetization (*i.e.,* free induction decay) as follows:

$$M_t = e^{(i\omega - R + K)t} M_0. \tag{17}$$

In this formula, M_0 is the complex magnetization at time $t = 0$. Subsequently, time-dependent data are Fourier transformed to yield an NMR spectrum of the exchanging system. In the case of a two-state exchange process $A \underset{k_{BA}}{\overset{k_{AB}}{\leftrightarrow}} B$, the terms in Equation (16) are defined by the following formulas:

$$m = \begin{pmatrix} M_A^+ \\ M_B^+ \end{pmatrix} \tag{18}$$

$$R = \begin{pmatrix} R_{2,A} + \Gamma_{2,A} & 0 \\ 0 & R_{2,B} + \Gamma_{2,B} \end{pmatrix} \tag{19}$$

$$K = \begin{pmatrix} k_{AB} & -k_{BA} \\ -k_{AB} & k_{BA} \end{pmatrix} \tag{20}$$

$$W = \begin{pmatrix} \Omega_A & 0 \\ 0 & \Omega_B \end{pmatrix}, \tag{21}$$

where M^+ is the transverse magnetization represented by a complex variable ($M_x + iM_y$) for the spin in states A and B, R_2 denotes the transverse relaxation rates in the two states, k_{AB} and k_{BA} stand for the kinetic rate constants for the A → B and B → A processes, respectively, and $\Omega/2\pi$ is the chemical shift frequency in Hz. In the paramagnetic state, the relaxation matrix $\boldsymbol{R}$ contains both the intrinsic R_2 and the PRE Γ_2 rates, while in the diamagnetic state the relaxation matrix $\boldsymbol{R}$ contains only the intrinsic R_2 rates. Equations (18)–(21) can be straightforwardly expanded to three-state exchange and a general *N*-state exchange process [109]. The solution of the matrix in equation (17) produces specific eigenvalues, of which the real and imaginary parts represent the decay rates and the resonance frequencies of the two states, respectively, and the populations of the exchanging states A and B influence the position and intensities of the resonance lines.

Biomolecular processes of conformational dynamics and molecular recognition are generally several orders of magnitude slower than the relevant diffusion timescale for the paramagnetic agent, which is on the order of 1 ns or faster [69,110]. Hence, different biomolecular conformational states can be probed, and measured sPREs represent an average value of sPREs for single conformational states. In the case of two-state exchange, the populations of the two interconverting states p_A and p_B, the values of the relative exchange rate between the two states ($k_{ex} = k_{AB} + k_{BA}$), and the chemical shift difference $\Delta\omega$ will influence the appearance of the NMR spectrum [1,111,112]. By comparing the exchange rate (in s^{-1}) with the chemical shift difference ($\Delta\omega$; in rad s^{-1}), different NMR time scales relevant to observed sPRE can be segregated into three distinct exchange regimes: slow exchange ($k_{ex} \ll |\Delta\omega|$), intermediate exchange ($k_{ex} \approx |\Delta\omega|$), and fast exchange ($k_{ex} \gg |\Delta\omega|$). In the slow exchange regime, resonance signals from both states are separately resolved in the NMR spectrum, enabling determination of the sPRE independently for both states. Fast exchange is at the opposite limit, where a single resonance line is observed in the NMR spectrum with a population-weighted chemical shift and relaxation rate, and thus the measured sPRE is also population weighted [99]. In the intermediate regime, the resonance linewidth is strongly increased due to the interconversion between the states [113], which precludes measurement of the sPRE. The additional contribution to relaxation arising from the presence of the paramagnetic probe modulates the measured NMR spectra. In the slow exchange regime, sPREs can be determined for each of the interconverting species individually, assuming that the exchange is slower than the sPRE observed in state A and B. In the fast exchange regime, the detected sPRE is a linear, population-weighted average of the sPREs observed in states A and B, with an assumption that the exchange is faster than the sPREs observed in state A and B:

$$\Gamma_2^{obs} = p_A \Gamma_{2,A} + p_B \Gamma_{2,B}. \tag{22}$$

It is important to note that the averaged sPRE provides quantitative information on the populations of the exchanging species, but not on the exchange rates between states. To obtain information about both structure and dynamics, the sPREs of individual states should be determined. The sPRE can be simulated computationally from structural models, or in the case of dynamically interacting protein complexes, sPREs can be measured for individual proteins in their unbound states [1,99]. Furthermore, the concentration dependence of the sPRE facilitates a modification of the Γ_2^{obs} aiming at inferring the presence of minor populated conformational states. As a result, an increased concentration of the paramagnetic agent would induce a stronger increase in the PRE of a spin localized in a solvent-exposed conformation, than of one for a buried spin. In fact, analysis of sPRE offers a unique opportunity of characterising some otherwise invisible, sparsely populated, states, even in the fast exchange regime [90]. It is imperative to be aware that quantitative analysis of minor species is only possible when a minor state exchanges with a major state at a rate much larger than the difference in PRE rates between the two states $k_{ex} \gg |\Gamma_2^{minor} - \Gamma_2^{major}|$; in contrast, when k_{ex} does not satisfy this inequality, information on k_{ex} and the chemical shift difference between corresponding states is required [99,111].

3. Paramagnetic co-solute probes

The choice of paramagnetic co-solute molecule is a critical step toward obtaining high quality sPRE data for structural and dynamic studies of biomolecules and their complexes. The main requirements for sPRE probes are high solubility in the solvent of interest, chemical inertness under experimental conditions (*i.e.* temperature, buffer, pH), and the lack of specific interactions with any type of functional group in the biomolecule. A notable exception to the latter criterion is when one aims to investigate weak, nonspecific and transient interactions between ions and a biomolecule. Recent studies have demonstrated that the use of analogous paramagnetic co-solutes differing only in their charges can be used in sPRE experiments i) to characterize ultra-weak paramagnetic co-solute-protein interactions and infer how co-solutes can shift the folding/unfolding equilibrium of a protein [114]; ii) to provide information about the spatial distribution of ions around biomolecules at residue level [115]; iii) to determine near-surface electrostatic potentials of biomolecules [116]. For quantitative applications in structural biology, the choice of the size of the probe can determine the level of granularity in mapping of solvent accessibility regions. For instance, smaller probes, such as oxygen, can infiltrate a lipid membrane environment and the hydrophobic cores of biomolecules. In contrast, larger probes, such as Gd_2(L7)$(H_2O)_2$ [117] (where L7 stands for 4,7,10,23,26,29-hexakis(carboxylmethyl)-2,12,21,31-tetraoxo-1,4,7,10,13,-20,23,26,29,32-decaazatricyclo-p-xylene), will be excluded from biomolecular complex cavities or interfaces, and are utilized in the determination of protein–protein interactions and aggregation processes. In this section, an overview of various sPRE probes will be outlined.

3.1. Oxygen

Due to its small size and ubiquity in biological processes, molecular oxygen (dioxygen) has been successfully used in several studies regarding protein immersion into membrane environments [118–121]. An oxygen concentration gradient can be established across the water–lipid membrane interface by applying a pressure of 20–60 bar for the observation of sPRE on ^{1}H or ^{19}F [122,123]. Measurements of membrane protein immersion depths can be obtained from either PREs or PCSs originating from the established concentration gradient of the paramagnetic probe. It is worth mentioning that the analysis can be complicated by variations in the accessibility of oxygen to protein surfaces due to the surface electrostatics [120,122]. Oxygen has also been utilized as a paramagnetic probe in studies of surface free energy differences of proteins [120,124], protein–protein interfaces [125], solvent exposure of unfolded and folded protein states [126], and in the detection of oxygen binding in internal protein cavities [127,128].

3.2. Aminoxyl radicals

Aminoxyl radicals, also known as nitroxides, constitute a class of compounds containing the aminoxyl moiety $R_2NO^{\bullet}$ as a source of the unpaired electron. Already in the 1970 s, simple organic aminoxyl radicals such as di-*tert*-butyl aminoxyl (DTBN) and 3-oxyl-2,2,4,4-tetramethyloxazolidine were used to decipher sPRE effects on DNA and cyclic peptides [129,130]. TEMPO (2,2,6,6-tetramethyl piperidin-1-yl)oxyl and its derivatives have been used as paramagnetic spin labels in numerous PRE studies [131–134]. For co-solute PRE applications, more soluble TEMPO derivatives were engineered through the addition of polar functional groups to the ring structure. One notable example is a hydroxy TEMPO derivative – TEMPOL (4-hydroxy-2,2,6,6-tetramethylpiperidin-1-oxyl), also referred to as hydroxy TEMPO or HyTEMPO [135]. Although the use of uncharged TEMPOL as a sPRE probe has been reported in studies of proteins [69], RNA [136] and enzyme-inhibitor complexes [137], it must be borne in mind that TEMPOL can potentially induce chemical shift changes at low millimolar concentrations [69]. Charged TEMPO derivatives have been exploited less often. owing to their tendency to form weak electrostatic interactions with charged groups on protein and DNA surfaces [138]. For example, a 4-amino-TEMPO has been shown to bind preferentially to exposed acidic amino acid residues [139], while a 3-carboxy-TEMPO has been demonstrated to interact with a solvent-accessible positive patch on ribonuclease A [140]. Nevertheless, these charged radicals are considered to be useful tools in mapping local electrostatic fields in proteins [116,139–141], or in investigating protein hydration [142].

3.3. First-row metal-transition ions

First-row transition metal ions are commonly used in paramagnetic NMR experiments [143–145]. Depending on the electron spin relaxation time, these metal ions tend to cause line-broadening effects in spectra of biomolecules. First-row transition metal ions possessing a long electronic relaxation time (10^{-8}–10^{-6} s), such as Mn^{2+} and Cu^{2+}, have a strong line-broadening effect via the increase of R_2 relaxation for biomolecular protons [59]. In contrast, ions with short electronic relaxation times (10^{-12}–10^{-9} s), such as Co^{2+} and Ni^{2+}, exhibit a weaker line-broadening effect and have a tendency to increase R_1 relaxation to a similar extent [146]. Of note, first-row transition-metal complexes, such as those of Ni^{2+}, also cause contact shifts and pseudocontact shifts (in the case of paramagnetic agents with anisotropic magnetic susceptibilities), and can be used as shift reagents [147]. In biomolecular NMR applications, metal ions with shorter electronic relaxation times can be harnessed when the desired effect is to enhance R_1 without a significant line broadening. For instance, Ni^{2+} coupled to 1,7-dicarboxymethyl-1,4,7,10 tetraazacyclododecane Ni(DO2A), has been used to enhance the efficiency of NMR data acquisition by reducing T_1 [146]. The use of Fe(DO3A) (with a high-spin iron(III) as an optimal transition metal) accelerated NMR analysis of the disordered protein α-synuclein and of a fibrillogenic peptide [148]. Furthermore, owing to their relatively small sizes, first-row transition metal ions are able to diffuse into biological membranes and establish a concentration gradient across the water–lipid interface, enabling measurements of insertion depths of membrane proteins [123,149].

3.4. Gd^{3+} chelates

Co-solute paramagnetic agents containing lanthanoid metal ions have been widely used in biomolecular NMR [150–154]. Out of all the lanthanides, gadolinium presents distinct advantages, as it is the only one that has a vanishing anisotropic component in its magnetic susceptibility tensor, meaning that Gd^{3+} does not induce PCS [53]. In addition, due to the large angular momentum of Gd^{3+}, with seven unpaired electrons (J = 7/2) (compare aminoxyl radicals that have J = 1/2), Gd^{3+} chelates have one of the largest radii of influence for the PRE effect, facilitating their use at lower concentrations. Therefore, Gd^{3+} is exceptionally well-suited for sPRE studies. Additional advantageous properties of Gd^{3+} chelates, such as their high chemical stability, high molar relaxivity and low hydrophobicity, have enabled their use as contrast agents in magnetic resonance imaging (MRI) applications [155,156]. Early sPRE studies, carried out with gadolinium chelates utilized charged Gd^{3+} derivatives such as $Gd(DOTA)^{-}$, $Gd(DO3A)^{-}$, $Gd(DTPA)^{2-}$ and $Gd(EDTA)^{-}$, with $Gd(DOTA)^{-}$ having the greatest *in vitro* stability among these [132,157–159]. However, undesired preferential binding of $Gd(DTPA)^{2-}$ and other charged Gd^{3+} derivates to carboxyl and amide groups has been reported [132,151]. With the development of neutral chelates that lack interaction bias, quantitative sPRE analyses were enabled and currently Gd(DTPA-BMA) (diethylenetriamine pentaacetic acid-bismethylamide) is the most commonly used probe of all Gd^{3+} chelates [69,70,160–163]. Gu *et al.* have developed a spherical and regular agent, TTHA-TMA (triethylenetetraamine hexaacetate trimethylamide), containing 10 coordination sites to the gadolinium ion, thus removing a free coordination site for a water molecule and avoiding enhancing the relaxation of protein backbone resonances through contributions from water-exchangeable protons [60,164]. Furthermore, aiming at the investigation of macromolecular complexes, larger probes, such as $Gd_2(L7)(H_2O)_2$ were developed to ensure complete exclusion of the probe from intermolecular surfaces [117,165].

3.5. Designing sPRE experiments and data processing

sPREs are measured as differences in relaxation rates (R_1 or R_2) or signal intensities of a biomolecule in the presence and absence of the paramagnetic probe, and can be obtained for any NMR-active nucleus (*e.g.* ^{1}H, ^{13}C, ^{15}N, ^{31}P) [99]. In general, a series of experiments is recorded with increasing concentrations of the paramagnetic agent (*e.g.* for detecting ^{13}C resonances: 10.0–50.0 mM Gd(DTPA-BMA)). To assess sPRE, any type of pulse sequence can be adapted by adding an R_1 or R_2 measurement block. Generally, R_1 relaxation values are obtained from a saturation-recovery block, whereas R_2 relaxation values are determined using a Carr-Purcell-Meiboom-Gill (CPMG) block. In terms of sPRE effect detection methods, 1D NMR spectroscopy could be used, but more commonly 2D NMR hetero-nuclear correlation experiments, such as ^{15}N-^{1}H HSQC [166–168], ^{13}C-^{1}H HSQC [69,169], ^{13}C-^{1}H HMQC [137], ^{15}N-^{1}H CRINEPT-HMQC [170] or

2D NOESY [168] have been selected as a readout. Also, in order to increase the accuracy of the analysis, one may analyze and compare results obtained from separate sPRE experiments where each experiment employs a different paramagnetic co-solute agent [69,132,167].

The values of sPRE of longitudinal relaxation (Γ_1) can be calculated from fitting an exponential recovery function to peak intensities according to the formula:

$$I = I_0\left(1 - e^{-R_1 t}\right), \tag{23}$$

where I_0 is the signal intensity after an infinite recovery delay, t stands for the recovery time, and R_1 represents the longitudinal relaxation rate. To extract accurate values of experimental errors, duplicates should be performed at two or more delay times. The sPRE values can then be determined from the slope of the relaxation rate against the probe concentration. In case the ^1H_N longitudinal relaxation data obtained are not mono-exponential, possibly due to rapid exchange with water or ^{1}H-^{1}H cross-relaxation effects, one should inspect fitting errors and exclude outliers [171].

sPRE of transverse relaxation (Γ_2) can be determined directly by fitting the following equation to signal intensities (I) at different concentrations of the probe:

$$I \approx \frac{1}{R_2^{dia}+c\Gamma_2} e^{-\left(R_2^{dia}+c\Gamma_2\right)\tau}, \tag{24}$$

where the first term corresponds to reduced signal intensities in the directly detected dimension, R_2^{dia} is the transverse relaxation rate under diamagnetic conditions, c represents the concentration of the paramagnetic probe, and τ stands for the total time during which nuclear spin magnetization is in the transverse plane prior to acquisition (*e.g.* the INEPT block in a pulse sequence)[59]. The Γ_2 rates can also be obtained by using a two-time-point measurement, in which transverse relaxation rates are determined from two delay time points (T ≈ 0 and ΔT) according to the equation:

$$\Gamma_2 = R_2^{para} - R_2^{dia} = \frac{1}{T_b - T_a} ln \frac{I^{dia}(T_b) I^{para}(T_a)}{I^{dia}(T_a) I^{para}(T_b)}, \tag{25}$$

where R_2^{para} is the transverse relaxation rate in the presence of the paramagnetic agent, $T_a \approx 0$ and $T_b > T_a$, represent delay times, I^{dia} and I^{para} stand for the peak intensities for the diamagnetic and paramagnetic states, respectively. In this experiment, two delay time points for transverse relaxation are chosen in a way to minimize the errors in the Γ_2 rates (an interested reader may find details elsewhere [100]).

4. Applications

In this section, we aim to illustrate the versatility of the technique in answering varied questions relating to the structures, dynamics, and functions of challenging biomolecules (Fig. 1, Table 1).

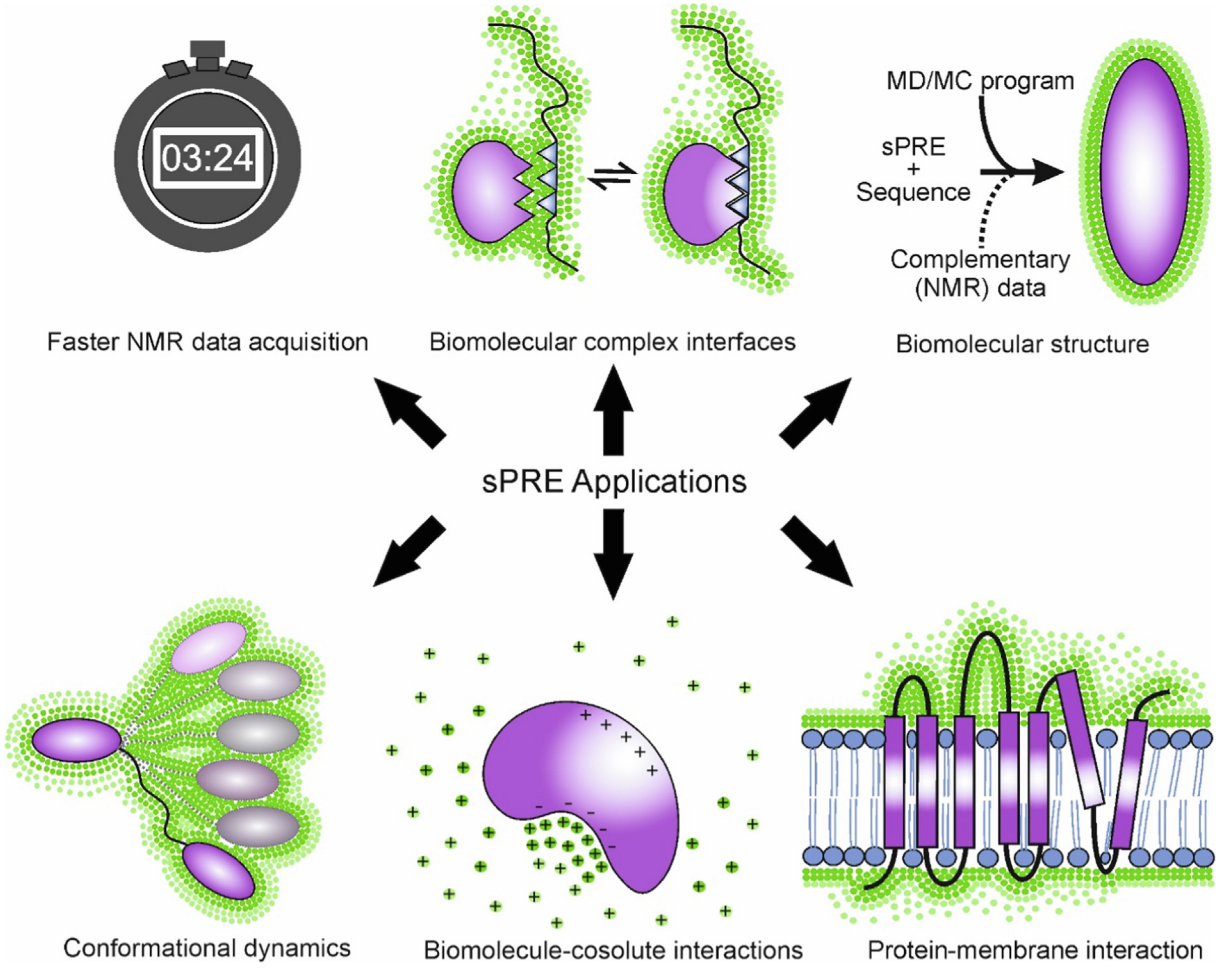

Fig. 1. sPRE enables a variety of different applications to biomolecules and their complexes, ranging from acceleration of NMR data acquisition, through determination of biomolecular structure and conformational dynamics, identification of interfaces of protein complexes and probing weak interactions between biomolecules and co-solutes, to characterization of protein immersion within a biological membrane. Paramagnetic agents are illustrated as green circles, and biomolecules are coloured in a gradient of purple to illustrate the dependence of sPRE on solvent accessibility.

Table 1
Summary of the use of sPRE methodology in a variety of applications in biomolecular sciences.

Application	sPRE study example
Increase sensitivity of recorded experiments and speed up data acquisition.	• Acquisition in 3 h of multidimensional NMR experiments of fibrillogenic peptide after addition of Fe(DO3A) probe [148] • Fast and quantitative NMR data acquisition of metabolomic samples [172,173]
Simplify crowded regions of NMR spectra.	• Simplification of NMR spectra for yeast ubiquitin and Qua1 homodimerization domain [59,174]
Help determine biomolecular structure.	• sPRE-derived solvent accessibility data on RNA samples used as restraints in structure determination [175–177] • Implementation of a sPRE-based scoring function into CS-ROSETTA *de novo* structure prediction and solvent accessibility data into Xplor-NIH structure calculation program [178,179] • sPREs used as restraints in MD/Monte Carlo simulations of protein conformational ensembles [60]
Identify interfaces of protein complexes.	• sPREs used to characterize a binding interface between constituents of a protein complex [158,180,181]
Infer information about conformational dynamics of biomolecules.	• Comparison of experimental and back-calculated sPREs reveals information about solvent exposure and conformational dynamics of the Tudor domain: dimethylated arginine complex [182] • sPRE rates used to detect low-population and/or transient conformational states of IDPs and enzymes [159,183] • sPRE, along with molecular simulations, used to visualize conformational ensembles of proteins undergoing dynamic movements at micro-to millisecond timescale, and large-scale dynamics [60,110] • sPREs used to distinguish between residues involved in the formation of weak specific complexes and nonspecific electrostatic interactions [162]
Study interactions between biomolecules and ions.	• sPRE used to visualize spatial distributions of ions around proteins, as well as for the *de novo* determination of near-surface electrostatic potential [115,116] • sPREs provide information on the dynamics and energetics of nonspecific, weak and transient protein-*co*-solute interactions at atomic level [114]
Make inferences about the structure of biomolecules inside biological membrane mimetics.	• sPRE values used to obtain distance restraints and information about the localization, orientation and immersion depth of a peptide within a biological membrane mimetic [168,184–186]

4.1. NMR signal enhancement

As mentioned in Section 3.3, sPRE agents with short electron relaxation times cause minimal line broadening and increase the rate of recovery of longitudinal magnetization (shorten T_1 relaxation time), allowing for reduced inter-scan recycle delays and improving the sensitivity of NMR experiments. This principle has been applied to a variety of biomolecular systems, ranging from small proteins to large protein complexes [146,170,187–189]. The limiting factor on the signal enhancement is the fact that sPRE strongly depends on the surface accessibility of residues, meaning that residues at the solvent-accessible surface experience a greater signal enhancement than residues buried in the interior of a biomolecule.

The addition of Gd(DTPA-BMA) to a uniformly ^{2}H-^{13}C-^{15}N-labeled 44 kDa trimeric *Bacillus Subtilis* chorismate mutase resulted in the reduction of ^{13}C T_1 relaxation times without compromising ^{13}C T_2 relaxation times, thus enabling a complete assignment of side-chain resonances [188]. However, the use of Gd^{3+} complexes may induce significant line broadening for ^{1}H resonances, due to the relatively long electronic relaxation time of the agent (nano- to microseconds), as demonstrated in the study of the 800 kDa GroEL complex where Gd^{3+} was added to assist in selective water suppression [170]. In the presence of $Gd(DOTA)^{-}$ at concentrations exceeding 1 mM, a reduction in water T_1 value was accompanied by a concomitant increase in R_2 relaxation rate of surface-exposed residues, whereas a line-broadening effect was not observed at lower concentrations of the paramagnetic probe. Notably, the sPRE-induced water suppression effect was also observed in solvent containing low concentrations of uncomplexed Gd^{3+}. The line broadening in the proton-detected experiments would not be severe in the presence of paramagnetic agents possessing short electronic relaxation times (pico- to nanosecond) [146].

Oktaviani *et al.* demonstrated that a high-spin Fe(DO3A) complex is an optimal sPRE probe for the study of intrinsically disordered proteins and fibrillogenic peptides, as its addition sped up the R_1 relaxation of amide protons and ^{13}C nuclei, facilitating complete backbone resonance assignment [148]. Fast 2D experiments, such as ^{1}H-^{15}N-SOFAST-HMQC [190] and carbon-detected (H-flip) ^{13}CO-^{15}N [191] employ selective excitation pulses on the protein resonances to increase the effects of R_1 relaxation. As a result of using these methods in the presence of 40 mM Ni(DO2A), the signal-to-noise ratios of intrinsically disordered proteins were enhanced 1.7-fold and 1.9-fold for ^{13}C-direct detected ^{13}CO-^{15}N and ^{1}H-^{15}N-SOFAST-HMQC experiments, respectively [187]. Building on these results, Chan *et al.* reported 4.5-fold enhancement of sensitivity of NMR diffusion experiments for a macromolecular assembly of ribosome–nascent chain complex after the addition of 40 mM Ni(DO2A) [192].

4.2. Spectral editing

The fact that sPRE agents cause line broadening of solvent-accessible proton resonances has led to their use as a spectral editing tool. This phenomenon can be beneficial for the analysis of biomolecular systems, such as disordered protein regions or biomolecular systems of a large size, in which spectral assignment is hampered by significant peak overlap. Based on this principle, Kellner *et al.* applied SEMPRE (spectral editing mediated by PRE) to simplify crowded ^{15}N-HSQC-type (including ^{15}N-edited NOESY) spectra of yeast ubiquitin by adding Gd(DPTA-BMA) [174]. This allowed them to distinguish resonances of ordered globular domains from resonances of disordered regions and solvent-accessible tails or linkers, simplifying the analysis of a crowded spectral region (~8-9 ppm for $^{1}H^{N}$).

In addition, it was shown for the Qua1 homodimerization domain from Sam68 (Src-associated during mitosis, 68 kDa) that amide resonances of solvent-exposed can be distinguished from buried residues in the dimer interface by comparison between their intensity profiles in the presence and absence of a paramagnetic agent [59]. Furthermore, this type of spectral editing can be applied to the study of transient and weak biomolecular interactions. For example, the addition of micromolar concentrations of Gd^{3+} salts accelerated the detection of interpolymer complex formation, cyclodextrin host–guest interactions, and the screening of DNA ligands by suppressing the NMR signals of interacting species in one- and two-dimensional experiments, while not impacting the non-competitive ligands [193].

4.3. Biomolecular structure determination

sPRE data can be used to determine structural parameters for a variety of biomolecular systems, including folded proteins [69] and large protein complexes [194], as well as challenging RNA molecules [136,175,195], and conformational ensembles of IDPs [183,196]. sPRE measurements provide structural information about solvent accessibility (*i.e.* atoms located in the surface vicinity will experience the largest sPRE) and about the minimum distance of the shielded atoms to the closest paramagnetic centre [70]. Back-calculation of theoretical sPREs for biomolecules, obtained by numerical integration with the use of the Otting-LeMaster approximation [59,64], for example, should match experiment. As this approach is computationally demanding, a modification was proposed in which dummy atoms mimicking paramagnetic probes were included in simulated-annealing molecular dynamics simulations [70]. Distance restraints were then obtained through iterative calculation of minimal distances from a spin of interest to the dummy atoms. Applications were shown for the rapid structure determination of ubiquitin (8 kDa) and maltodextrin-binding protein (42 kDa).

A promising and time-efficient improvement for structure calculation with sPRE data has been proposed by Wang *et al.* through the introduction of an empirically-determined solvent accessibility potential implemented in the Xplor-NIH program [179,197]. In this approach, an explicit probe is replaced by an implicit energy term reflecting solvent accessibility (an inverse relationship to the level of "crowding" of neighbouring atoms) for each residue in the simulated-annealing protocol. As residues located near or at the protein surface tend to be surrounded by fewer heavy atoms (within a certain distance cut-off R_c) compared to buried residues, the calculated level of solvent accessibility (S^c_{Acc}) can be determined according to the following equation:

$$S^c_{Acc} = \left[\sum_{i=1}^{N} \frac{1}{r_i^2}\right]^{-1}, \tag{26}$$

where solvent accessibility is expressed in Å^2, r_i is the distance (in Å) between an amide proton and heavy atom i, and N is the number of heavy atoms within a distance R_c. By using the 10 lowest-energy NMR structures of the model protein ubiquitin and a cut-off radius of 20 Å and performing linear regression (calculated S^c_{Acc} against measured solvent accessibility), Wang *et al.* derived an empirical formula correlating experimental sPRE data (*eg.* intensity ratios) with the effective solvent area S^m_{Acc} for their specific dataset:

$$S^m_{Acc} = 0.353\Gamma_{PRE} + 0.128. \tag{27}$$

A combination of this empirical function with equation (26) yields the solvent accessibility energy term E_{Acc}, which they implemented in the Xplor-NIH protocol, expressed as a harmonic potential:

$$E_{Acc} = k\left(S^c_{Acc} - S^m_{Acc}\right)^2, \tag{28}$$

in which the force constant k, was optimal at 300 kcal/Å. The inclusion of sPRE data in the Xplor-NIH protocol significantly improved the accuracy and convergence of structural models of the protein BAX, ubiquitin, and Qua1 homodimer [179] (though each case required a separate empirical parametrization of the relationship between S^c_{Acc} and Γ_{PRE}; the values shown in Eq. (27) are specific for the ubiquitin experiments).

An alternative approach, optimized for fast performance and time-efficiency, in which a model structure is used and mapped onto a three-dimensional bit array representing a regularly spaced grid, was reported by Hartlmüller *et al.* [178]. In this protocol, a uniform grid with a typical spacing of 0.5–2 Å is first generated around the structural model (by default, the grid boundaries are located minimum 10 Å away from every atom of the protein). Subsequently, the positions of atoms in the biomolecule are discretized on the grid by replacing the Cartesian coordinates of the atom with the coordinates of the nearest grid point. Next, grid positions located within the van der Waals region of the biomolecule are selected as occupied. All radii of atoms are increased by the radius of the paramagnetic agent (by default 3.5 Å), marking all the positions of the grid inaccessible to the paramagnetic probe molecules. In the next step, the sPRE value for every atom is defined by the sum over all the grid positions within an integration radius that have not been marked as occupied in the previous step:

$$sPRE_i^{model} = \sum_{r_{i,j}<d_{int}}^{N} \frac{1}{r_{i,j}^6} \times m_j, \tag{29}$$

where i refers to the index of the protein atom, j refers to the index of the grid point, N is the number of grid points, $sPRE_i^{model}$ stands for the approximated sPRE value for the ith atom of a given biomolecular structure, $r_{i,j}$ denotes the discretized distance on the grid between the ith atom and the jth grid position, d_{int} is the integration radius, and

$$m_j = \begin{cases} 0 \text{ if the } j\text{th grid point marked as occupied} \\ 1 \text{ otherwise} \end{cases}. \tag{30}$$

As the atoms of the biomolecule and the grid positions are discretized on the same grid, the $\frac{1}{r_{i,j}^6}$ value is calculated beforehand and stored in a lookup table, simplifying the required computations to grid-based operations. Calculations are accelerated as lookup tables contain all possible grid-based $\frac{1}{r_{i,j}^6}$ weighted distances and only a single calculation step is required. This fast back-calculation approach was used in ROSETTA-based *de novo* structure prediction (Fig. 2) [178]. In this work, authors implemented a novel sPRE-based scoring function in the ROSETTA protocol comparing experimental sPREs with back-calculated sPREs in accordance with a $score_{PRE} = As_{score}$ relationship, where $score_{PRE}$ denotes a score computed based on Spearman's correlation, s_{score} is a raw score, and A is a scaling factor to scale the PRE score to ROSETTA weight sets. The authors demonstrated the potential of using sPRE data for ROSETTA-based *de novo* structure prediction by performing a benchmark of classical ROSETTA (CS-ROSETTA) as well as CS-ROSETTA combined with sPRE (sPRE-CS-ROSETTA) calculations and comparing results with complementary NMR data. It was found that the implementation of sPRE data improves conformational sampling and scoring of CS-ROSETTA and provides more accurate and better converged structural models for most of the proteins tested. Surface accessibility data from sPRE provides orthogonal restraints compared to other NMR parameters, and guides structure calculations by defining solvent-exposed and buried residues, which is particularly crucial in the early folding of the peptide chain when positions and orientations of key secondary structural elements are being defined. Furthermore, the authors observed that even a restricted set of sPRE data are sufficient to improve the quality of computed structures, indicating that sPRE restraints can be beneficial for *de novo* structure prediction of larger proteins, for which complete chemical shift assignments are demanding to obtain.

The work by Harjes *et al.* on yeast IMPACT Homolog 1 (Yih1) can serve as a recent example of using sPRE experiments to characterize a protein structural model [198]. Yih1 negatively regulates Gcn2 protein (General Control Non-derepressible 2), which is involved in reducing initiation of translation during amino-acid starvation. Yih1 consists of approximately 260 residues folded into two domains – the *N*-terminal RWD domain and the C-terminal Ancient Domain – connected by a 26-residue linker. Measured

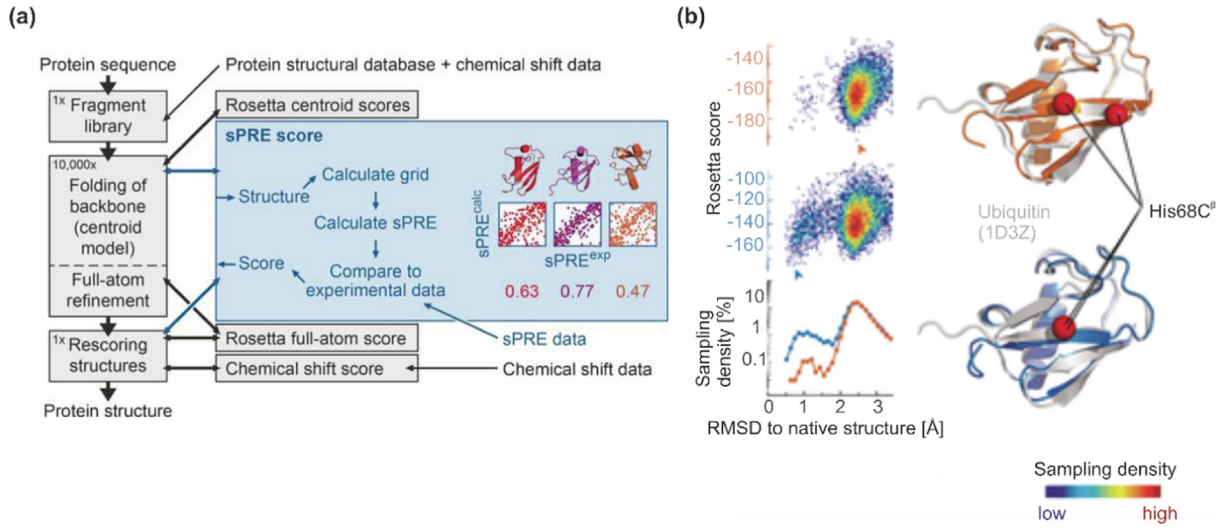

Fig. 2. *De novo* protein structure prediction with incorporation of sPRE-derived solvent accessibility information. (a) Schematic principle of sPRE-CS-Rosetta, where sPRE score is implemented as a scoring function that scores centroid and full-atom models. (b) Comparison of lowest-energy models obtained with CS-Rosetta (orange), CS-sPRE-Rosetta (blue), and NMR solution structure (grey) of ubiquitin. For both Rosetta methods, the corresponding Rosetta score is shown on the left and the distribution of the Cα-RMSD of the sampled structures is plotted below on a logarithmic scale. Adapted with permission from [178] under the Creative Commons CC BY license.

sPRE values indicated that residue Gly96 of Yih1, which is located in a loop between helices two and three of the RWD domain, can be placed within an inter-domain interface as its relaxation rates remain relatively unchanged with increasing concentration of Gd (DTPA-BMA). Additionally, the authors determined structural ensembles of full-length Yih1 by combining intra-domain NOE, SAXS and RDC data, and they observed lower than average values of calculated sPREs for residues in the putative interdomain interface. Furthermore, a comparison of sPRE rates, back-calculated using the grid-based algorithm described above [178], for the full-length protein model versus calculations for the two domains treated as independent entities identified regions with distinct solvent exposure. Further analysis revealed that sPREs calculated for full-length models parallel the measured sPREs more closely than PREs calculated for the two separate domains. Of note, Yih1 regions exhibiting the highest differences of sPRE calculated for isolated domains versus the full-length model correspond to residues forming the inter-domain interface.

4.4. Biomolecular structure validation and refinement

As sPRE measurements probe solvent accessibility, sPRE data can be used to validate structures and secondary structural features of peptides/proteins exposed to two different environments. To give an illustration of this application, sPRE data for an antimicrobial 15-residue peptide CM1534 in membrane-mimetic micelles revealed a wave-like pattern in the data originating from the α-helical region of the peptide, which facilitated a refinement of the orientation of the peptide within the micelle [168]. A similar wave-like pattern of the sPRE data was also reported for the GXXXG motifs of plasticins in the membrane milieu [161]. The presence of such an sPRE pattern is thought to be characteristic of any α-helix exposed to two environments, differing in their level of solvent accessibility, on opposing faces of the helix. Furthermore, Zhang *et al.* compared experimental solvent PRE rates to the rates back-calculated from the ensemble of NMR structures after the addition of Gd(DTPA-BMA), to validate the structure of the *N*-terminal domain of splicing factor 1 [199]. Therein, experimentally-derived sPRE rates for flexible regions were higher than back-calculated ones, whereas for structured helical regions these sPRE rates remained in agreement. In addition, a comparison of measured and back-calculated sPRE rates after the addition of Gd(DTPA-BMA) enabled an assessment of the quality of NMR structures of Sam68 Qua1 homodimer [200].

It is worth noting that although NMR spectroscopy-based methods have proven to be indispensable in probing the structure and dynamics of RNA molecules [201–203], yet still poor chemical shift dispersion, low proton density, small number of intramolecular interactions, and the necessity to collect a substantial set of restraints to define RNA torsion angles constitute technical limitations. Since sPRE uses inert probes and does not require tagging the RNA with paramagnetic probes or enriching samples with NMR-active isotopes, it has prompted researchers to elucidate how it could complement standard NMR restraints in RNA structure refinement.

In this regard, Hartlmüller *et al.* demonstrated that acquiring proton longitudinal relaxation rates of a UUCG RNA tetraloop and a GTP-bound GTP aptamer with increasing concentrations of Gd (DTPA-BMA) resulted in experimental sPRE data that provided solvent-accessibility information; these data correlated well with structural features and could be further used as orthogonal restraints in the determination of the RNA structure (Fig. 3) [175]. Moreover, Gong *et al.* showed that the use of sparse sPRE restraints can improve the accuracy and precision of refined structures of RNAs with complex topologies, as demonstrated for a pseudoknot and a four-way junction tRNA [177]. In their study, the authors used triethylenetetramine hexaacetate-trimethylamide gadolinium chelate Gd(TTHA-TMA), which contains no coordination sites for water molecules and enhances relaxation via the outer-sphere mechanism, as a paramagnetic probe [164]. More recently, LeBlanc *et al.* reported the use of sPRE measurements to gain information on solvent accessibility and aid modeling of the solution structure of hepatitis B virus 61-nucleotide-long *cis*-acting RNA regulatory signal epsilon ε [195].

In recent work, Bottaro *et al.* presented a conformational ensemble of the dynamic RNA UUCG stem-loop obtained through a combination of MD simulations with NMR experimental data (NOEs, chemical shifts, scalar couplings, RDCs, cross-correlated relaxation rates, relaxation-dispersion experiments and sPREs) [176]. When computational ensembles were compared with different sets of NMR data using available PDB structures as a reference (PDB codes: 6BY5 and 2KOC), discrepancies were noted. The MD

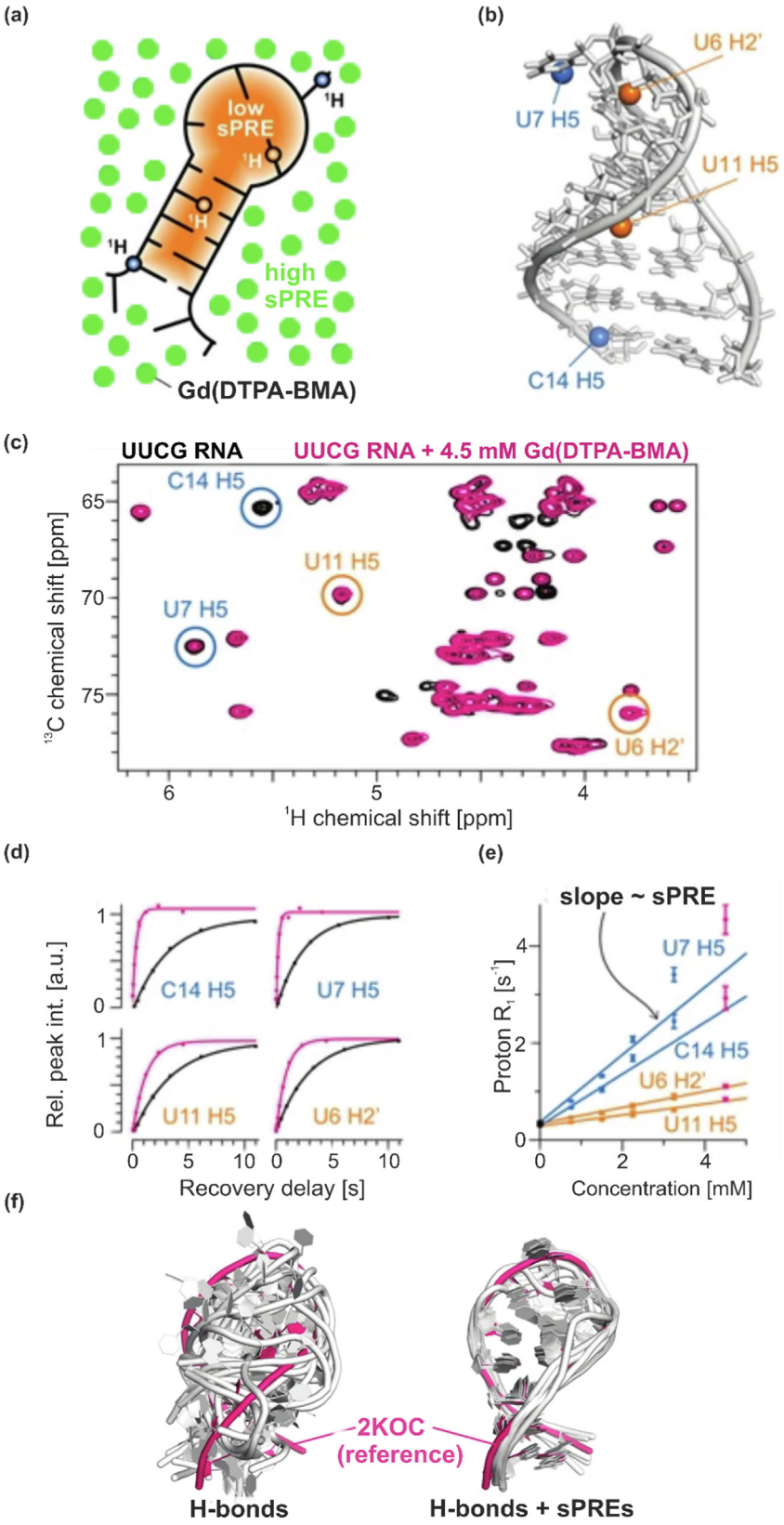

Fig 3. sPREs can be used as restraints in RNA structure determination. (a) After the titration of paramagnetic agent Gd(DTPA-BMA) to UUCG tetraloop RNA, sample sPREs can be measured and distance-to-surface information can be derived. (b) Solution NMR structure of UUCG RNA tetraloop (PDB accession code: 2KOC), with examples of solvent-exposed and -buried protons shown in blue and orange, respectively. (c) Overlay of NMR spectra of UUCG tetraloop in the absence (black) or the presence (pink) of 4.5 mM Gd (DTPA-BMA) (spectra recorded on Avance III Bruker 900 MHz NMR spectrometer), where signals from protons highlighted in Fig. 2b are indicated with orange and blue circles. (d) Measurements of proton R_1 relaxation in the presence of paramagnetic Gd(DTPA-BMA) agent deliver quantitative sPRE data on UUCG tetraloop (colour code as in Fig. 2c). (e) The longitudinal proton R_1 rates obtained increase linearly with concentration of Gd(DTPA-BMA), and the slopes correspond to the sPRE values of the respective protons. (f) Structural models of UUCG tetraloop calculated using the Xplor-NIH program with (right side) or without (left side) sPRE restraints. The figure was adapted with permission from [175] under the Creative Commons CC BY license.

ensemble was refined by using a maximum entropy refinement and including experimental datasets in simulations. Plotting a histogram of distances of refined ensembles from a consensus PDB structure revealed the presence of a previously unreported, sparsely populated second conformational state B. It is of note that in the ensemble refined with sPRE data, the population of the dominant state A was significantly reduced, to approximately 44 ± 10 %, compared to the initial ensemble. The authors employed a machine learning based random-forest classifier to assign structural features distinguishing between the two states, and state B was defined by the absence of a characteristic *trans*-sugar Watson U6–G9 interaction with the C8 and G9 bases exposed to solution. Summarizing, the approach undertaken proved to be suitable for complex biomolecular systems such as dynamic RNAs, and suggested that the incorporation of experimental NMR data (including sPREs) into MD simulations can reveal RNA motions and the presence of sparsely populated conformational states.

In another example, Xie and Frank carried out computational calculations for a dynamic S-adenosylmethionine-responsive riboswitch ensemble, during which the authors included an ensemble reweighting step using data on the solvent-accessible surface area of the C8 purine residues derived experimentally from "light-activated structural examination of RNA" experiments, a novel technique for probing nucleobase solvent accessibility inside cells [204,205]. The structural ensembles that they obtained were consistent with the previously published data, thus demonstrating that the incorporation of solvent-accessibility data (not only sPRE-derived) on RNA molecules significantly improves the quality of the structural RNA ensembles inferred.

4.5. Identification of protein-complex interfaces

sPRE data provide residue-resolved information for molecular surfaces and binding interfaces in biomolecular complexes, complementing parameters obtained from conventional NMR-based methods such as CSP analysis, hydrogen exchange, differential line broadening analysis, and dipolar interaction detecting techniques such as cross-saturation transfer or isotope-edited/filtered intermolecular NOEs [75]. The surface accessibility data obtained from sPRE analysis thus offer an alternative approach to determining binding interfaces that is helpful when the aforementioned methods cannot be applied and can be used to characterize any type of biomolecular complex over a wide range of binding affinities and time scales. By comparing differences in signal intensities in the presence and absence of a binding partner one can identify residues in the interface that are shielded from the paramagnetic agent, and this can be monitored separately for residues from each partner in the complex in separate experiments. Residues experiencing a smaller sPRE in the bound state than in the unbound state indicate the presence of a binding interface [75,88].

An early example of probing a protein–protein complex interface with this approach is in work reported by Arumugan *et al.* [158], in which the authors mapped the binding interface between a catalytic domain of human metalloproteinase 3 (MMP-3) and a tissue inhibitor of metalloproteinases 1 (TIMP-1), by comparing amide proton line-broadening after the addition of the paramagnetic $Gd(EDTA)^{-}$ complex in the presence and absence of a binding partner.

Experimental sPRE data were also used to gain insight into structural changes in human peroxisomal biogenesis factor 19 (PEX19), a key protein in transport of peroxisomal membrane proteins, in the presence and absence of post-translational farnesylation [206]. A comparison of sPRE values for farnesylated and non-modified PEX19 indicated that the C-terminal residues exhibit reduced solvent exposure after farnesylation, and the NMR analysis revealed that farnesylation enhances the binding of PEX19 to peroxisomal membrane proteins via an allosteric mechanism.

In another example study, solvent PRE analysis was used to augment modeling of the structure of the Sulfolobus solfataricus (*Sso*) minichromosome maintenance complex (MCM), a hexameric holoenzyme, comprised of an *N*-terminal domain, a catalytical AAA+ domain, and a less well-characterized C-terminal domain possessing winged helix (WH) topology [180]. The authors recorded PRE rates for the WH domain construct, including the linker and the AAA+ domain, in the absence and presence of *Sso* MCMΔWH domain upon the addition of Gd(DTPA-bis (methylamide), enabling them to map residues of the WH domain that are protected from solvent by the adjacent AAA+ domain of the MCM molecule (*i.e.* residues that showed reduced sPRE values in the presence of *Sso* MCMΔWH).

Similarly, Tomlinson *et al.* measured sPREs for FusB fusidic acid resistance protein bound to a fragment of elongation factor G lacking *N*-terminal domains (EF-GC3), constituting a drug target for FusB that it acts to protect [181]. The recorded solvent PREs were used as restraints in MD simulated annealing calculations using Xplor-NIH to determine structures of individual domains and define the orientations of domains upon complex formation.

In a study of a 150 kDa ternary nuclear export complex, Sattler and coworkers incorporated sPRE data into *in silico* docking procedures using the HADDOCK docking software (high ambiguity driven docking) to enable modeling of the structure of the complex [194]. The nuclear export complex that was studied comprised the 123 kDa nuclear export receptor CRM1, the 20 kDa guanine nucleotide-binding protein Ran in its GTP-bound state, and a peptide with the prototypic nuclear export signal of the protein kinase A inhibitor, thus constituting a paradigm to test the computational procedure outlined below. In the protocol that was developed, an ensemble of structures was first generated using the standard HADDOCK rigid-body docking algorithm. From this initial ensemble, the best subset of structural models was identified based on the standard HADDOCK score, and then refined with a semi-flexible interface region in explicit solvent. The resulting structural models were clustered based on root mean-square deviation (RMSD) criteria. In the next step, docking clusters were scored using the experimentally determined sPRE data, and the PRE score, reflecting the agreement between back-calculated sPRE data with experimental sPRE data, was calculated and added to the conventional HADDOCK score. In this manner the readjusted cluster distribution could resolve much of the docking ambiguity resulting from sparse restraint density. In the last step, a final refinement was carried out for the top-scoring structural models, using the molecular dynamics simulated annealing software ARIA/CNS [207] and employing all restraints. This rescoring procedure was repeated in an iterative way until all restraint violations were satisfied and the backbone RMSD to the previous model decreased below 1.0 Å. By using this protocol, the accuracy and precision of the final structural models were significantly improved, and the quality of the resulting models could be validated by comparing experimental and back-calculated sPREs.

4.6. Conformational dynamics

Conformational dynamics and molecular recognition are important for numerous biomolecular processes, including enzyme catalysis and allosteric regulation of cellular signaling. NMR observables and nuclear spin relaxation phenomena can directly sense conformational exchange in biomolecules and biomolecular complexes (*e.g.* transient encounter complexes, alternative binding modes, domain reorientation) [92,99,208,209]. sPRE data analysis can provide structural information on biomolecular ensembles that exist as a predominant ground-state in exchange with sparsely popu-

lated excited conformations present in solution. In fact, sPRE offers a distinct advantage compared to conventional NMR parameters (that contain both distance and conformational exchange information which can be difficult to deconvolute) as it reports on solvent accessibility, and a comparison of back-calculated to experimental sPRE profiles can indicate whether dynamics are present in the biomolecular system [60].

The use of sPRE to determine solvent exposure and conformational dynamics was already reported in the proton-relaxation analysis of gramicidin S in the early 1980s [210]. Tripsianes *et al.* used co-solute PREs to monitor ligand solvent exposure to study a weak binding process between the Tudor domain of human survival of motor neuron (SMN) protein and post-translationally dimethylated arginine [182]. By means of a simple comparison beween back-calculated and experimental sPRE data, the authors uncovered a dynamic process that was not evident from the crystal structure. This dynamic process involves a rotation of a dimethylarginine side chain in the recognition site, which, due to conformational averaging between arginine methyl groups and the recognition site, was not immediately apparent in the NOE data for the complex. Both methyl groups had the same level of sPRE and were equally inaccessible from the solvent, which can only be explained by a dynamic model. Additionally, the sPRE data back-calculated from the NMR model remained consistent with the dynamic process, unlike data back-calculated from the crystal structure.

Another example is provided by the study of Sun *et al.,* where sPRE analysis was employed to probe solvent accessibility and dynamic properties of the human DNA repair enzyme uracil DNA glycosylase (hUNG) in its *apo* and nonspecifically-DNA-bound states [159]. A comparison of back-calculated and experimental values of sPRE rates for backbone amides enabled detection of transiently populated conformational states of hUNG, as well as revealing that structural rearrangements of hUNG after DNA binding were smaller than predicted from crystal structures. Moreover, the sPRE analysis revealed that the disordered C-terminal tail of 2-deoxyribose-5-phosphate aldolase samples conformations with low solvent accessibility [211].

Hartlmüller *et al.* demonstrated that sPRE data are highly sensitive to low populations of residual structure in IDPs, as shown for α-synuclein and the *N*-terminal transactivation domain of p53 [183]. Similar results were shown by Kooshapur *et al.* [196] for urea-denatured ubiquitin; a combination of sPRE data with RDCs and SAXS-derived parameters as restraints in Xplor-NIH simulated annealing calculations significantly improved the convergence of the conformational ensemble to the final structure.

Gong *et al.* used sPRE data in conjunction with molecular dynamics simulations to visualize protein structural ensembles of two model proteins, an *N*-terminal domain of a bacterial phosphotransferase enzyme I (EIN) and *E. coli* adenylate kinase (AdK), which are known to interconvert between two conformational states at a micro-to millisecond timescale [110]. For both systems, the observed differences between experimental and back-calculated sPRE values correspond to protein regions that have already been shown to undergo micro-to millisecond dynamic movements affecting solvent accessibility. In the case of the EIN protein, the authors fitted observed sPRE values to a varying set of back-calculated sPRE profiles of each of the known conformers, in order to analyze the domain motion quantitatively. To assess dynamic interconversion of AdK, a structural ensemble was generated and snapshots from extended molecular dynamics simulations trajectories were taken to fit to the experimental sPRE data.

Based on this work, Gong *et al.* harnessed sPRE data to visualize large-scale dynamics of a ligand-free Ca^{2+}-loaded calmodulin (Ca^{2+}-CaM) [60], a protein consisting of *N*-terminal and C-terminal domains connected by a flexible linker in which the domains undergo a large twisting movement upon binding to ligand, effectively forming a switch from an open to a closed conformation. The sPRE rates obtained for the ligand-free Ca^{2+}-CaM did not agree with sPRE rates back-calculated for a published open structure of Ca^{2+}-CaM, with the linker residues showing the highest discrepancy. By using Xplor-NIH a conformer library for Ca^{2+}-CaM was created, which allowed for full torsion-angle freedom of the linker residues and relative orientation between two domains in MD simulations. This procedure yielded conformers in the closed or partially closed states, whereas simultaneously performed MD simulations started from the known open structure of Ca^{2+}-CaM resulted in sampling mostly open conformations. In the next step, the authors chose from the pre-generated library an ensemble structure comprising open and closed state conformers, and systematically varied the relative percentages of the two populations in calculations of the theoretical sPRE values. A comparison of ensemble-averaged sPRE values to the experimental data led to selection from the library of an ensemble comprising 55 % of the open state and 45 % of the closed state that showed the highest consistency with the observed sPRE values and accounted for the conformational variation within the linker region.

Notably, Merle *et al.* applied sPRE to investigate properties of a dynamic fuzzy complex between two intrinsically disordered proteins, SERF1a (a member of the Modifier of aggregation-4/Small EDRK-rich factor (MOAG-4/SERF) family) and alpha-synuclein [212]. The authors observed that alpha-synuclein in a complex with SERF1a exhibits a higher surface accessibility to the paramagnetic probe Gd(DTPA-BMA) than alpha-synuclein in the apo state. Deprotection of the alpha-synuclein surface by SERF1a, in particular the aggregation-prone domain, enhances amyloid formation of alpha-synuclein. Intriguingly, sPRE can also be utilized to probe order-to-disorder transition, as shown for bacterial acid-resistant chaperone HdeA [213]. The sPRE analysis demonstrated that HdeA exists in an inactive dimer state at pH 6 and most of its residues remain minimally perturbed in the presence of a paramagnetic probe $Gd(EDTA)^{-}$, whereas several protein regions exhibit enhanced solvent accessibility at pH values of 3 and 4.

Another key aspect to note is that co-solute PREs can also be used to investigate nonspecific transient protein–protein interactions, as reported in the study of a weak self-association of human growth hormone by Johansson *et al.*, where transverse ^{1}H sPREs induced by the addition of the uncharged paramagnetic Gd^{3+} relaxation probe gadodiamide (Gd(DTPA-BMA)) were determined [162]. The authors reported a novel approach to discriminating between residues involved in transient, nonspecific protein–protein interactions and residues involved in the formation of weak, specific protein complexes, which was possible through measuring sPRE values at varying protein concentrations and at a constant concentration of the Gd(DTPA-BMA) agent. For transient, nonspecific interactions induced by long-range electrostatic interactions between protein molecules, sPREs will increase linearly with protein concentration due to increased crowding near the protein surface and the reduced diffusion rate. In contrast, in the case of residues forming specific associations, additionally stabilized by short-range, hydrophobic interactions and hydrogen bonds, sPREs will decrease at higher protein concentrations due to an increase in the population of oligomeric states of protein and reduced accessibility of the paramagnetic agent to the binding site. For the purpose of experimental data analysis, the authors applied the Hwang-Freed model for spin relaxation by translational diffusion [87], although similar results would be expected assuming a transient, nonspecific, yet rotationally correlated complex.

Hunashal *et al.* used a previously reported approach to map residues involved in exchange processes occurring on the milli-to microsecond timescale in two model proteins, human β_2-

microglobulin and hen egg white lysozyme [214]. The authors recorded a series of NMR experiments (^{1}H 1D, 2D TOCSY, ^{15}N–^{1}H HSQC), in which they set the relaxation delay so as to generate either (A) fully, or (B) partly recovered longitudinal magnetization in the presence and absence of the paramagnetic co-solute probe TEMPOL. Their results indicate a possible use for information from paramagnetic perturbation of NMR spectra recorded far from magnetization equilibrium conditions, assuming no specific interactions occur with the paramagnetic agent. In addition, these findings were confirmed by a comparison to measured relaxation dispersion data.

In summary, sPRE measurements can be successfully applied to probe the conformational dynamics of macromolecules, and one can envision that sPRE data will in future increasingly be combined with other experiments to study transient states and map weak interactions.

4.7. sPRE measurements probe electrostatics, energetics, and dynamics of protein-co-solute interactions

Despite the fact that ionic interactions are essential for proteins and nucleic acids to carry out their functions, little is known about how ions behave around biomolecules and the phenomenon remains largely neglected in literature. The significance of these interactions, and how the type of ions in a solution of biomolecules affect their activity, has been illustrated by biochemical experiments in which the replacement of chloride with glutamate ions yields as much as a 100-fold increase in the affinity for DNA for certain DNA-binding proteins [215]. The difficulties in unravelling ion-macromolecule interactions stem from the mobile nature of ions around nucleic acids and proteins, which is reflected in the fact that many high-resolution crystal structures of biomolecules contain unresolved electron densities for monovalent cations and anions.

The term "ion atmosphere" can be used to describe a zone around the macromolecular surface where the density of mobile ions is higher than the background due to electrostatic interactions between ions and the macromolecule [216–219]. It has been realized that in the case of nucleic acids, cations acting as counterions will accumulate in the ion atmosphere and anions acting as co-ions will be excluded from the ion atmosphere. Due to the presence of a negative charge at every residue in nucleic acids, these macromolecules can be treated as linear polyelectrolytes and their interactions with ions predicted using counterion condensation theory [220–222]. In contrast, proteins possess a significantly smaller net charge than nucleic acids, and the charge distribution on the protein molecular surface is uneven and protein-specific. Hence, to predict a spatial distribution of ions around a protein at particular ionic strength one can use Poisson-Boltzmann theory, provided that a three-dimensional structure is available [223]. Currently, protein-*co*-solute interactions are experimentally studied using (bio)physical methods such as anomalous SAXS, atomic emission spectroscopy coupled to mass spectrometry, and NMR spectroscopy [216,224].

As evidenced in recent work by Yu *et al.* [115], sPRE measurements can be harnessed to visualize the spatial distribution of anions around proteins. Through NMR-based quantification and diffusion experiments, these authors demonstrated that the number of accumulated anions around positively charged proteins is smaller than the overall charge valence of the protein. Next, they measured Γ_2 sPREs of ubiquitin (overall charge: 0e), the Antp homeodomain (+12e), and the Antp homeodomain-DNA complex (-16e) in the presence of the aminoxyl radicals carboxy-PROXYL or carbamoyl-PROXYL. The authors noticed that the differences $\Delta\Gamma_2$ between the Γ_2 rates for the carboxy-PROXYL and carbamoyl-PROXYL samples at a given sPRE concentration were relatively small for ubiquitin ($\Delta\Gamma_2 < 20$ s^{-1}), while large positive $\Delta\Gamma_2$ values were noted for many residues in positively charged regions of the Antp homeodomain, implying the accumulation of anions around the protein surface. In contrast, negative $\Delta\Gamma_2$ values were reported for the majority of residues of the Antp homeodomain-DNA complex. As Γ_2 rates for the carbamoyl-PROXYL sample were higher than those for the carboxy-PROXYL sample, indicating the exclusion of carboxy-PROXYL from the surface of the Antp homeodomain upon the formation of the protein-DNA complex (negatively charged DNA has an impact on the surface electrostatic potential of the Antp homeodomain) (Fig. 4). Protein-ion interactions are considerably weaker and more transient than typical protein–ligand interactions, yet the sPRE approach can provide information about the spatial distributions and dynamic properties of counterions around biomolecules at an atomic level.

Another example highlighting the applicability of sPRE to probing the electrostatic repulsion between a paramagnetic probe and a dynamic protein is shown in the study by Dass *et al.*[225]. In this work, the authors demonstrated that addition of negatively charged gadoteric acid to a solution of alpha-synuclein induced line broadening of the resonances of the negatively charged C-terminal protein region, but much less compared to the addition of the neutral species gadoteridol (the two probes are physicochemically equivalent, except for their net charge). The depletion of anions around the acidic tail was faithfully reflected in the depression of OH^--catalysed hydrogen exchange rates.

Even more recently, Yu *et al.* reported how the ratio of Γ_2 rates arising from cationic and anionic probes added at the same concentration can be utilized for *de novo* determination of near-surface electrostatic potentials, even in the absence of a three-dimensional structure. For this they compared sPRE due to amino-methyl-PROXYL and carboxy-PROXYL probes (*i.e.* two PROXYL derivates differing only in a charge at neutral pH with amino-methyl-PROXYL bearing a positive (+1e) and carboxy-PROXYL a negative (−1e) charge) [116]. Experimentally derived electrostatic potentials for backbone H_N atoms were in accord with potentials derived from Poisson–Boltzmann theory, as demonstrated for secondary structural elements of ubiquitin and the highly charged biosystem of the Antp homeodomain: DNA complex. Nonetheless, discrepancies between experimental and theoretical electrostatic potentials were noticeable for residues in conformationally flexible loop regions of ubiquitin and the Antp homeodomain: DNA complex. These can plausibly be explained by limitations of the theoretical approach such as a lack of ion correlation around the protein and the fact that currently available models can fail to capture structural differences and dynamics of biomolecules [116,141]. The authors also investigated the impact of higher ionic strength on electrostatic potentials, and observed smaller magnitudes of PREs in the sample containing 130 mM salt concentration compared to the one with 30 mM salt, indicating weaker electrostatic interactions between the protein and the charged co-solutes at the higher ionic strength. Nevertheless, the sPRE-derived electrostatic potential remained in reasonable agreement with the Poisson–Boltzmann theory-based predictions under higher ionic strength conditions.

Moreover, Toyama *et al.* developed a pseudo-4D NMR experiment based on the haCONHA pulse sequence scheme recording ($^{13}CO_i$,$^{15}N_{i+1}$,$^1H_i^{\alpha}$) correlations for collecting backbone $^1H^{\alpha}$ transverse relaxation rates in IDPs, thus enabling the acquisition of a high-quality NMR spectra for IDPs even at neutral pH values (where solvent exchange leads to amide spectra of a poor quality) [226]. The study laid the foundation for the determination of the surface electrostatic potential of RNA-binding protein CAPRIN1 in both phase-separated (incl. the "condensed" phase of high protein concentration) and single-phase states at the residue-specific level [227].

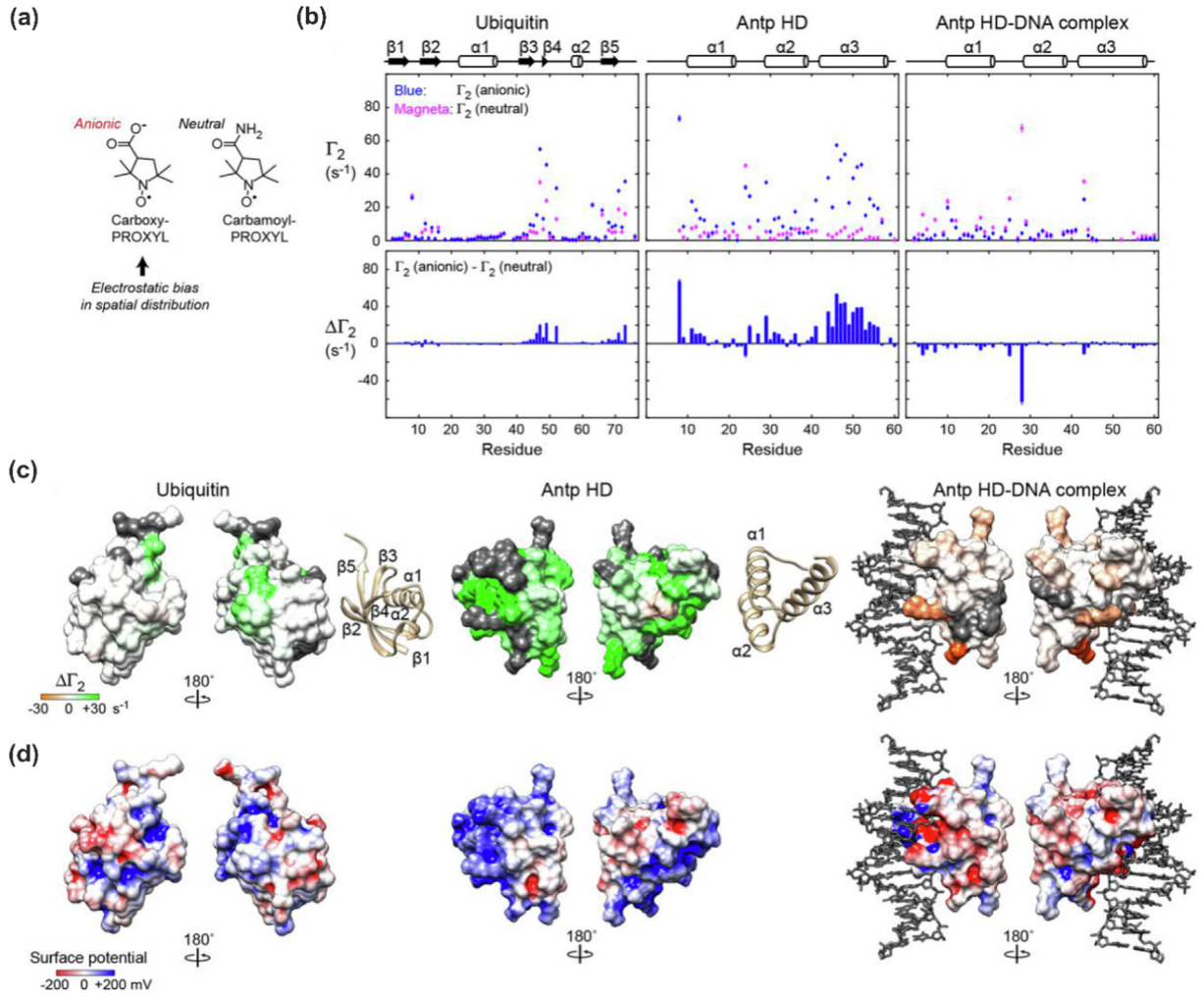

Fig. 4. sPRE data provide information on the spatial distributions of anions around protein surfaces. (a) Structures of negatively charged carboxy-PROXYL and neutral carbamoyl-PROXYL paramagnetic probes. (b) On the upper panel are illustrated protein backbone $^{1}H_N$ transverse sPRE rates Γ_2 collected for ubiquitin (left panel), Antp homeodomain (middle panel) and the Antp homeodomain-DNA complex (right panel) arising after the addition of 10 mM of either carboxy-PROXYL (blue) or carbamoyl-PROXYL (magenta). On the bottom panel are displayed calculated differences ($\Delta\Gamma_2$) between the PRE Γ_2 rates for anionic and neutral paramagnetic co-solutes. (c) $\Delta\Gamma_2$ values mapped on the protein surfaces for ubiquitin, the Antp homeodomain, and the Antp homeodomain–DNA complex, coloured in a gradient from orange to green to indicate negative and positive $\Delta\Gamma_2$ magnitudes, respectively. (d) Surface electrostatic potentials for ubiquitin, the Antp homeodomain, and the Antp homeodomain–DNA complex (structures and orientation as in Fig. 4c). Reprinted with permission from [115] under License 4.0 (CC BY-NC-ND).

Despite the fact that interactions between proteins and co-solutes modulate protein stability, dynamics, and function, the molecular mechanisms governing these interactions remain largely unresolved, mostly due to their extremely weak (binding affinity in excess of 1 M), nonspecific and transient character [114,228]. Conventional spectroscopic techniques, including NMR, often cannot detect these weak interactions due to the intrinsic complexity and dynamics of biomolecular three-dimensional structures. Okuno *et al.* developed a novel approach to obtaining quantitative information about the energetics and dynamics of protein-*co*-solute interactions from sPRE measurements [171]. They introduced an approximate non-Lorentzian spectral density function, which was used to fit experimental spectral densities calculated from measured Γ_1 and Γ_2 sPRE rates at multiple magnetic fields, given by:

$$J_{approx}(\omega) = \frac{J(0)}{\left(1+a\omega+b\sqrt{\omega}\right)^2}, \tag{31}$$

where a is a site-specific fitted parameter varying between atoms in the protein, and b can be obtained according to the following formula:

$$b = \frac{\sqrt{2}\pi n_s}{9D_{trans}^{3/2}J(0)}, \tag{32}$$

in which n_S stands for the number density (*i.e.* a number of co-solute spins per unit volume or concentration) of the paramagnetic co-solute, D_{trans} denotes the relative translational diffusion constant for the interacting molecules, and the field-independent value of $J(0)$ can be calculated using the equation:

$$J(0) = \frac{5\left(\Gamma_2(\omega_H) - \frac{\Gamma_1(\omega_H)}{2}\right)}{\left(\frac{\mu_0}{4\pi}\right)^2\hbar^2\gamma_H^2\gamma_e^2}. \tag{33}$$

Here, μ_0 is the magnetic permeability of vacuum, γ_H and γ_e are the gyromagnetic ratios of the proton spin of interest on the protein and the electron spin of co-solute, respectively, and ω_H denotes the Larmor proton frequency at a given spectrometer field. Experimental Γ_1 and Γ_2 rates are related to spectral density as follows:

$$\Gamma_1(\omega_H) = \frac{3}{10}\left(\frac{\mu_0}{4\pi}\right)^2\hbar^2\gamma_H^2\gamma_e^2 J(\omega_H), \tag{34}$$

$$\Gamma_2(\omega_H) = \frac{1}{5}\left(\frac{\mu_0}{4\pi}\right)^2\hbar^2\gamma_H^2\gamma_e^2\left(J(0) + \frac{3}{4}J(\omega_H)\right). \tag{35}$$

In Eq. (32) D_{trans} can be derived either experimentally from pulsed field gradient diffusion measurements, or from fitting sPRE data recorded at multiple spectrometer fields as a global parameter. Furthermore, the authors introduced a new parameter, the co-solute concentration-normalized equilibrium average of protein-*co*-solute interspin distance $\langle r^{-6}\rangle_{norm}$, that reports on the strength of interactions between the unpaired electron on the co-solute and the proton of interest on the investigated biomolecule, the values of which are independent of dynamics [171]; recall that in the case of a fluctuating interspin distance, the distance is incorporated into the definition of the correlation function, and hence into the spectral density functions, as for instance in Eq. (13) (see ref. [171] for further details).

$$\langle r^{-6}\rangle_{\text{norm}} = \frac{2}{n_S \pi}\int_0^\infty J(\omega)d\omega, \tag{36}$$

where $J(\omega)$ can only be determined at a small number of frequencies due to the limited sampling of the spectral density by relaxation at available NMR spectrometer fields.

Site-specific electrostatic and hydrophobic interactions and excluded volume interactions between the protein and co-solute govern $\langle r^{-6}\rangle_{norm}$. A comparison of $\langle r^{-6}\rangle_{norm}$ with $\langle r^{-6}\rangle_{norm}^{exc}$ (defined for systems with no intermolecular interactions except the excluded volume; this can be directly computed from atomic coordinates) might be used to determine the attractive ($\langle r^{-6}\rangle_{norm} > \langle r^{-6}\rangle_{norm}^{exc}$) or repulsive ($\langle r^{-6}\rangle_{norm} < \langle r^{-6}\rangle_{norm}^{exc}$) character of the interaction between co-solute and the protein at the residue level.

An effective residue-dependent correlation time τ_c, reporting on the timescale of fluctuations of the inter-spin vector $\vec{r}$, that stems from translational and rotational diffusion and is affected by both short- and long-range intermolecular interactions, is defined as follows:

$$\tau_c = \frac{J(0)}{n_S\langle r^{-6}\rangle_{\text{norm}}}. \tag{37}$$

Hence, through deriving values of $\langle r^{-6}\rangle_{norm}$ and τ_c this approach permits characterization of the energetics and dynamics of co-solute-protein interactions at residue-specific level. In their study, the authors investigated the interaction between ^{2}H-^{15}N labeled ubiquitin and aminoxyl radicals, 3-carboxy-PROXYL and 3-carbamoyl-PROXYL. The sPRE data analysis showed the presence of two preferential interaction sites, clustered within hydrophobic areas and involving residues located in flexible regions [171]. A caveat may be that aminoxyl radicals are known to preferentially interact with charged amino acids in proteins, biasing the quantitative interpretation [140].

The same procedure was more recently applied to unravelling interactions between paramagnetic co-solutes, 3-carboxy-PROXYL and 3-carbamoyl-PROXYL, and the drkN SH3 protein domain, a protein that exists in a dynamic equilibrium between native and unfolded states that are in the slow exchange limit on the chemical shift timescale [114]. By comparing $\langle r^{-6}\rangle_{norm}$ and ($\langle r^{-6}\rangle_{norm}$- $\langle r^{-6}\rangle_{norm}^{exc}$) profiles for backbone amides and a side-chain $N_{\varepsilon 1}H$ indole proton of Trp36, the authors showed that there was preferential binding of both co-solutes to the unfolded state of drkN SH3 relative to the native state, which can be explained by the higher solvent accessibility of backbone amides and solvent-exposed side-chains in the unfolded state. In addition, for the native state at 298 K, the value determined for τ_c was longer for 3-carboxyl-PROXYL than for 3-carbamoyl-PROXYL, whereas for the unfolded state the opposite was seen. At 277 K, the positive correlation between τ_c for 3-carboxyl-PROXYL and for 3-carbamoyl-PROXYL implies similar residence times of both co-solutes in the proximity of the corresponding backbone amides for both protein states. Correlation plots of calculated $\langle r^{-6}\rangle_{norm}$ values at 298 and 277 K for both probes exhibited a slope of approximately 1 for the native state and values greater than 1 for the unfolded state with $\langle r^{-6}\rangle_{norm}$ higher at 298 K, which was explained by the existence of stronger protein-*co*-solute interactions, possessing unfavourable enthalpic contributions in the unfolded state.

Taken together, these examples emphasize the use of sPRE analysis in probing weak, transient interactions between proteins and ions/co-solutes, which are otherwise inaccessible.

4.8. Structure determination of proteins in biological membrane mimetics

Despite the fact that membranes and membrane-associated biomolecules increasingly constitute drug targets, mechanistic details regarding membrane-biomolecule interactions and transmembrane signaling events often remain elusive [229]. Therefore, defining the structure and localization (orientation/immersion depth) of the biomolecule on or within the membrane is essential for understanding the mode of action of these biomolecules and for an ensuing drug design process. Due to the upper size limit of solution NMR spectroscopy, the number of suitable membrane-mimetic systems is limited, and membrane-mimetic environments such as micelles, bicelles and small unilamellar vesicles are most often employed in solution NMR experiments [161,230–233]. Because lipids have high proton densities they need to be deuterated for NMR studies; consequently the systems most often applied are those commercially available in deuterated form, such as sodium dodecylsulfate (SDS), dodecylphosphocholine (DPC) and dimyristoylphosphatodylcholine (DMPC) [59,229–231]. Paramagnetically-labeled lipids, such as 5-, 12- or 16-doxylstearic acid (5-DSA; 12-DSA; 16-DSA), have also been designed and used in the studies of protein and peptide insertions into the membrane [229,234–236]. However, the use of co-solute paramagnetic agents for detection of sPRE proved to be a more flexible, efficient, and cost-effective tool for monitoring of insertion of proteins and peptides in micellar environments.

Small paramagnetic probes, such as oxygen, can diffuse across a membrane and create a paramagnetic gradient inside a membrane-mimetic environment, allowing probing of the orientation and the depth of insertion of peptides or proteins with respect to the surface of a micelle [119]. Small metal ion probes, such as Mn^{2+} or Ni^{2+}, could in principle also be used to probe the localization of proteins/peptides inside membranes, but their disadvantage is the formation of interactions with polar groups of amino acids or the micelle [229,237]. Large sPRE probes can be used to monitor the solvent exposure of the membrane proteins or amphipathic peptides.

As an example of a paramagnetic probe that is inert in aqueous solution, Gd(DTPA-BMA) was shown by NMR and EPR spectroscopy studies to possess no binding specificity for micelles or peptides [69,238], and can be used at lower concentrations than aminoxyl radicals because it exerts larger paramagnetic effects. Furthermore, solvent exposure and immersion depth information can be obtained by taking measurements on addition of the paramagnetic agent to a solution surrounding the micelle, rather than by introducing the paramagnetic probe into the micelle itself [239,240]. In this scenario, spins located in the proximity of the micelle surface experience a higher sPRE, than those in the core of the micelle. A formula for the total relaxation enhancement can be obtained by integration over the whole volume containing the paramagnetic agent, weighted by r^{-6} and multiplied by the probability of finding a paramagnetic centre in a particular volume element, for a nucleus immersed under the solvent-exposed surface, such as in a micelle:

$$PRE = \frac{k\pi}{6(d+l)^3}, \quad (38)$$

where d denotes the distance to the closest point on the surface, l accounts for the solvent layer and radius of the paramagnetic probe, and k is a constant combining terms from equations (5) or (6) with the probe concentration. For a planar surface, and to a good approximation for large spherical systems such as micelles, this integrated PRE depends on d^{-3}, where d denotes the immersion depth. This relation was described in the study by Respondek *et al.* [168], in which the authors added the paramagnetic probe Gd(DTPA-BMA) to a solution containing a 15-residue CM antimicrobial peptide (CM-15) and the *trans*-membrane helix TM7 of yeast V-ATPase in membrane mimetics. They observed that the sPRE values depended on the distance to the surface of the micelle, and the tilt and azimuthal angles of the peptide were determined from a least-squares fitting of experimental sPREs to a wave-like function with a 3.6 residue periodicity corresponding to the helical portions of the peptides (Fig. 5). The sPREs obtained could be further converted to distance restraints to determine the localization and orientation within the membrane by using equation (38) and used for calculations of the structure of a peptide bound to the membrane.

Several subsequent studies investigated the immersion of peptides/proteins in biological membrane mimetics. Li *et al.* performed solvent PRE experiments on a construct comprising a transmembrane domain and a juxtamembrane region of erythropoietin receptor in the presence and absence of $Gd(DTPA)^{2-}$ [184]. The

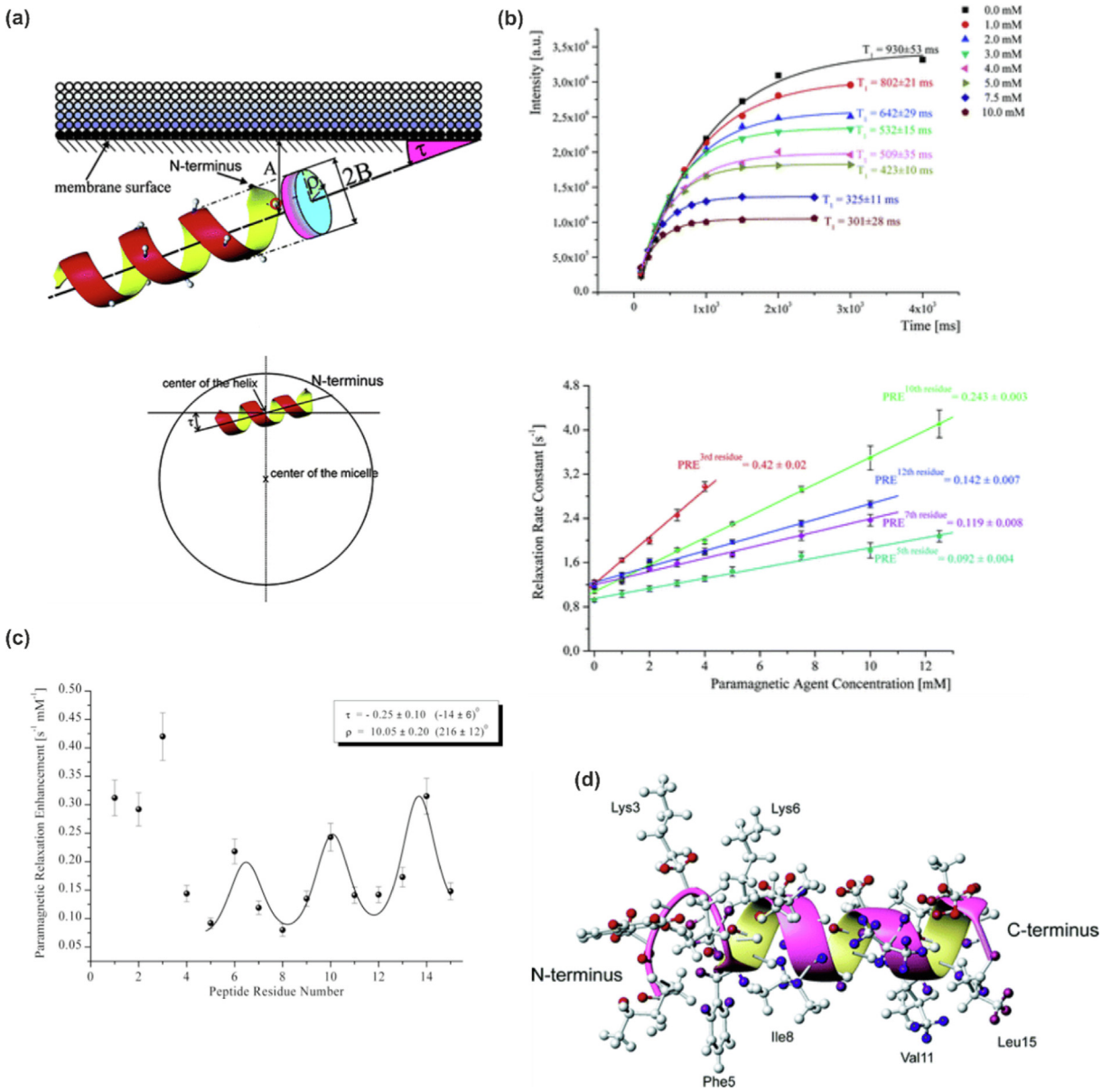

Fig. 5. sPRE-derived data report on the structure and arrangement of helical peptides within biological membranes. (a) A definition of parameters required for the description of PRE rates on helical peptides in membranes (upper panel) and for the definition of the tilt angle in micellar systems (bottom panel). A tilt angle τ is measured between the membrane surface and the helical axis. The azimuthal angle ρ is found between the first α-proton and a line perpendicular to the helix axis and pointing towards the membrane surface. (b) Signal saturation recovery (upper panel) and sPRE rates (lower panel) of Ala10-Hα of CM-15 plotted as a function of Gd(DTPA-BMA) concentration. (c) sPRE values of Hα nuclei of CM-15 plotted as a function of amino acids number. Least squares fitting was used to account for the sinusoidal character between residues 5 and 15, and the tilt and azimuthal angles obtained are shown in the inset. (d) Calculated structural model of CM-15 peptide coloured according to sPREs values ranging from blue (low values) to red (high PREs). Protons for which sPREs could not be obtained unambiguously are indicated as white. Some exposed residues are annotated. Adapted with permission from [168]. Copyright 2007 American Chemical Society.

data collected demonstrated that the C-terminal juxtamembrane region is accessible to the solvent, whereas the *N*-terminal part of the construct is protected from the paramagnetic agent and can interact with micelles.

Hohlweg *et al.* showed that Arg735 in vacuolar ATPase forms a cation-π interaction with Trp733 and Trp737, and used sPRE to estimate an immersion depth of Arg735 in DPC micelles using the addition of Gd(DTPA-BMA) [185]. The sPRE value for a double mutant lacking the aromatic residues (Y733A/W737L) was higher (Arg735 Hδ sPRE, 0.42 ± 0.02 $s^{-1}mM^{-1}$) than that determined for a wild-type peptide (Arg735 Hδ sPRE, 0.32 ± 0.02 $s^{-1}mM^{-1}$), indicating shallower membrane immersion and lack of additional shielding by the aromatic groups in the mutant. The authors deduced that the sPRE value of wild-type protein corresponded to an immersion depth of approximately 12 Å from the micelle surface, while the sPRE value determined for the mutant implied an immersion depth of approximately 10 Å from the surface.

Lee *et al.* measured sPRE values for the GTPase (guanosine triphosphatase) KRAS in the absence and presence of Gd(DTPA-BMA) in order to decipher changes in KRAS solvent accessibility upon membrane-dependent dimerization [186]. For their study the authors prepared two KRAS samples. In one, ^{13}C-^{15}N-labeled KRAS was irreversibly attached to the lipid bilayer of a nanodisc through maleimide conjugation (MC-KRAS), while the other comprised isotopically unlabeled, fully processed KRAS with C-terminal farnesylation and carboxy-methylation (FP-KRAS). After addition of an equimolar amount of FP-KRAS to MC-KRAS, reduced sPRE values were observed for ^{13}C-labeled methyl groups in ILV (Ile, Leu, Val) in the α4–α5 dimer interface and the α3-loop region of MC-KRAS, both in the presence of the non-cleavable GTPγS substrate analogue and inactive GDP-bound states, indicating that these regions are solvent inaccessible upon KRAS dimerization on the membrane. Furthermore, the authors observed that sPRE values for the β-sheet effector-binding site were increased after dimerization in the GTPγS-bound state, but the values were decreased in the inactive form, suggesting that dimerization of GTPγS-bound KRAS promotes solvent exposure of this region.

In work by Soubias *et al.*, methyl sPRE rates of a pleckstrin homology (PH) domain of the Arf GTPase–activating protein (Arf-GAP) ASAP1 in free and nanodisc-bound states were measured in the presence of a paramagnetic probe Gadavist (Gd^{3+}) [241]. Analysis of sPRE rates revealed that the methyl groups of residues I353, V356, and A374 - located in a β1/β2 loop - exhibited reduced normalized relaxation rates, and hence were solvent protected, in the nanodisc-bound state.

As exemplified by a recent study of Bai *et al.*, one can also observe solvent PRE effects using ^{19}F NMR experiments [242]. In this work, authors recorded sPRE spectra of ^{19}F-labeled cytochrome b5 reconstituted in lipid nanodiscs after the addition of Gd(DTPA-BMA), in which an observed reduction in signal intensity for W27 led to the conclusion that this residue remains accessible to the solution whereas other tryptophan residues that were unaffected are buried within the lipid bilayer. Additionally, sPRE data can be combined with PREs obtained from membrane-embedded paramagnetic tags to determine the orientation of biomolecules with respect to a micelle [186,234,241,243]. Furthermore, sPRE data can be used to assist molecular modeling in defining the orientation of peptides in the membrane [230].

5. Miscellaneous topics

5.1. Intrinsically disordered proteins and regions

Over the last two decades, intrinsically disordered regions (IDRs) and intrinsically disordered proteins (IDPs) have been recognized to occur very widely and to play significant functional roles in cellular processes such as signal transduction, cell-cycle control, molecular recognition, transcription and translation regulation [244–246], thus challenging the conventional protein structure–function paradigm [247,248]. According to bioinformatic analyses, approximately 15–45 percent of eukaryotic proteins contain disordered regions comprising at least 30 residues [249–251]. It has been shown that these regions are characterized by distinct amino acid compositions that are rich in polar and charged residues and depleted in bulky and hydrophobic residues, which often results in a high net charge and a low mean hydrophobicity for these sequences [252–254]. Amino acid sequence signatures of IDRs and IDPs are generally associated with populations of distinct near-isoenergetic multiple conformations as a result of their much flatter free-energy landscapes compared to those of globular proteins [255]. These highly flexible proteins exist as an ensemble of interconverting states [254,256,257]. Protein structural disorder serves crucial biological roles; these regions are frequently involved in the formation of protein complexes, in which they can either lose their conformational heterogeneity during binding-induced folding, or alternatively can retain it by forming so-called "fuzzy" complexes [245,258,259]. The inherent dynamics of IDPs often allow them to act as hubs in signaling networks [244,260]. Significantly, misregulation of the function of several IDPs has been linked to protein aggregation, and consequently to the onset and progression of neurodegenerative diseases, cancer, and diabetes [261,262]. Mounting evidence indicates that weak multivalent interactions between IDRs can mediate the process of liquid–liquid phase separation (LLPS), in which a biomolecule (protein, protein/nucleic acid complex) condenses into a dense phase and a surrounding dilute phase, coexisting in dynamic equilibrium [263–265]. Protein phase separation is an emerging important concept in cellular signaling, underlies the formation of membraneless organelles, and can be regulated by binding of ligands and chaperones or by post-translational modifications (PTMs) [266].

Due to their structural heterogeneity, IDPs are usually not amenable to structural characterization by means of X-ray crystallography or cryo-electron microscopy, except for IDP complexes in which folding-upon-binding occurs or where protein disorder is limited to a small confined peptide region [245,267]. In addition to this, conformational analysis of IDPs and IDRs is complicated by their higher average solvent accessibility compared to folded proteins and their higher sensitivity to solvent characteristics. Therefore, use of complementary biophysical techniques such as NMR spectroscopy, SAXS/SANS, smFRET, mass spectrometry and computational molecular simulations has emerged as the current state of the art in the integrative determination of structural and dynamic properties of IDPs in isolated, complex, and phase separated states [38,245,268–271]. The rugged free energy surface for IDPs and their extensive dynamics on time scales, ranging from milliseconds to microseconds, substantially increases the computational costs of conformational sampling during all-atom explicit solvent simulations [272–274]. To address this challenge, all-atom implicit solvent simulations [275], coarse-grained models [276], and enhanced-sampling techniques [277] are increasingly being applied to study IDPs, IDRs, their complexes, and LLPS [278–283]. In this regard, the incorporation of sPRE-derived surface accessibility information on IDPs and their complexes into modeling could, for instance, be used to further increase the accuracy of prediction of (un)structure and dynamics of such biomolecular systems, or, as shown by Okuno *et al.*, to calculate the ensemble of structures that reflect the preferential interactions between proteins and co-solutes [114].

In spite of the higher sensitivity of NMR experiments with IDPs, which results from their favourable relaxation properties deter-

mined by fast internal motions, IDPs have posed a challenge to characterization by NMR spectroscopy due to their low chemical shift dispersion for proton resonances, and to chemical exchange with bulk water decreasing the intensities of $^{1}H^{N}$ signals [245,268,284]. Recent improvements in NMR technology and methodology have largely overcome this challenge and enhanced the spectral resolution for IDPs that is now accessible. These improvements include higher-field NMR spectrometers, the development of ^{13}C- and ^{15}N-direct detection experiments combined with cryoprobe technology [25,285–288], the introduction of non-uniform sampling technologies [289–291], the exploitation of relaxation-optimized pulse schemes [292,293], and the use of uniform- and selective-labeling schemes and isotope-edited pulse sequences [291,294,295].

NMR observables such as chemical shifts, scalar couplings, nuclear spin relaxation, RDCs, PREs, NMR exchange rates, and NOESY cross-peak intensities are frequently used in combination to study structural and dynamic properties of IDPs, IDRs and their complexes [257,296–298]. Interestingly, the progress of in-cell NMR technology now enables the probing of alterations in structure and dynamics of IDPs and IDRs after ligand binding or post-translational modifications in living cells [296,299,300]. As mentioned earlier, sPRE methodology has already been employed to i) accelerate NMR data collection for IDP and IDR samples, enabling the acquisition of multidimensional experiments within a few hours [148]; ii) probe residual structure and long-range interactions in IDPs and IDRs [183]; iii) determine conformational ensembles of IDPs and IDRs at an atomic resolution when combined with restraints obtained from complementary methods [196]; iv) detect surface accessibility changes upon ligand binding in fuzzy complexes [212]; and v) follow protein unfolding [213].

In a further advance, Yu *et al.* and Dass *et al.* demonstrated that paramagnetic probes bearing a charge are valuable in investigating the electrostatic interactions between disordered proteins and surrounding ions [115,225], hence sPRE methodology can be employed to explore protein phase separation, as such interactions drive the formation of liquid droplets. In this regard, we can also envision the use of sPRE to dissect which residues are involved in the formation of liquid droplets, as well as their accessibility and dynamics. As outlined in Section 4.4, the inclusion of solvent accessibility data greatly improves refinement of RNA structures, hence sPRE methodology shows promise for exploring structural details of RNA molecules within biomolecular condensates. Recently, sPRE methodology has been employed to determine changes in the surface electrostatic potential of CAPRIN1 along the trajectory of its ATP-induced phase separation [227].

All things considered, various NMR techniques, including the use of sPRE effects, have greatly facilitated studies of IDPs and IDRs and promise to continue to accelerate the progress of this research field in the future (Fig. 6).

5.2. NMR-based metabolomics

Metabolomics is a rapidly-expanding technology-driven discipline with a strong focus on the detection and quantification of small molecules (metabolites) in biological samples [301]. Metabolomics experiments can provide insights into human health through measuring changes in the concentration of metabolites. Altered metabolite levels are often associated with disease, and NMR spectroscopy has proven to be a valuable tool in metabolomics and biomarker research [302–304]. Notably, Mulder *et al.* reported that in the case of metabolomic samples containing a mixture of small molecules, the addition of a commercially available contrast agent at a low concentration (~0.5 mM) increases the R_1 relaxation rate and enables fast and quantitative NMR analysis [172]. The authors demonstrated that for established standard operating procedures (SOPs), NMR signal intensities were incorrect for many metabolites in a diamagnetic, synthetic mixture of metabolites common for human urine, as reduction in the magnetization recovery time caused a decrease in signal intensity for a number of metabolites. Addition of Gd^{3+} chelates at a low concentration to the sample enabled a significant reduction in experiment time, as well as decreasing the range of relaxation times for different metabolites while simultaneously providing full restoration of relaxation data. Importantly, the co-solute paramagnetic agents employed in the study (*i.e.* gadoteri-

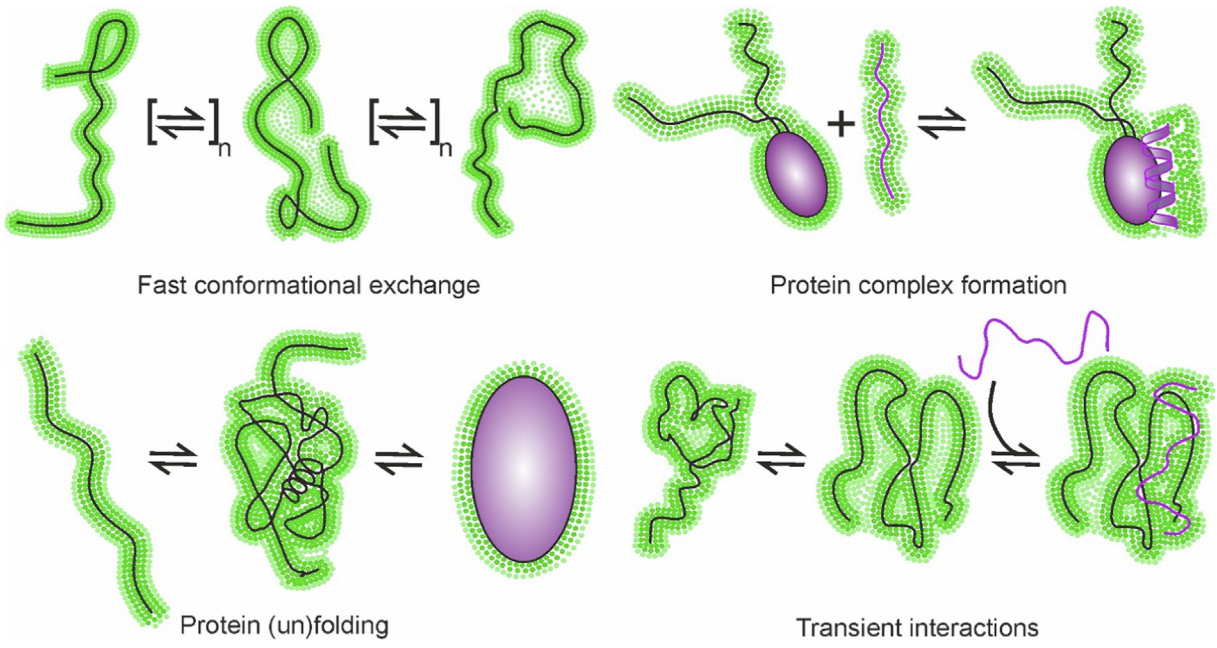

Fig. 6. Applications of sPRE methods for investigating structural and dynamic properties of intrinsically disordered proteins and protein regions. Changes in solvent accessibility derived from sPRE data report on the formation of protein complexes, the presence of transient inter- and intramolecular interactions, and rearrangements of secondary and tertiary structural elements, and probe conformational dynamics. All of these aspects are important in the study of dynamic IDPs and IDRs.

dol and gadobutrol) appear to have no specific interactions with metabolites.

More recently, Honrao *et al.* reported that a combination of non-uniform sampling and the addition of gadolinium to standard human plasma resulted in a further increase of mean NMR peak intensities (1.12-fold for standard human plasma and 1.25-fold for a model mixture) and improved the detection of low-abundance metabolites [173].

5.3. Drug discovery

NMR spectroscopy is a gold standard method for investigating interactions of ligands with biomolecules; its advantages include the fact that molecules are studied in solution and are free of labels, enabling the screening of mixtures of multiple compounds to identify directly those compounds that interact. These factors have made NMR one of the main biophysical methods of choice in drug discovery [305–307]. Usually, NMR experiments such as measurements of CSPs, relaxation rates, exchange rates of backbone amide hydrogens, translational diffusion, paramagnetic data, or using NOE-based approaches are applied to report on the interaction of a drug with a biomolecule of interest, including its affinity, binding kinetics, changes in molecular structure upon binding, or its translational and rotational diffusion [58,308,309]. However, sPRE data can also provide information about alterations in surface accessibility in a biomolecule upon ligand binding, and thereby also assist in the identification and validation of interactions between biomolecules and drugs. For instance, Clark *et al.* employed sPRE analysis to investigate solvent accessibility and conformational dynamics of the adenosine receptor A_2AR reconstituted in a micellar environment in its inverse-agonist bound state [310].

As a particular example of the use of sPRE measurements in NMR-based drug design, we describe below the work of Spitz *et al.* in more detail [311]. These authors investigated interactions between the pro-apoptotic BCL-2 protein BAX and the small-molecule drug, Eltrombopag. BCL-2 family proteins are crucial regulators of apoptotic cell death, where apoptogenic factors are released into the cytosol during a process of mitochondrial outer membrane permeabilization. In healthy cells, pro-apoptotic BAX and BAK proteins exist as inactive monomers, autoinhibited homodimers, or are bound to anti-apoptotic BCL-2 family members. Binding of a pro-apoptotic BH3-only protein to the *N*-terminal trigger site of BAX via its BH3-domain helix induces conformational changes of BAX, which in turn translocates from the cytosol to the mitochondrial outer membrane. Once inserted, BAX forms homo-oligomeric pores permeabilizing the outer membrane of mitochondria.

The authors identified Eltrombopag as a promising BAX modulator by searching and testing a library of FDA-approved small molecules. They showed that Eltrombopag binds to BAX with a binding affinity of 143 nM, and demonstrated that the activation of BAX is inhibited by Eltrombopag at an early stage by blocking binding of the BH3-only activator and stabilizing BAX in a soluble inactive form. CSP analysis of BAX in the presence of Eltrombopag showed that changes localize to the *N*-terminal BAX trigger site as well as to residues in helices α4, α7 (proximal to trigger site) and in the C-terminal helix α9. In addition, molecular docking and NMR analysis revealed that Eltrombopag forms contacts with a shallow hydrophobic pocket between helices α1and α6 of BAX, as well as forming a crucial ionic interaction with R145 and a secondary hydrogen bond with R134 of BAX. Molecular dynamics simulations and root-mean-square fluctuation (RMSF) analysis uncovered increased heterogeneity of the α4–α5 loop and helix α7, and decreased fluctuation of the α3–α4 loop and helix α9 (considered to form the opening of a canonical site).

The authors proposed that these conformational changes distal to the canonical site via changes in helices α4 and α7, and the α4–α5 loop result in the inhibition of BAX activation, and hence stabilize BAX in its inactive form. Notably, the authors validated this hypothesis by measuring sPRE effects caused by addition of hydroxyl-TEMPO to ^{15}N-labeled-BAX in its apo state and in the complex with Eltrombopag, recording ^{1}H-^{15}N-HSQC spectra in each case. Reduced sPRE values were observed for residues involved in direct interaction with Eltrombopag, especially those surrounding the hydrophobic pocket between helices α1 and α6, and on residues surrounding the interface of helix α7 and the α4–α5 loop and residues of helices α3, α5, and α9 forming the canonical site. Importantly, sPRE values remained unchanged for residues forming the α1–α2 loop, a displacement of which was reported to be critical in BAX activation. These data indicate that addition of Eltrombopag changed the sPRE profile of BAX by directly blocking binding of hydroxyl-TEMPO to the BAX trigger site and altering the surface topology of BAX, thus strongly corroborating the NMR and MD results. In conclusion, this example illustrates how sPRE can complement other biophysical and NMR-based methods in detecting the changes in protein structure and dynamics caused by binding of a drug compound.

5.4. Limitations

Although sPRE methodology has many strengths, including being a label-free method that imposes no requirements for introducing mutations or conjugations, and that it offers possibilities to investigate solvent accessibility for any NMR-active nucleus, some limitations to the sPRE method exist that one should bear in mind during experimental design and analysis. Firstly, with the exception of dioxygen binding to high-affinity sites, sPRE causes smaller effects (*i.e.* a tenfold difference in relaxation rates between surface exposed and buried residues) than does traditional PRE, where the paramagnetic probe is directly attached to the molecule of interest and can cause relaxation rate changes up to several thousand s^{-1} [99,131]. sPRE analysis is therefore at its most valuable in exploring biomolecular processes that are accompanied by significant alterations in solvent exposure. Secondly, to ensure the accuracy of sPRE data collection, the paramagnetic probe employed should be inert and not interact with a biomolecule under investigation, *i.e.* stickiness of the probe to certain residues would bias analysis when high concentrations of the probe are used; however, a notable exception to this is when an experiment is deliberately designed to disentangle electrostatic and/or transient, weak interactions, as described in Section 4.7. Thirdly, a combination of sPRE data with conformational sampling methods that generate a large library of conformers, such as molecular dynamics or Monte-Carlo-based sampling, has already been proven successful for refining structures of protein and RNA molecules [60,176], determining the structures and orientations of domains within a protein complex [181], and for cross-validation in revealing protein: drug interactions [311]. Achieving sufficient conformational sampling for a biomolecule and the surrounding paramagnetic agent imposes a high computational cost that represents the main challenge for these methods. Furthermore, although one of the assets of sPRE is that the data recorded are sensitive to molecular motions at millisecond time scale, numerical integration during sPRE back-calculation may be imprecise for a system experiencing dynamics at pico- to nanosecond timescale (the electron relaxation times). This can be further complicated by diffusional motion of the paramagnetic probe and thus rotational modulation of dipole–dipole interactions between the probe and the biomolecule may need to be taken into account [60,110].

6. Conclusions and future perspectives

In this review, we have given an overview of the pertinent theory, recent developments, and applications of solvent paramagnetic relaxation enhancements to investigate the structure, dynamics and function of biomolecules and macromolecular complexes. The implementation of sPRE measurement blocks in pulse sequences is relatively straightforward and requires minimal setup cost, however, careful experimental design is needed to obtain quantitative information. The method is particularly suitable for studying high molecular mass and conformationally dynamic biomolecules and their complexes, for which structural analysis by means of conventional techniques can be challenging. By providing surface-to-distance information in a tuneable manner, co-solute PREs can nicely complement sparse data obtained using other NMR approaches and other structural biology techniques. Solvent PREs may also be harnessed to accelerate NMR data acquisition and improve signal sensitivity, which is potentially useful not only for dynamic and unstable biomolecules but also for metabolomic samples. Moreover, recent evidence indicates that sPRE measurements employing carefully designed paramagnetic co-solute probes can provide a useful tool to probe the dynamics and energetics of weak, transient and sparse ion-macromolecule interactions. Such measurements can deliver information on the spatial distribution of co-solute ions around a biomolecule and on the near-surface electrostatic potential of macromolecules, thus filling gaps in our understanding of these dynamic interactions otherwise not accessible to conventional biophysical methods.

A combination of NMR spectroscopy with complementary techniques has emerged as a highly effective approach for unravelling structural and functional properties at the atomic level for dynamic biomolecules such as IDPs, nucleic acids and their complexes across different time scales. Future challenges will include, but are not limited to, integration of parameters obtained from different methods to characterize protein phase separation phenomena and its regulation, as well as transient dynamic interactions involving IDPs. In this regard, we envision that the incorporation of sPRE-obtained surface accessibility information into modeling schemes could increase predictive accuracy for such dynamic processes. Moreover, a combination of sPRE-obtained parameters (*i.e.* changes in surface accessibility upon complex formation, information on transient protein interactions, depth of membrane embeddedness) with AlphaFold2-predicted protein structures could significantly aid in drug discovery. With further extension, we expect that sPRE will continue to be a prominent method in the NMR spectroscopist's toolkit, providing detailed quantitative insights into the dynamic properties and interactions of macromolecules.

Data availability

No data was used for the research described in the article.

Declaration of Competing Interest

The authors declare that they have no known competing financial interests or personal relationships that could have appeared to influence the work reported in this paper.

Acknowledgements

T.M. was supported by Austrian Science Fund (FWF) grants P28854, I3792, DOC-130, and DK-MCD W1226; Austrian Research Promotion Agency (FFG) grants 864690 and 870454; the Integrative Metabolism Research Center Graz; the Austrian Infrastructure Program 2016/2017, the Styrian Government (Zukunftsfonds, doc.-fund program); the City of Graz; and BioTechMed-Graz (flagship project). A.L. was trained within the frame of the Ph.D. program Metabolic and Cardiovascular Disease (DK-MCD) at the Medical University of Graz.

References

[1] E. Spreitzer, S. Usluer, T. Madl, Probing surfaces in dynamic protein interactions, J. Mol. Biol. 432 (2020) 2949–2972.
[2] C. Göbl, T. Madl, B. Simon, M. Sattler, NMR approaches for structural analysis of multidomain proteins and complexes in solution, Prog. Nucl. Magn. Reson. Spectrosc. 80 (2014) 26–63.
[3] A. Ilari, C. Savino, Protein structure determination by x-ray crystallography, Methods Mol. Biol. 452 (2008) 63–87.
[4] J.T. Seffernick, S. Lindert, Hybrid methods for combined experimental and computational determination of protein structure, J. Chem. Phys. 153 (2020) 240901.
[5] B. Brutscher, I.C. Felli, S. Gil-Caballero, T. Hošek, R. Kümmerle, A. Piai, R. Pierattelli, Z. Sólyom, NMR methods for the study of instrinsically disordered proteins structure, dynamics, and interactions: general overview and practical guidelines, Adv. Exp. Med. Biol. 870 (2015) 49–122.
[6] A. Bax, G.M. Clore, Protein NMR: boundless opportunities, J. Magn. Reson. 306 (2019) 187–191.
[7] T.R. Alderson, L.E. Kay, NMR spectroscopy captures the essential role of dynamics in regulating biomolecular function, Cell 184 (2021) 577–595.
[8] A.K. Mittermaier, L.E. Kay, Observing biological dynamics at atomic resolution using NMR, Trends Biochem. Sci. 34 (2009) 601–611.
[9] C.M. Quinn, M. Wang, T. Polenova, NMR of macromolecular assemblies and machines at 1 GHz and beyond: new transformative opportunities for molecular structural biology, Methods Mol. Biol. 1688 (2018) 1–35.
[10] H. Schwalbe, Editorial: New 1.2 GHz NMR spectrometers-new horizons? Angew. Chem. Int. Ed. Engl. 56 (2017) 10252–10253.
[11] E. Luchinat, L. Barbieri, M. Cremonini, L. Banci, Protein in-cell NMR spectroscopy at 1.2 GHz, J. Biomol. NMR 75 (2021) 97–107.
[12] P. Styles, N.F. Soffe, C.A. Scott, An improved cryogenically cooled probe for high-resolution NMR, J. Magn. Reson. 84 (1989) (1969) 376–378.
[13] J. Yao, J. Yoon, Low-noise electrometer and its low-noise cryogenic probe with completely guarded sample chamber, Rev. Sci. Instrum. 71 (2000) 1776–1780.
[14] M.W. Voehler, G. Collier, J.K. Young, M.P. Stone, M.W. Germann, Performance of cryogenic probes as a function of ionic strength and sample tube geometry, J. Magn. Reson. 183 (2006) 102–109.
[15] F. Delaglio, S. Grzesiek, G.W. Vuister, G. Zhu, J. Pfeifer, A. Bax, NMRPipe: a multidimensional spectral processing system based on UNIX pipes, J. Biomol. NMR 6 (1995) 277–293.
[16] J.M. Thompson, N.G. Sgourakis, G. Liu, P. Rossi, Y. Tang, J.L. Mills, T. Szyperski, G.T. Montelione, D. Baker, Accurate protein structure modeling using sparse NMR data and homologous structure information, Proc. Natl. Acad. Sci. U. S. A. 109 (2012) 9875–9880.
[17] K. Pervushin, R. Riek, G. Wider, K. Wüthrich, Attenuated T2 relaxation by mutual cancellation of dipole-dipole coupling and chemical shift anisotropy indicates an avenue to NMR structures of very large biological macromolecules in solution, Proc. Natl. Acad. Sci. U. S. A. 94 (1997) 12366–12371.
[18] A. Eletsky, A. Kienhöfer, K. Pervushin, TROSY NMR with partially deuterated proteins, J. Biomol. NMR 20 (2001) 177–180.
[19] R. Riek, K. Pervushin, K. Wüthrich, TROSY and CRINEPT: NMR with large molecular and supramolecular structures in solution, Trends Biochem. Sci. 25 (2000) 462–468.
[20] S. Schütz, R. Sprangers, Methyl TROSY spectroscopy: a versatile NMR approach to study challenging biological systems, Prog. Nucl. Magn. Reson. Spectrosc. 116 (2020) 56–84.
[21] T.L. Religa, A.M. Ruschak, R. Rosenzweig, L.E. Kay, Site-directed methyl group labeling as an NMR probe of structure and dynamics in supramolecular protein systems: applications to the proteasome and to the ClpP protease, J. Am. Chem. Soc. 133 (2011) 9063–9068.
[22] K. Tripsianes, U. Schütz, L. Emmanouilidis, G. Gemmecker, M. Sattler, Selective isotope labeling for NMR structure determination of proteins in complex with unlabeled ligands, J. Biomol. NMR 73 (2019) 183–189.
[23] K. Takeuchi, H. Arthanari, I. Shimada, G. Wagner, Nitrogen detected TROSY at high field yields high resolution and sensitivity for protein NMR, J. Biomol. NMR 63 (2015) 323–331.
[24] I.C. Felli, B. Brutscher, Recent advances in solution NMR: fast methods and heteronuclear direct detection, ChemPhysChem 10 (2009) 1356–1368.
[25] E.B. Gibbs, R.W. Kriwacki, Direct detection of carbon and nitrogen nuclei for high-resolution analysis of intrinsically disordered proteins using NMR spectroscopy, Methods 138–139 (2018) 39–46.
[26] H. Arthanari, K. Takeuchi, A. Dubey, G. Wagner, Emerging solution NMR methods to illuminate the structural and dynamic properties of proteins, Curr. Opin. Struct. Biol. 58 (2019) 294–304.
[27] P. Schanda, E. Kupce, B. Brutscher, SOFAST-HMQC experiments for recording two-dimensional heteronuclear correlation spectra of proteins within a few seconds, J. Biomol. NMR 33 (2005) 199–211.

[28] A.-H. Emwas, M. Alghrably, S. Al-Harthi, B. Gabriel Poulson, K. Szczepski, K. Chandra, M. Jaremko, New Advances in Fast Methods of 2D NMR Experiments, IntechOpen, 2019.
[29] D. Gołowicz, P. Kasprzak, V. Orekhov, K. Kazimierczuk, Fast time-resolved NMR with non-uniform sampling, Prog. Nucl. Magn. Reson. Spectrosc. 116 (2020) 40–55.
[30] K. Zangger, Pure shift NMR, Prog. Nucl. Magn. Reson. Spectrosc. 86–87 (2015) 1–20.
[31] C. Charlier, T.R. Alderson, J.M. Courtney, J. Ying, P. Anfinrud, A. Bax, Study of protein folding under native conditions by rapidly switching the hydrostatic pressure inside an NMR sample cell, Proc. Natl. Acad. Sci. U. S. A. 115 (2018) E4169–E4178.
[32] C.A. Barnes, A.J. Robertson, J.M. Louis, P. Anfinrud, A. Bax, Observation of beta-amyloid peptide oligomerization by pressure-jump NMR spectroscopy, J. Am. Chem. Soc. 141 (2019) 13762–13766.
[33] J.M. Plitzko, B. Schuler, P. Selenko, Structural biology outside the box-inside the cell, Curr. Opin. Struct. Biol. 46 (2017) 110–121.
[34] F. Delhommel, F. Gabel, M. Sattler, Current approaches for integrating solution NMR spectroscopy and small-angle scattering to study the structure and dynamics of biomolecular complexes, J. Mol. Biol. 432 (2020) 2890–2912.
[35] M.P. Rout, A. Sali, Principles for integrative structural biology studies, Cell 177 (2019) 1384–1403.
[36] M. Turk, W. Baumeister, The promise and the challenges of cryo-electron tomography, FEBS Lett. 594 (2020) 3243–3261.
[37] D.F. Gauto, L.F. Estrozi, C.D. Schwieters, G. Effantin, P. Macek, R. Sounier, A.C. Sivertsen, E. Schmidt, R. Kerfah, G. Mas, J.P. Colletier, P. Güntert, A. Favier, G. Schoehn, P. Schanda, J. Boisbouvier, Integrated NMR and cryo-EM atomic-resolution structure determination of a half-megadalton enzyme complex, Nat. Commun. 10 (2019) 2697.
[38] G.W. Gomes, M. Krzeminski, A. Namini, E.W. Martin, T. Mittag, T. Head-Gordon, J.D. Forman-Kay, C.C. Gradinaru, Conformational ensembles of an intrinsically disordered protein consistent with NMR, SAXS, and single-molecule FRET, J. Am. Chem. Soc. 142 (2020) 15697–15710.
[39] J. Jumper, R. Evans, A. Pritzel, T. Green, M. Figurnov, O. Ronneberger, K. Tunyasuvunakool, R. Bates, A. Zidek, A. Potapenko, A. Bridgland, C. Meyer, S.A. A. Kohl, A.J. Ballard, A. Cowie, B. Romera-Paredes, S. Nikolov, R. Jain, J. Adler, T. Back, S. Petersen, D. Reiman, E. Clancy, M. Zielinski, M. Steinegger, M. Pacholska, T. Berghammer, S. Bodenstein, D. Silver, O. Vinyals, A.W. Senior, K. Kavukcuoglu, P. Kohli, D. Hassabis, Highly accurate protein structure prediction with AlphaFold, Nature 596 (2021) 583–589.
[40] K. Tunyasuvunakool, J. Adler, Z. Wu, T. Green, M. Zielinski, A. Zidek, A. Bridgland, A. Cowie, C. Meyer, A. Laydon, S. Velankar, G.J. Kleywegt, A. Bateman, R. Evans, A. Pritzel, M. Figurnov, O. Ronneberger, R. Bates, S.A.A. Kohl, A. Potapenko, A.J. Ballard, B. Romera-Paredes, S. Nikolov, R. Jain, E. Clancy, D. Reiman, S. Petersen, A.W. Senior, K. Kavukcuoglu, E. Birney, P. Kohli, J. Jumper, D. Hassabis, Highly accurate protein structure prediction for the human proteome, Nature 596 (2021) 590–596.
[41] M. Baek, F. DiMaio, I. Anishchenko, J. Dauparas, S. Ovchinnikov, G.R. Lee, J. Wang, Q. Cong, L.N. Kinch, R.D. Schaeffer, C. Millán, H. Park, C. Adams, C.R. Glassman, A. DeGiovanni, J.H. Pereira, A.V. Rodrigues, A.A. van Dijk, A.C. Ebrecht, D.J. Opperman, T. Sagmeister, C. Buhlheller, T. Pavkov-Keller, M.K. Rathinaswamy, U. Dalwadi, C.K. Yip, J.E. Burke, K.C. Garcia, N.V. Grishin, P.D. Adams, R.J. Read, D. Baker, Accurate prediction of protein structures and interactions using a three-track neural network, Science 373 (2021) 871–876.
[42] J. Pereira, A.J. Simpkin, M.D. Hartmann, D.J. Rigden, R.M. Keegan, A.N. Lupas, High-accuracy protein structure prediction in CASP14, Proteins 89 (2021) 1687–1699.
[43] A. Kryshtafovych, T. Schwede, M. Topf, K. Fidelis, J. Moult, Critical assessment of methods of protein structure prediction (CASP)-Round XIV, Proteins 89 (2021) 1607–1617.
[44] R. Evans, M. O'Neill, A. Pritzel, N. Antropova, A. Senior, T. Green, A. Žídek, R. Bates, S. Blackwell, J. Yim, O. Ronneberger, S. Bodenstein, M. Zielinski, A. Bridgland, A. Potapenko, A. Cowie, K. Tunyasuvunakool, R. Jain, E. Clancy, P. Kohli, J. Jumper, D. Hassabis, Protein complex prediction with AlphaFold-Multimer, bioRxiv (2021) 2021.2010.2004.463034.
[45] M.L. Hekkelman, I. de Vries, R.P. Joosten, A. Perrakis, AlphaFill: enriching the AlphaFold models with ligands and co-factors, bioRxiv (2021) 2021.2011.2026.470110.
[46] G. Masrati, M. Landau, N. Ben-Tal, A. Lupas, M. Kosloff, J. Kosinski, Integrative structural biology in the era of accurate structure prediction, J. Mol. Biol. 433 (2021) 167127.
[47] P. Klukowski, R. Riek, P. Güntert, Leveraging deep learning for fully automated NMR protein structure determination, arXiv preprint (2022).
[48] P.R. Markwick, T. Malliavin, M. Nilges, Structural biology by NMR: structure, dynamics, and interactions, PLoS Comput. Biol. 4 (2008) 1–7.
[49] A. Bax, G. Kontaxis, N. Tjandra, Dipolar couplings in macromolecular structure determination, Methods Enzymol. 339 (2001) 127–174.
[50] M. Blackledge, Recent progress in the study of biomolecular structure and dynamics in solution from residual dipolar couplings, Prog. Nucl. Magn. Reson. Spec. 46 (2005) 23–61.
[51] J.H. Prestegard, C.M. Bougault, A.I. Kishore, Residual dipolar couplings in structure determination of biomolecules, Chem. Rev. 104 (2004) 3519–3540.
[52] C. Nitsche, G. Otting, Pseudocontact shifts in biomolecular NMR using paramagnetic metal tags, Prog. Nucl. Magn. Reson. Spectrosc. 98–99 (2017) 20–49.
[53] G. Otting, Protein NMR using paramagnetic ions, Annu. Rev. Biophys. 39 (2010) 387–405.
[54] G.M. Clore, Practical aspects of paramagnetic relaxation enhancement in biological macromolecules, Methods Enzymol. 564 (2015) 485–497.
[55] A.J. Pell, G. Pintacuda, C.P. Grey, Paramagnetic NMR in solution and the solid state, Prog. Nucl. Magn. Reson. Spectrosc. 111 (2019) 1–271.
[56] A. Cavalli, X. Salvatella, C.M. Dobson, M. Vendruscolo, Protein structure determination from NMR chemical shifts, Proc. Natl. Acad. Sci. U. S. A. 104 (2007) 9615–9620.
[57] X.C. Su, G. Otting, Paramagnetic labelling of proteins and oligonucleotides for NMR, J. Biomol. NMR 46 (2010) 101–112.
[58] C.A. Softley, M.J. Bostock, G.M. Popowicz, M. Sattler, Paramagnetic NMR in drug discovery, J. Biomol. NMR 74 (2020) 287–309.
[59] H.G. Hocking, K. Zangger, T. Madl, Studying the structure and dynamics of biomolecules by using soluble paramagnetic probes, ChemPhysChem 14 (2014) 3082–3094.
[60] Z. Gong, C.D. Schwieters, C. Tang, Theory and practice of using solvent paramagnetic relaxation enhancement to characterize protein conformational dynamics, Methods 148 (2018) 48–56.
[61] R. Linser, U. Fink, B. Reif, Probing surface accessibility of proteins using paramagnetic relaxation in solid-state NMR spectroscopy, J. Am. Chem. Soc. 131 (2009) 13703–13708.
[62] C. Öster, S. Kosol, C. Hartlmüller, J.M. Lamley, D. Iuga, A. Oss, M.L. Org, K. Vanatalu, A. Samoson, T. Madl, J.R. Lewandowski, Characterization of protein-protein interfaces in large complexes by solid-state NMR solvent paramagnetic relaxation enhancements, J. Am. Chem. Soc. 139 (2017) 12165–12174.
[63] D. Aucoin, Y. Xia, T. Theint, P.S. Nadaud, K. Surewicz, W.K. Surewicz, C.P. Jaroniec, Protein-solvent interfaces in human Y145Stop prion protein amyloid fibrils probed by paramagnetic solid-state NMR spectroscopy, J. Struct. Biol. 206 (2019) 36–42.
[64] V.V. Bernini, O. Spiga, N., Niccolai, Probing protein surface accessibility with solvent and paramagnetic molecules, Prog. Nucl. Magn. Reson. Spec. 54 (2009) 278–289.
[65] I. Bertini, C. Luchinat, G. Parigi, Paramagnetic constraints: an aid for quick solution structure determination of paramagnetic metalloproteins, Concepts Magn. Reson. 14 (2002) 259–286.
[66] J. Peters, J. Huskens, D. Raber, Lanthanide induced shifts and relaxation rate enhancements, Prog. Nucl. Magn. Reson. Spec. 28 (1996) 283–350.
[67] I. Bertini, C. Luchinat, G. Parigi, Magnetic susceptibility in paramagnetic NMR, Prog. Nucl. Magn. Reson. Spec. 3 (2002) 249–273.
[68] G. Parigi, E. Ravera, C. Luchinat, Magnetic susceptibility and paramagnetism-based NMR, Prog. Nucl. Magn. Reson. Spectrosc. 114–115 (2019) 211–236.
[69] G. Pintacuda, G. Otting, Identification of protein surfaces by NMR measurements with a pramagnetic Gd(III) chelate, J. Am. Chem. Soc. 124 (2002) 372–373.
[70] T. Madl, W. Bermel, K. Zangger, Use of relaxation enhancements in a paramagnetic environment for the structure determination of proteins using NMR spectroscopy, Angew. Chem. Int. Ed. Engl. 48 (2009) 8259–8262.
[71] L.P. Hwang, J.H. Freed, Generalized Einstein relations for rotational and translational diffusion of molecules including spin, J. Chem. Phys. 63 (1975) 118–130.
[72] C.F. Polnaszek, R.G. Bryant, Nitroxide radical induced solvent proton relaxation: measurement of localized translational diffusion, J. Chem. Phys. 81 (1984) 4038–4045.
[75] T. Madl, F.A. Mulder, Small paramagnetic co-solute molecules, in: Paramagnetism in Experimental Biomolecular NMR, 2018, pp. 283–309.
[81] G. Parigi, C. Luchinat, Chapter 1: NMR consequences of the nucleus-electron spin interactions, in: Paramagnetism in Experimental Biomolecular NMR, 2018, pp. 1–41.
[82] I. Solomon, Relaxation processes in a system of two spins, Phys. Rev. 99 (1955) 559–565.
[83] N. Bloembergen, L. Morgan, Proton relaxation times in paramagnetic solutions. Effects of electron spin relaxation, J. Chem. Phys. 34 (1961) 842–850.
[84] M. Guéron, Nuclear relaxation in macromolecules by paramagnetic ions: a novel mechanism, J. Magn. Reson. 19 (1975) (1969) 58–66.
[85] T.J. Swift, R.E. Connick, NMR-relaxation mechanisms of O17 in aqueous solutions of paramagnetic cations and the lifetime of water molecules in the first coordination sphere, J. Chem. Phys. 37 (1962) 307–320.
[86] A.J. Vega, D. Fiat, Nuclear relaxation processes of paramagnetic complexes the slow-motion case, Mol. Phys. 31 (1976) 347–355.
[87] L.-P.-F. Hwang, H. Jack, Dynamic effects of pair correlation functions on spin relaxation by translational diffusion in liquids, J. Chem. Phys. 63 (1975) 4017–4025.
[88] H.G. Hocking, K. Zangger, T. Madl, Solution PRE NMR, in: Protein NMR, Springer, 2015, pp. 133–157.
[89] D. Kruk, J. Kowalewski, General treatment of paramagnetic relaxation enhancement associated with translational diffusion, J. Chem. Phys. 130 (2009) 174104.
[90] G.M. Clore, Exploring sparsely populated states of macromolecules by diamagnetic and paramagnetic NMR relaxation, Prot. Sci.: Publ. Prot. Soc. 20 (2011) 229–246.
[92] I.R. Kleckner, M.P. Foster, An introduction to NMR-based approaches for measuring protein dynamics, BBA 2011 (1814) 942–968.

[93] K. Henzler-Wildman, D. Kern, Dynamic personalities of proteins, Nature 450 (2007) 964–972.
[94] A.M. Mandel, M. Akke, A.G. Palmer 3rd, Backbone dynamics of *Escherichia coli* ribonuclease HI: correlations with structure and function in an active enzyme, J. Mol. Biol. 246 (1995) 144–163.
[95] T.I. Igumenova, K.K. Frederick, A.J. Wand, Characterization of the fast dynamics of protein amino acid side chains using NMR relaxation in solution, Chem. Rev. 106 (2006) 1672–1699.
[96] M.S. Marlow, J. Dogan, K.K. Frederick, K.G. Valentine, A.J. Wand, The role of conformational entropy in molecular recognition by calmodulin, Nat. Chem. Biol. 6 (2010) 352–358.
[97] D. Yang, L.E. Kay, Contributions to conformational entropy arising from bond vector fluctuations measured from NMR-derived order parameters: application to protein folding, J. Mol. Biol. 263 (1996) 369–382.
[98] N. Popovych, S. Sun, R.H. Ebright, C.G. Kalodimos, Dynamically driven protein allostery, Nat. Struct. Mol. Biol. 13 (2006) 831–838.
[99] G.M. Clore, J. Iwahara, Theory, practice, and applications of paramagnetic relaxation enhancement for the characterization of transient low-population states of biological macromolecules and their complexes, Chem. Rev. 109 (2009) 4108–4139.
[100] J. Iwahara, C. Tang, G. Marius Clore, Practical aspects of (1)H transverse paramagnetic relaxation enhancement measurements on macromolecules, J. Magn. Reson. 184 (2007) 185–195.
[101] G. Lipari, A. Szabo, Model-free approach to the interpretation of nuclear magnetic resonance relaxation in macromolecules. 1. Theory and range of validity, J. Am. Chem. Soc. 104 (1982) 4546–4559.
[102] J. Iwahara, C.D. Schwieters, G.M. Clore, Ensemble approach for NMR structure refinement against (1)H paramagnetic relaxation enhancement data arising from a flexible paramagnetic group attached to a macromolecule, J. Am. Chem. Soc. 126 (2004) 5879–5896.
[103] J. Iwahara, G.M. Clore, Structure-independent analysis of the breadth of the positional distribution of disordered groups in macromolecules from order parameters for long, variable-length vectors using NMR paramagnetic relaxation enhancement, J. Am. Chem. Soc. 132 (2010) 13346–13356.
[104] R. Brüschweiler, B. Roux, M. Blackledge, C. Griesinger, M. Karplus, R.R. Ernst, Influence of rapid intramolecular motion on NMR cross-relaxation rates. A molecular dynamics study of antamanide in solution, J. Am. Chem. Soc. 114 (1992) 2289–2302.
[105] E. Olejniczak, C. Dobson, M. Karplus, R. Levy, Motional averaging of proton nuclear Overhauser effects in proteins. Predictions from a molecular dynamics simulation of lysozyme, J. Am. Chem. Soc. 106 (1984) 1923–1930.
[106] M. Rubinstein, A. Baram, Z. Luz, Electronic and nuclear relaxation in solutions of transition metal ions with spin S= 3/2 and 5/2, Mol. Phys. 20 (1971) 67–80.
[107] A. Mittermaier, L.E. Kay, New tools provide new insights in NMR studies of protein dynamics, Science 312 (2006) 224–228.
[108] H.M. McConnell, Reaction rates by nuclear magnetic resonance, J. Chem. Phys. 28 (1958) 430–431.
[109] J.J. Led, D.M. Grant, Carbon-13 relaxation in paramagnetic complexes of amino acids. Structural and dynamical information on nickel(II) complexes of histidine, J. Am. Chem. Soc. 99 (1977) 5845–5858.
[110] Z. Gong, X.H. Gu, D.C. Guo, J. Wang, C. Tang, Protein structural ensembles visualized by solvent paramagnetic relaxation enhancement, Angew. Chem. Int. Ed. Engl. 56 (2017) 1002–1006.
[111] N.J. Anthis, G.M. Clore, Visualizing transient dark states by NMR spectroscopy, Q. Rev. Biophys. 48 (2015) 35–116.
[112] K. Teilum, M.B. Kunze, S. Erlendsson, B.B. Kragelund, (S)Pinning down protein interactions by NMR, Prot. Sci.: Publ. Prot. Soc. 26 (2017) 436–451.
[113] A.G. Palmer, C.D. Kroenke, J. Patrick Loria, [10] - Nuclear magnetic resonance methods for quantifying microsecond-to-millisecond motions in biological macromolecules, in: T.L. James, V. Dötsch, U. Schmitz (Eds.) Methods in Enzymology, Academic Press, 2001, pp. 204–238.
[114] Y. Okuno, J. Yoo, C.D. Schwieters, R.B. Best, H.S. Chung, G.M. Clore, Atomic view of cosolute-induced protein denaturation probed by NMR solvent paramagnetic relaxation enhancement, Proc. Natl. Acad. Sci. U. S. A. 118 (2021).
[115] B. Yu, C.C. Pletka, J. Iwahara, Quantifying and visualizing weak interactions between anions and proteins, Proc. Natl. Acad. Sci. U. S. A. 118 (2021).
[116] B. Yu, C.C. Pletka, B.M. Pettitt, J. Iwahara, De novo determination of near-surface electrostatic potentials by NMR, Proc. Natl. Acad. Sci. U. S. A. 118 (2021).
[117] A. Bernini, O. Spiga, V. Venditti, F. Prischi, L. Bracci, A.P. Tong, W.T. Wong, N. Niccolai, NMR studies of lysozyme surface accessibility by using different paramagnetic relaxation probes, J. Am. Chem. Soc. 128 (2006) 9290–9291.
[118] F. Evanics, P.M. Hwang, Y. Cheng, L.E. Kay, R.S. Prosser, Topology of an outer-membrane enzyme: measuring oxygen and water contacts in solution NMR studies of PagP, J. Am. Chem. Soc. 128 (2006) 8256–8264.
[119] P.A. Luchette, R.S. Prosser, C.R. Sanders, Oxygen as a paramagnetic probe of membrane protein structure by cysteine mutagenesis and (19)F NMR spectroscopy, J. Am. Chem. Soc. 124 (2002) 1778–1781.
[120] C.L. Teng, B. Hinderliter, R.G. Bryant, Oxygen accessibility to ribonuclease a: quantitative interpretation of nuclear spin relaxation induced by a freely diffusing paramagnet, J. Phys. Chem. A 110 (2006) 580–588.
[121] R.S. Prosser, P.A. Luchette, An NMR study of the origin of dioxygen-induced spin-lattice relaxation enhancement and chemical shift perturbation, J. Magn. Reson. 171 (2004) 225–232.
[122] I. Bezsonova, J. Forman-Kay, R.S. Prosser, Molecular oxygen as a paramagnetic NMR probe of protein solvent exposure and topology, Concept Magn. Reson. A 32a (2008) 239–253.
[123] M.S. Al-Abdul-Wahid, C. Neale, R. Pomès, R.S. Prosser, A solution NMR approach to the measurement of amphiphile immersion depth and orientation in membrane model systems, J. Am. Chem. Soc. 131 (2009) 6452–6459.
[124] G. Hernández, C.L. Teng, R.G. Bryant, D.M. LeMaster, O2 penetration and proton burial depth in proteins: applicability to fold family recognition, J. Am. Chem. Soc. 124 (2002) 4463–4472.
[125] M. Sakakura, S. Noba, P.A. Luchette, I. Shimada, R.S. Prosser, An NMR method for the determination of protein-binding interfaces using dioxygen-induced spin-lattice relaxation enhancement, J. Am. Chem. Soc. 127 (2005) 5826–5832.
[126] I. Bezsonova, F. Evanics, J.A. Marsh, J.D. Forman-Kay, R.S. Prosser, Oxygen as a paramagnetic probe of clustering and solvent exposure in folded and unfolded states of an SH3 domain, J. Am. Chem. Soc. 129 (2007) 1826–1835.
[127] R. Kitahara, Y. Yoshimura, M. Xue, T. Kameda, F.A. Mulder, Detecting O2 binding sites in protein cavities, Sci. Rep. 6 (2016) 20534.
[128] T. Kawamura, T. Wakamoto, S. Kitazawa, S. Sakuraba, T. Kameda, R. Kitahara, Analysis of O2-binding sites in proteins using gas-pressure NMR spectroscopy: outer surface protein A, Biophys. J. 112 (2017) 1820–1828.
[129] I. Morishima, T. Inubushi, T. Yonezawa, Y. Kyogoku, Proton magnetic resonance studies of specific association of nucleic acid constitutent bases in a nonaqueous solvent. Utility of DTBN radical to probe the affinity of hydrogen bonding involved in complementary base pairs1, J. Am. Chem. Soc. 99 (1977) 4299–4305.
[130] K.D. Kopple, T.J. Schamper, Proton magnetic resonance line broadening produced by association with a nitroxide radical in studies of amide and peptide conformation, J. Am. Chem. Soc. 94 (1972) 3644–3646.
[131] C. Tang, C.D. Schwieters, G.M. Clore, Open-to-closed transition in apo maltose-binding protein observed by paramagnetic NMR, Nature 449 (2007) 1078–1082.
[132] A.M. Petros, L. Mueller, K.D. Kopple, NMR identification of protein surfaces using paramagnetic probes, Biochemistry 29 (1990) 10041–10048.
[133] G. Esposito, H. Molinari, M. Pegna, N. Niccolai, L. Zetta, A 1H NMR study on the interaction of aminoxyl paramagnetic probes with unfolded peptides, J. Chem. Soc., Perkin Trans. 2 (1993) 1531–1534.
[134] O.H. Griffith, A. Waggoner, Nitroxide free radicals: spin labels for probing biomolecular structure, Acc. Chem. Res. 2 (1969) 17–24.
[135] N. Niccolai, O. Spiga, A. Bernini, M. Scarselli, A. Ciutti, I. Fiaschi, S. Chiellini, H. Molinari, P.A. Temussi, NMR studies of protein hydration and TEMPOL accessibility, J. Mol. Biol. 332 (2003) 437–447.
[136] V. Venditti, N. Niccolai, S.E. Butcher, Measuring the dynamic surface accessibility of RNA with the small paramagnetic molecule TEMPOL, Nucleic Acids Res. 36 (2008) e20.
[137] S.W. Fesik, G. Gemmecker, E.T. Olejniczak, A.M. Petros, Identification of solvent-exposed regions of enzyme-bound ligands by nuclear magnetic resonance, J. Am. Chem. Soc. 113 (1991) 7080–7081.
[138] S.M. Hahn, L. Wilson, C.M. Krishna, J. Liebmann, W. DeGraff, J. Gamson, A. Samuni, D. Venzon, J.B. Mitchell, Identification of nitroxide radioprotectors, Radiat. Res. 132 (1992) 87–93.
[139] G.I. Likhtenshtein, I. Adin, A. Novoselsky, A. Shames, I. Vaisbuch, R. Glaser, NMR studies of electrostatic potential distribution around biologically important molecules, Biophys. J. 77 (1999) 443–453.
[140] C.L. Teng, R.G. Bryant, Spin relaxation measurements of electrostatic bias in intermolecular exploration, J. Magn. Reson. 179 (2006) 199–205.
[141] F.A.A. Mulder, NMR spectroscopy charges into protein surface electrostatics, Proc. Natl. Acad. Sci. U. S. A. 118 (2021).
[142] N. Niccolai, A. Ciutti, O. Spiga, M. Scarselli, A. Bernini, L. Bracci, D. Di Maro, C. Dalvit, H. Molinari, G. Esposito, P.A. Temussi, NMR studies of protein surface accessibility, J. Biol. Chem. 276 (2001) 42455–42461.
[143] I. Bertini, C. Luchinat, G. Parigi, E. Ravera, Chapter 7 - Transition metal ions: shift and relaxation, in: I. Bertini, C. Luchinat, G. Parigi, E. Ravera (Eds.), NMR of Paramagnetic Molecules, second edition., Elsevier, Boston, 2017, pp. 175–253.
[144] M.R. Jensen, C. Lauritzen, S.W. Dahl, J. Pedersen, J.J. Led, Binding ability of a HHP-tagged protein towards Ni2+ studied by paramagnetic NMR relaxation: the possibility of obtaining long-range structure information, J. Biomol. NMR 29 (2004) 175–185.
[145] N. Niccolai, E. Tiezzi, G. Valensin, Manganese (II) as magnetic relaxation probe in the study of biomechanisms and of biomacromolecules, Chem. Rev. 82 (1982) 359–384.
[146] S. Cai, C. Seu, Z. Kovacs, A.D. Sherry, Y. Chen, Sensitivity enhancement of multidimensional NMR experiments by paramagnetic relaxation effects, J. Am. Chem. Soc. 128 (2006) 13474–13478.
[147] B.C. Mayo, Lanthanide shift reagents in nuclear magnetic resonance spectroscopy, Chem. Soc. Rev. 1 (1973) 49–74.
[148] N.A. Oktaviani, M.W. Risør, Y.H. Lee, R.P. Megens, D.H. de Jong, R. Otten, R.M. Scheek, J.J. Enghild, N.C. Nielsen, T. Ikegami, F.A. Mulder, Optimized co-solute paramagnetic relaxation enhancement for the rapid NMR analysis of a highly fibrillogenic peptide, J. Biomol. NMR 62 (2015) 129–142.

[149] R.S. Prosser, F. Evanics, J.L. Kitevski, S. Patel, The measurement of immersion depth and topology of membrane proteins by solution state NMR, Biochim. Biophys. Acta. 1768 (2007) 3044–3051.
[150] G. Otting, Prospects for lanthanides in structural biology by NMR, J. Biomol. NMR 42 (2008) 1–9.
[151] S. Aime, N. D'Amelio, M. Fragai, Y.M. Lee, C. Luchinat, E. Terreno, G. Valensin, A paramagnetic probe to localize residues next to carboxylates on protein surfaces, J. Biol. Inorg. Chem. 7 (2002) 617–622.
[152] C.M. Dobson, S.J. Ferguson, F.M. Poulsen, R.J. Williams, Complete assignment of aromatic 1H nuclear magnetic resonances of the tyrosine residues of hen lysozyme, Eur. J. Biochem. 92 (1978) 99–103.
[153] M. Sattler, S.W. Fesik, Resolving resonance overlap in the NMR spectra of proteins from differential lanthanide-induced shifts, J. Am. Chem. Soc. 119 (1997) 7885–7886.
[154] M. Franzmann, D. Otzen, R. Wimmer, Quantitative use of paramagnetic relaxation enhancements for determining orientations and insertion depths of peptides in micelles, ChemBioChem 10 (2009) 2339–2347.
[155] H.W. Eichstaedt, R. Felix, O. Danne, F.C. Dougherty, H. Schmutzler, Imaging of acute myocardial infarction by magnetic resonance tomography (MRT) using the paramagnetic relaxation substance gadolinium-DTPA, Cardiovasc. Drugs Ther. 3 (1989) 779–788.
[156] S. Aime, C. Cabella, S. Colombatto, S. Geninatti Crich, E. Gianolio, F. Maggioni, Insights into the use of paramagnetic Gd(III) complexes in MR-molecular imaging investigations, J. Magn. Reson. Imaging 16 (2002) 394–406.
[157] J.C. Bousquet, S. Saini, D.D. Stark, P.F. Hahn, M. Nigam, J. Wittenberg, J.T. Ferrucci Jr., Gd-DOTA: characterization of a new paramagnetic complex, Radiology 166 (1988) 693–698.
[158] S. Arumugam, C.L. Hemme, N. Yoshida, K. Suzuki, H. Nagase, M. Berjanskii, B. Wu, S.R. Van Doren, TIMP-1 contact sites and perturbations of stromelysin 1 mapped by NMR and a paramagnetic surface probe, Biochemistry 37 (1998) 9650–9657.
[159] Y. Sun, J.I. Friedman, J.T. Stivers, Cosolute paramagnetic relaxation enhancements detect transient conformations of human uracil DNA glycosylase, hUNG, Biochemistry 50 (2011) 10724–10731.
[160] A. Bernini, V. Venditti, O. Spiga, A. Ciutti, F. Prischi, R. Consonni, L. Zetta, I. Arosio, P. Fusi, A. Guagliardi, N. Niccolai, NMR studies on the surface accessibility of the archaeal protein Sso7d by using TEMPOL and Gd(III) (DTPA-BMA) as paramagnetic probes, Biophys. Chem. 137 (2008) 71–75.
[161] L. Carlier, P. Joanne, L. Khemtemourian, C. Lacombe, P. Nicolas, C. El Amri, O. Lequin, Investigating the role of GXXXG motifs in helical folding and self-association of plasticins, Gly/Leu-rich antimicrobial peptides, Biophys. Chem. 196 (2015) 40–52.
[162] H. Johansson, M.R. Jensen, H. Gesmar, S. Meier, J.M. Vinther, C. Keeler, M.E. Hodsdon, J.J. Led, Specific and nonspecific interactions in ultraweak protein-protein associations revealed by solvent paramagnetic relaxation enhancements, J. Am. Chem. Soc. 136 (2014) 10277–10286.
[163] J. Iwahara, M. Zweckstetter, G.M. Clore, NMR structural and kinetic characterization of a homeodomain diffusing and hopping on nonspecific DNA, Proc. Natl. Acad. Sci. U. S. A. 103 (2006) 15062–15067.
[164] X.H. Gu, Z. Gong, D.C. Guo, W.P. Zhang, C. Tang, A decadentate Gd(III)-coordinating paramagnetic cosolvent for protein relaxation enhancement measurement, J. Biomol. NMR 58 (2014) 149–154.
[165] A. Bernini, O. Spiga, V. Venditti, F. Prischi, M. Botta, G. Croce, A.P. Tong, W.T. Wong, N. Niccolai, The use of a ditopic Gd(III) paramagnetic probe for investigating alpha-bungarotoxin surface accessibility, J. Inorg. Biochem. 112 (2012) 25–31.
[166] E. Liepinsh, M. Baryshev, A. Sharipo, M. Ingelman-Sundberg, G. Otting, S. Mkrtchian, Thioredoxin fold as homodimerization module in the putative chaperone ERp29: NMR structures of the domains and experimental model of the 51 kDa dimer, Structure 9 (2001) 457–471.
[167] M.L. Deschamps, E.S. Pilka, J.R. Potts, I.D. Campbell, J. Boyd, Probing protein-peptide binding surfaces using charged stable free radicals and transverse paramagnetic relaxation enhancement (PRE), J. Biomol. NMR 31 (2005) 155–160.
[168] M. Respondek, T. Madl, C. Göbl, R. Golser, K. Zangger, Mapping the orientation of helices in micelle-bound peptides by paramagnetic relaxation waves, J. Am. Chem. Soc. 129 (2007) 5228–5234.
[169] H. Molinari, G. Esposito, L. Ragona, M. Pegna, N. Niccolai, R.M. Brunne, A.M. Lesk, L. Zetta, Probing protein structure by solvent perturbation of NMR spectra: the surface accessibility of bovine pancreatic trypsin inhibitor, Biophys. J. 73 (1997) 382–396.
[170] S. Hiller, G. Wider, T. Etezady-Esfarjani, R. Horst, K. Wüthrich, Managing the solvent water polarization to obtain improved NMR spectra of large molecular structures, J. Biomol. NMR 32 (2005) 61–70.
[171] Y. Okuno, A. Szabo, G.M. Clore, Quantitative Interpretation of Solvent Paramagnetic Relaxation for Probing Protein-Cosolute Interactions, J. Am. Chem. Soc. 142 (2020) 8281–8290.
[172] F.A.A. Mulder, L. Tenori, C. Luchinat, Fast and quantitative NMR metabolite analysis afforded by a paramagnetic co-solute, Angew. Chem. Int. Ed. Engl. 58 (2019) 15283–15286.
[173] C. Honrao, N. Teissier, B. Zhang, R. Powers, E.M. O'Day, Gadolinium-based paramagnetic relaxation enhancement agent enhances sensitivity for NUS multidimensional NMR-based metabolomics, Molecules 26 (2021).
[174] R. Kellner, C. Mangels, K. Schweimer, S.J. Prasch, P.R. Weiglmeier, P. Rösch, S. Schwarzinger, SEMPRE: spectral editing mediated by paramagnetic relaxation enhancement, J. Am. Chem. Soc. 131 (2009) 18016–18017.
[175] C. Hartlmüller, J.C. Günther, A.C. Wolter, J. Wöhnert, M. Sattler, T. Madl, RNA structure refinement using NMR solvent accessibility data, Sci. Rep. 7 (2017) 5393.
[176] S. Bottaro, P.J. Nichols, B. Vögeli, M. Parrinello, K. Lindorff-Larsen, Integrating NMR and simulations reveals motions in the UUCG tetraloop, Nucleic Acids Res. 48 (2020) 5839–5848.
[177] Z. Gong, S. Yang, Q.-F. Yang, Y.-L. Zhu, J. Jiang, C. Tang, Refining RNA solution structures with the integrative use of label-free paramagnetic relaxation enhancement NMR, Biophys. Rep. 5 (2019) 244–253.
[178] C. Hartlmüller, C. Göbl, T. Madl, Prediction of protein structure using surface accessibility data, Angew. Chem. Int. Ed. Engl. 55 (2016) 11970–11974.
[179] Y. Wang, C.D. Schwieters, N. Tjandra, Parameterization of solvent-protein interaction and its use on NMR protein structure determination, J. Magn. Reson. 221 (2012) 76–84.
[180] C. Wiedemann, A. Szambowska, S. Häfner, O. Ohlenschläger, K.H. Gührs, M. Görlach, Structure and regulatory role of the C-terminal winged helix domain of the archaeal minichromosome maintenance complex, Nucleic Acids Res. 43 (2015) 2958–2967.
[181] J.H. Tomlinson, G.S. Thompson, A.P. Kalverda, A. Zhuravleva, A.J. O'Neill, A target-protection mechanism of antibiotic resistance at atomic resolution: insights into FusB-type fusidic acid resistance, Sci. Rep. 6 (2016) 19524.
[182] K. Tripsianes, T. Madl, M. Machyna, D. Fessas, C. Englbrecht, U. Fischer, K.M. Neugebauer, M. Sattler, Structural basis for dimethylarginine recognition by the Tudor domains of human SMN and SPF30 proteins, Nat. Struct. Mol. Biol. 18 (2011) 1414–1420.
[183] C. Hartlmüller, E. Spreitzer, C. Göbl, F. Falsone, T. Madl, NMR characterization of solvent accessibility and transient structure in intrinsically disordered proteins, J. Biomol. NMR 73 (2019) 305–317.
[184] Q. Li, Y.L. Wong, Q. Huang, C. Kang, Structural insight into the transmembrane domain and the juxtamembrane region of the erythropoietin receptor in micelles, Biophys. J. 107 (2014) 2325–2336.
[185] W. Hohlweg, G.E. Wagner, H.F. Hofbauer, F. Sarkleti, M. Setz, N. Gubensäk, S. Lichtenegger, S.F. Falsone, H. Wolinski, S. Kosol, C. Oostenbrink, S.D. Kohlwein, K. Zangger, A cation-pi interaction in a transmembrane helix of vacuolar ATPase retains the proton-transporting arginine in a hydrophobic environment, J. Biol. Chem. 293 (2018) 18977–18988.
[186] K.Y. Lee, Z. Fang, M. Enomoto, G. Gasmi-Seabrook, L. Zheng, S. Koide, M. Ikura, C.B. Marshall, Two distinct structures of membrane-associated homodimers of GTP- and GDP-bound KRAS4B revealed by paramagnetic relaxation enhancement, Angew. Chem. Int. Ed. Engl. 59 (2020) 11037–11045.
[187] F.X. Theillet, A. Binolfi, S. Liokatis, S. Verzini, P. Selenko, Paramagnetic relaxation enhancement to improve sensitivity of fast NMR methods: application to intrinsically disordered proteins, J. Biomol. NMR 51 (2011) 487–495.
[188] A. Eletsky, O. Moreira, H. Kovacs, K. Pervushin, A novel strategy for the assignment of side-chain resonances in completely deuterated large proteins using 13C spectroscopy, J. Biomol. NMR 26 (2003) 167–179.
[189] N.P. Wickramasinghe, M. Kotecha, A. Samoson, J. Past, Y. Ishii, Sensitivity enhancement in (13)C solid-state NMR of protein microcrystals by use of paramagnetic metal ions for optimizing (1)H T(1) relaxation, J. Magn. Reson. 184 (2007) 350–356.
[190] P. Schanda, B. Brutscher, Very fast two-dimensional NMR spectroscopy for real-time investigation of dynamic events in proteins on the time scale of seconds, J. Am. Chem. Soc. 127 (2005) 8014–8015.
[191] W. Bermel, I. Bertini, I.C. Felli, R. Pierattelli, Speeding up (13)C direct detection biomolecular NMR spectroscopy, J. Am. Chem. Soc. 131 (2009) 15339–15345.
[192] S.H.S. Chan, C.A. Waudby, A.M.E. Cassaignau, L.D. Cabrita, J. Christodoulou, Increasing the sensitivity of NMR diffusion measurements by paramagnetic longitudinal relaxation enhancement, with application to ribosome-nascent chain complexes, J. Biomol. NMR 63 (2015) 151–163.
[193] L.F. Pinto, J. Correa, L. Zhao, R. Riguera, E. Fernandez-Megia, Fast NMR screening of macromolecular complexes by a paramagnetic spin relaxation filter, ACS Omega 3 (2018) 2974–2983.
[194] T. Madl, T. Güttler, D. Görlich, M. Sattler, Structural analysis of large protein complexes using solvent paramagnetic relaxation enhancements, Angew. Chem. Int. Ed. Engl. 50 (2011) 3993–3997.
[195] R.M. LeBlanc, W.K. Kasprzak, A.P. Longhini, L.T. Olenginski, F. Abulwerdi, S. Ginocchio, B. Shields, J. Nyman, M. Svirydava, C. Del Vecchio, J. Ivanic, J.S. Schneekloth Jr., B.A. Shapiro, T.K. Dayie, S.F.J. Le Grice, Structural insights of the conserved "priming loop" of hepatitis B virus pre-genomic RNA, J. Biomol. Struct. Dyn. (2021) 1–13.
[196] H. Kooshapur, C.D. Schwieters, N. Tjandra, Conformational ensemble of disordered proteins probed by solvent paramagnetic relaxation enhancement (sPRE), Angew. Chem. Int. Ed. Engl. 57 (2018) 13519–13522.
[197] C.D. Schwieters, G.A. Bermejo, G.M. Clore, Xplor-NIH for molecular structure determination from NMR and other data sources, Prot. Sci.: Publ. Prot. Soc. 27 (2018) 26–40.
[198] E. Harjes, G.B. Jameson, Y.H. Tu, N. Burr, T.S. Loo, A.K. Goroncy, P.J.B. Edwards, S. Harjes, B. Munro, C. Göbl, E. Sattlegger, G.E. Norris, Experimentally based structural model of Yih1 provides insight into its function in controlling the key translational regulator Gcn2, FEBS Lett. 595 (2021) 324–340.
[199] Y. Zhang, T. Madl, I. Bagdiul, T. Kern, H.S. Kang, P. Zou, N. Mausbacher, S.A. Sieber, A. Kramer, M. Sattler, Structure, phosphorylation and U2AF65 binding of the N-terminal domain of splicing factor 1 during 3'-splice site recognition, Nucleic Acids Res. 41 (2013) 1343–1354.

[200] N.H. Meyer, K. Tripsianes, M. Vincendeau, T. Madl, F. Kateb, R. Brack-Werner, M. Sattler, Structural basis for homodimerization of the Src-associated during mitosis, 68-kDa protein (Sam68) Qua1 domain, J. Biol. Chem. 285 (2010) 28893–28901.
[201] M.P. Latham, D.J. Brown, S.A. McCallum, A. Pardi, NMR methods for studying the structure and dynamics of RNA, ChemBioChem 6 (2005) 1492–1505.
[202] B. Furtig, C. Richter, J. Wöhnert, H. Schwalbe, NMR spectroscopy of RNA, ChemBioChem 4 (2003) 936–962.
[203] S.S. Wijmenga, B.N.M. van Buuren, The use of NMR methods for conformational studies of nucleic acids, Prog. Nucl. Magn. Reson. Spec. 32 (1998) 287–387.
[204] J. Xie, A.T. Frank, RNA ensembles from solvent accessibility data: application to the SAM-I riboswitch aptamer domain, J. Phys. Chem. B 125 (2021) 3486–3493.
[205] C. Feng, D. Chan, J. Joseph, M. Muuronen, W.H. Coldren, N. Dai, I.R. Corrêa Jr., F. Furche, C.M. Hadad, R.C. Spitale, Light-activated chemical probing of nucleobase solvent accessibility inside cells, Nat. Chem. Biol. 14 (2018) 325.
[206] L. Emmanouilidis, U. Schütz, K. Tripsianes, T. Madl, J. Radke, R. Rucktäschel, M. Wilmanns, W. Schliebs, R. Erdmann, M. Sattler, Allosteric modulation of peroxisomal membrane protein recognition by farnesylation of the peroxisomal import receptor PEX19, Nat. Commun. 8 (2017) 14635.
[207] J.P. Linge, M. Habeck, W. Rieping, M. Nilges, ARIA: automated NOE assignment and NMR structure calculation, Bioinformatics 19 (2003) 315–316.
[208] N.L. Fawzi, J. Ying, D.A. Torchia, G.M. Clore, Probing exchange kinetics and atomic resolution dynamics in high-molecular-weight complexes using dark-state exchange saturation transfer NMR spectroscopy, Nat. Protoc. 7 (2012) 1523–1533.
[209] N.L. Fawzi, J. Ying, R. Ghirlando, D.A. Torchia, G.M. Clore, Atomic-resolution dynamics on the surface of amyloid-beta protofibrils probed by solution NMR, Nature 480 (2011) 268–272.
[210] G.V. Neri Niccolai, C. Rossi, W.A. Gibbons, The stereochemistry and dynamics of natural products and biopolymers from proton relaxation spectroscopy: spin-label delineation of inner and outer protons of gramicidin S including hydrogen bonds, J. Am. Chem. Soc. 104 (1982) 1534–1537.
[211] M. Schulte, D. Petrović, P. Neudecker, R. Hartmann, J. Pietruszka, S. Willbold, D. Willbold, V. Panwalkar, Conformational sampling of the intrinsically disordered C-terminal tail of DERA is important for enzyme catalysis, ACS Catal. 8 (2018) 3971–3984.
[212] D.A. Merle, A. Witternigg, C. Tam-Amersdorfer, C. Hartlmüller, E. Spreitzer, E. Schrank, S. Wagner-Lichtenegger, O. Werzer, K. Zangger, A.J. Kungl, T. Madl, N.H. Meyer, S.F. Falsone, Increased aggregation tendency of alpha-synuclein in a fully disordered protein complex, J. Mol. Biol. 431 (2019) 2581–2598.
[213] X.C. Yu, Y. Hu, J. Ding, H. Li, C. Jin, Structural basis and mechanism of the unfolding-induced activation of HdeA, a bacterial acid response chaperone, J. Biol. Chem. 294 (2019) 3192–3206.
[214] Y. Hunashal, C. Cantarutti, S. Giorgetti, L. Marchese, H. Molinari, N. Niccolai, F. Fogolari, G. Esposito, Exploring exchange processes in proteins by paramagnetic perturbation of NMR spectra, Phys. Chem. Chem. Phys. 22 (2020) 6247–6259.
[215] S. Leirmo, C. Harrison, D.S. Cayley, R.R. Burgess, M.T. Record Jr., Replacement of potassium chloride by potassium glutamate dramatically enhances protein-DNA interactions in vitro, Biochemistry 26 (1987) 2095–2101.
[216] B. Yu, J. Iwahara, Experimental approaches for investigating ion atmospheres around nucleic acids and proteins, Comput. Struct. Biotechnol. J. 19 (2021) 2279–2285.
[217] G.S. Manning, The molecular theory of polyelectrolyte solutions with applications to the electrostatic properties of polynucleotides, Q. Rev. Biophys. 11 (1978) 179–246.
[218] M.T. Record, C.F. Anderson, T.M. Lohman, Thermodynamic analysis of ion effects on the binding and conformational equilibria of proteins and nucleic acids: the roles of ion association or release, screening, and ion effects on water activity, Q. Rev. Biophys. 11 (1978) 103–178.
[219] C.F. Anderson, M.T. Record, Ion distributions around DNA and other cylindrical polyions: theoretical descriptions and physical implications, Annu. Rev. Biophys. Biophys. Chem. 19 (1990) 423–463.
[220] G.S. Manning, Limiting laws and counterion condensation in polyelectrolyte solutions I. Colligative properties, J. Chem. Phys. 51 (1969) 924–933.
[221] G.S. Manning, Limiting laws and counterion condensation in polyelectrolyte solutions II. Self-diffusion of the small ions, J. Chem. Phys. 51 (1969) 934–938.
[222] M.T. Record Jr, T.M. Lohman, P. De Haseth, Ion effects on ligand-nucleic acid interactions, J. Mol. Biol. 107 (1976) 145–158.
[223] F. Fogolari, A. Brigo, H. Molinari, The Poisson-Boltzmann equation for biomolecular electrostatics: a tool for structural biology, J. Mol. Recognit. 15 (2002) 377–392.
[224] B. Yu, K.G. Bien, C.C. Pletka, J. Iwahara, Dynamics of cations around DNA and protein as revealed by (23)Na diffusion NMR spectroscopy, Anal. Chem. (2022).
[225] R. Dass, E. Corlianò, F.A.A. Mulder, The contribution of electrostatics to hydrogen exchange in the unfolded protein state, Biophys. J. 120 (2021) 4107–4114.
[226] Y. Toyama, A.K. Rangadurai, L.E. Kay, Measurement of (1)H(alpha) transverse relaxation rates in proteins: application to solvent PREs, J. Biomol. NMR 76 (2022) 137–152.
[227] Y. Toyama, A.K. Rangadurai, J.D. Forman-Kay, L.E. Kay, Mapping the per-residue surface electrostatic potential of CAPRIN1 along its phase-separation trajectory, Proc. Natl. Acad. Sci. U. S. A. 119 (2022) e2210492119.
[228] S.N. Timasheff, Thermodynamic binding and site occupancy in the light of the Schellman exchange concept, Biophys. Chem. 101–102 (2002) 99–111.
[229] E. Schrank, G.E. Wagner, K. Zangger, Solution NMR studies on the orientation of membrane-bound peptides and proteins by paramagnetic probes, Molecules 18 (2013) 7407–7435.
[230] C. Göbl, S. Kosol, T. Stockner, H.M. Rückert, K. Zangger, Solution structure and membrane binding of the toxin fst of the par addiction module, Biochemistry 49 (2010) 6567–6575.
[231] D.A. Kallick, M.R. Tessmer, C.R. Watts, C.Y. Li, The use of dodecylphosphocholine micelles in solution NMR, J. Magn. Reson., Ser B 109 (1995) 60–65.
[232] P.A. Keifer, A. Peterkofsky, G. Wang, Effects of detergent alkyl chain length and chemical structure on the properties of a micelle-bound bacterial membrane targeting peptide, Anal. Biochem. 331 (2004) 33–39.
[233] N.J. Traaseth, R. Verardi, K.D. Torgersen, C.B. Karim, D.D. Thomas, G. Veglia, Spectroscopic validation of the pentameric structure of phospholamban, Proc. Natl. Acad. Sci. U. S. A. 104 (2007) 14676–14681.
[234] C. Hilty, G. Wider, C. Fernández, K. Wüthrich, Membrane protein-lipid interactions in mixed micelles studied by NMR spectroscopy with the use of paramagnetic reagents, ChemBioChem 5 (2004) 467–473.
[235] F. Porcelli, B. Buck, D.K. Lee, K.J. Hallock, A. Ramamoorthy, G. Veglia, Structure and orientation of pardaxin determined by NMR experiments in model membranes, J. Biol. Chem. 279 (2004) 45815–45823.
[236] E. Schievano, T. Calisti, I. Menegazzo, R. Battistutta, E. Peggion, S. Mammi, G. Palu, A. Loregian, pH-Dependent conformational changes and topology of a herpesvirus translocating peptide in a membrane-mimetic environment, Biochemistry 43 (2004) 9343–9351.
[237] M.A. Fazal, B.C. Roy, S. Sun, S. Mallik, K.R. Rodgers, Surface recognition of a protein using designed transition metal complexes, J. Am. Chem. Soc. 123 (2001) 6283–6290.
[238] K. Zangger, M. Respondek, C. Göbl, W. Hohlweg, K. Rasmussen, G. Grampp, T. Madl, Positioning of micelle-bound peptides by paramagnetic relaxation enhancements, J. Phys. Chem. B 113 (2009) 4400–4406.
[239] A. Piai, Q. Fu, J. Dev, J.J. Chou, Optimal Bicelle Size q for Solution NMR Studies of the Protein Transmembrane Partition, Chemistry 23 (2017) 1361–1367.
[240] F. Lv, F. Qi, Z. Zhang, M. Wen, J. Kale, A. Piai, L. Du, S. Wang, L. Zhou, Y. Yang, B. Wu, Z. Liu, J. Del Rosario, J. Pogmore, J.J. Chou, D.W. Andrews, J. Lin, B. OuYang, An amphipathic Bax core dimer forms part of the apoptotic pore wall in the mitochondrial membrane, EMBO J. 40 (2021) e106438.
[241] O. Soubias, S. Pant, F. Heinrich, Y. Zhang, N.S. Roy, J. Li, X. Jian, M.E. Yohe, P.A. Randazzo, M. Lösche, E. Tajkhorshid, R.A. Byrd, Membrane surface recognition by the ASAP1 PH domain and consequences for interactions with the small GTPase Arf1, Sci. Adv. 6 (2020).
[242] J. Bai, J. Wang, T. Ravula, S.C. Im, G.M. Anantharamaiah, L. Waskell, A. Ramamoorthy, Expression, purification, and functional reconstitution of (19) F-labeled cytochrome b5 in peptide nanodiscs for NMR studies, Biochim. Biophys. Acta, Biomembr. 1862 (2020) 183194.
[243] J. Jarvet, J. Danielsson, P. Damberg, M. Oleszczuk, A. Gräslund, Positioning of the Alzheimer Abeta(1–40) peptide in SDS micelles using NMR and paramagnetic probes, J. Biomol. NMR 39 (2007) 63–72.
[244] P.E. Wright, H.J. Dyson, Intrinsically disordered proteins in cellular signalling and regulation, Nat. Rev. Mol. Cell Biol. 16 (2015) 18–29.
[245] N. Rezaei-Ghaleh, M. Blackledge, M. Zweckstetter, Intrinsically disordered proteins: from sequence and conformational properties toward drug discovery, ChemBioChem 13 (2012) 930–950.
[246] A.K. Dunker, I. Silman, V.N. Uversky, J.L. Sussman, Function and structure of inherently disordered proteins, Curr. Opin. Struct. Biol. 18 (2008) 756–764.
[247] P.E. Wright, H.J. Dyson, Intrinsically unstructured proteins: re-assessing the protein structure-function paradigm, J. Mol. Biol. 293 (1999) 321–331.
[248] V.N. Uversky, Natively unfolded proteins: a point where biology waits for physics, Prot. Sci.: Publ. Prot. Soc. 11 (2002) 739–756.
[249] P. Tompa, Intrinsically disordered proteins: a 10-year recap, Trends Biochem. Sci. 37 (2012) 509–516.
[250] M.E. Oates, P. Romero, T. Ishida, M. Ghalwash, M.J. Mizianty, B. Xue, Z. Dosztányi, V.N. Uversky, Z. Obradovic, L. Kurgan, A.K. Dunker, J. Gough, D(2)P (2): database of disordered protein predictions, Nucleic Acids Res. 41 (2013) D508–D516.
[251] R. van der Lee, M. Buljan, B. Lang, R.J. Weatheritt, G.W. Daughdrill, A.K. Dunker, M. Fuxreiter, J. Gough, J. Gsponer, D.T. Jones, P.M. Kim, R.W. Kriwacki, C.J. Oldfield, R.V. Pappu, P. Tompa, V.N. Uversky, P.E. Wright, M.M. Babu, Classification of intrinsically disordered regions and proteins, Chem. Rev. 114 (2014) 6589–6631.
[252] P. Tompa, The interplay between structure and function in intrinsically unstructured proteins, FEBS Lett. 579 (2005) 3346–3354.
[253] A.K. Dunker, C.J. Oldfield, J. Meng, P. Romero, J.Y. Yang, J.W. Chen, V. Vacic, Z. Obradovic, V.N. Uversky, The unfoldomics decade: an update on intrinsically disordered proteins, BMC Genomics 9 (Suppl 2) (2008) S1.
[254] I. Pritišanac, R.M. Vernon, A.M. Moses, J.D. Forman Kay, Entropy and Information within Intrinsically Disordered Protein Regions, Entropy (Basel) 21 (2019).
[255] H. Frauenfelder, S.G. Sligar, P.G. Wolynes, The energy landscapes and motions of proteins, Science 254 (1991) 1598–1603.

[256] A. Huang, C.M. Stultz, Finding order within disorder: elucidating the structure of proteins associated with neurodegenerative disease, Future, Med. Chem. 1 (2009) 467–482.
[257] M.R. Jensen, M. Zweckstetter, J.R. Huang, M. Blackledge, Exploring free-energy landscapes of intrinsically disordered proteins at atomic resolution using NMR spectroscopy, Chem. Rev. 114 (2014) 6632–6660.
[258] R. Sharma, Z. Raduly, M. Miskei, M. Fuxreiter, Fuzzy complexes: specific binding without complete folding, FEBS Lett. 589 (2015) 2533–2542.
[259] M. Fuxreiter, Fuzziness in protein interactions-a historical perspective, J. Mol. Biol. 430 (2018) 2278–2287.
[260] V. Csizmok, A.V. Follis, R.W. Kriwacki, J.D. Forman-Kay, Dynamic protein interaction networks and new structural paradigms in signaling, Chem. Rev. 116 (2016) 6424–6462.
[261] V.N. Uversky, C.J. Oldfield, U. Midic, H. Xie, B. Xue, S. Vucetic, L.M. Iakoucheva, Z. Obradovic, A.K. Dunker, Unfoldomics of human diseases: linking protein intrinsic disorder with diseases, BMC Genomics 10 (Suppl 1) (2009) S7.
[262] V.N. Uversky, C.J. Oldfield, A.K. Dunker, Intrinsically disordered proteins in human diseases: introducing the D2 concept, Annu. Rev. Biophys. 37 (2008) 215–246.
[263] S. Boeynaems, S. Alberti, N.L. Fawzi, T. Mittag, M. Polymenidou, F. Rousseau, J. Schymkowitz, J. Shorter, B. Wolozin, L. Van Den Bosch, P. Tompa, M. Fuxreiter, Protein phase separation: a new phase in cell biology, Trends Cell Biol. 28 (2018) 420–435.
[264] G.L. Dignon, R.B. Best, J. Mittal, Biomolecular phase separation: from molecular driving forces to macroscopic properties, Annu. Rev. Phys. Chem. 71 (2020) 53–75.
[265] S. Alberti, A. Gladfelter, T. Mittag, Considerations and challenges in studying liquid-liquid phase separation and biomolecular condensates, Cell 176 (2019) 419–434.
[266] A. Bah, J.D. Forman-Kay, Modulation of intrinsically disordered protein function by post-translational modifications, J. Biol. Chem. 291 (2016) 6696–6705.
[267] A. Prestel, K. Bugge, L. Staby, R. Hendus-Altenburger, B.B. Kragelund, Characterization of dynamic IDP complexes by NMR spectroscopy, Methods Enzymol. 611 (2018) 193–226.
[268] E.B. Gibbs, S.A. Showalter, Quantitative biophysical characterization of intrinsically disordered proteins, Biochemistry 54 (2015) 1314–1326.
[269] R. Beveridge, Q. Chappuis, C. Macphee, P. Barran, Mass spectrometry methods for intrinsically disordered proteins, Analyst 138 (2013) 32–42.
[270] N. Sibille, P. Bernadó, Structural characterization of intrinsically disordered proteins by the combined use of NMR and SAXS, Biochem. Soc. Trans. 40 (2012) 955–962.
[271] A.C. Murthy, N.L. Fawzi, The (un)structural biology of biomolecular liquid-liquid phase separation using NMR spectroscopy, J. Biol. Chem. 295 (2020) 2375–2384.
[272] V. Spiwok, Z. Sucur, P. Hosek, Enhanced sampling techniques in biomolecular simulations, Biotechnol. Adv. 33 (2015) 1130–1140.
[273] R. Lazim, D. Suh, S. Choi, Advances in molecular dynamics simulations and enhanced sampling methods for the study of protein systems, Int. J. Mol. Sci. 21 (2020).
[274] J.E. Shea, R.B. Best, J. Mittal, Physics-based computational and theoretical approaches to intrinsically disordered proteins, Curr. Opin. Struct. Biol. 67 (2021) 219–225.
[275] A. Vitalis, R.V. Pappu, ABSINTH: a new continuum solvation model for simulations of polypeptides in aqueous solutions, J. Comput. Chem. 30 (2009) 673–699.
[276] S. Kmiecik, D. Gront, M. Kolinski, L. Wieteska, A.E. Dawid, A. Kolinski, Coarse-grained protein models and their applications, Chem. Rev. 116 (2016) 7898–7936.
[277] R.C. Bernardi, M.C.R. Melo, K. Schulten, Enhanced sampling techniques in molecular dynamics simulations of biological systems, Biochim. Biophys. Acta. 1850 (2015) 872–877.
[278] G.H. Zerze, C.M. Miller, D. Granata, J. Mittal, Free energy surface of an intrinsically disordered protein: comparison between temperature replica exchange molecular dynamics and bias-exchange metadynamics, J. Chem. Theory Comput. 11 (2015) 2776–2782.
[279] J.M. Choi, R.V. Pappu, Improvements to the ABSINTH force field for proteins based on experimentally derived amino acid specific backbone conformational statistics, J. Chem. Theory Comput. 15 (2019) 1367–1382.
[280] W. Zheng, G.L. Dignon, N. Jovic, X. Xu, R.M. Regy, N.L. Fawzi, Y.C. Kim, R.B. Best, J. Mittal, Molecular details of protein condensates probed by microsecond long atomistic simulations, J. Phys. Chem. B 124 (2020) 11671–11679.
[281] A.C. Murthy, G.L. Dignon, Y. Kan, G.H. Zerze, S.H. Parekh, J. Mittal, N.L. Fawzi, Molecular interactions underlying liquid-liquid phase separation of the FUS low-complexity domain, Nat. Struct. Mol. Biol. 26 (2019) 637–648.
[282] J.A. Joseph, A. Reinhardt, A. Aguirre, P.Y. Chew, K.O. Russell, J.R. Espinosa, A. Garaizar, R. Collepardo-Guevara, Physics-driven coarse-grained model for biomolecular phase separation with near-quantitative accuracy, Nat. Comput. Sci. 1 (2021) 732–743.
[283] C. Cragnell, E. Rieloff, M. Skepö, Utilizing coarse-grained modeling and Monte Carlo simulations to evaluate the conformational ensemble of intrinsically disordered proteins and regions, J. Mol. Biol. 430 (2018) 2478–2492.
[284] R. Konrat, NMR contributions to structural dynamics studies of intrinsically disordered proteins, J. Magn. Reson. 241 (2014) 74–85.
[285] W. Bermel, I. Bertini, J. Chill, I.C. Felli, N. Haba, M.V.V. Kumar, R. Pierattelli, Exclusively heteronuclear (13) C-detected amino-acid-selective NMR experiments for the study of intrinsically disordered proteins (IDPs), ChemBioChem 13 (2012) 2425–2432.
[286] I.C. Felli, R. Pierattelli, Novel methods based on (13)C detection to study intrinsically disordered proteins, J. Magn. Reson. 241 (2014) 115–125.
[287] S. Chhabra, P. Fischer, K. Takeuchi, A. Dubey, J.J. Ziarek, A. Boeszoermenyi, D. Mathieu, W. Bermel, N.E. Davey, G. Wagner, H. Arthanari, (15)N detection harnesses the slow relaxation property of nitrogen: delivering enhanced resolution for intrinsically disordered proteins, Proc. Natl. Acad. Sci. U. S. A. 115 (2018) E1710–E1719.
[288] T.M. Perdikari, N. Jovic, G.L. Dignon, Y.C. Kim, N.L. Fawzi, J. Mittal, A predictive coarse-grained model for position-specific effects of post-translational modifications, Biophys. J. 120 (2021) 1187–1197.
[289] K. Kazimierczuk, A. Zawadzka-Kazimierczuk, W. Koźmiński, Non-uniform frequency domain for optimal exploitation of non-uniform sampling, J. Magn. Reson. 205 (2010) 286–292.
[290] K. Kazimierczuk, J. Stanek, A. Zawadzka-Kazimierczuk, W. Koźmiński, Random sampling in multidimensional NMR spectroscopy, Prog. Nucl. Magn. Reson. Spectrosc. 57 (2010) 420–434.
[291] C. Wiedemann, N. Goradia, S. Häfner, C. Herbst, M. Görlach, O. Ohlenschläger, R. Ramachandran, HN-NCA heteronuclear TOCSY-NH experiment for (1)H(N) and (15)N sequential correlations in ((13)C, (15)N) labelled intrinsically disordered proteins, J. Biomol. NMR 63 (2015) 201–212.
[292] P. Schanda, H. Van Melckebeke, B. Brutscher, Speeding up three-dimensional protein NMR experiments to a few minutes, J. Am. Chem. Soc. 128 (2006) 9042–9043.
[293] Z. Solyom, M. Schwarten, L. Geist, R. Konrat, D. Willbold, B. Brutscher, BEST-TROSY experiments for time-efficient sequential resonance assignment of large disordered proteins, J. Biomol. NMR 55 (2013) 311–321.
[294] A. Dubey, R.V. Kadumuri, G. Jaipuria, R. Vadrevu, H.S. Atreya, Rapid NMR Assignments of Proteins by Using Optimized Combinatorial Selective Unlabeling, ChemBioChem 17 (2016) 334–340.
[295] J.P. Brady, P.J. Farber, A. Sekhar, Y.H. Lin, R. Huang, A. Bah, T.J. Nott, H.S. Chan, A.J. Baldwin, J.D. Forman-Kay, L.E. Kay, Structural and hydrodynamic properties of an intrinsically disordered region of a germ cell-specific protein on phase separation, Proc. Natl. Acad. Sci. U. S. A. 114 (2017) E8194–E8203.
[296] S. Milles, N. Salvi, M. Blackledge, M.R. Jensen, Characterization of intrinsically disordered proteins and their dynamic complexes: from in vitro to cell-like environments, Prog. Nucl. Magn. Reson. Spectrosc. 109 (2018) 79–100.
[297] R. Schneider, M. Blackledge, M.R. Jensen, Elucidating binding mechanisms and dynamics of intrinsically disordered protein complexes using NMR spectroscopy, Curr. Opin. Struct. Biol. 54 (2019) 10–18.
[298] E.B. Gibbs, E.C. Cook, S.A. Showalter, Application of NMR to studies of intrinsically disordered proteins, Arch. Biochem. Biophys. 628 (2017) 57–70.
[299] I.C. Felli, R. Pierattelli, Recent progress in NMR spectroscopy: toward the study of intrinsically disordered proteins of increasing size and complexity, IUBMB Life 64 (2012) 473–481.
[300] F.X. Theillet, A. Binolfi, B. Bekei, A. Martorana, H.M. Rose, M. Stuiver, S. Verzini, D. Lorenz, M. van Rossum, D. Goldfarb, P. Selenko, Structural disorder of monomeric alpha-synuclein persists in mammalian cells, Nature 530 (2016) 45–50.
[301] E. Riekeberg, R. Powers, New frontiers in metabolomics: from measurement to insight, F1000Res 6 (2017) 1148.
[302] D.S. Wishart, NMR metabolomics: a look ahead, J. Magn. Reson. 306 (2019) 155–161.
[303] A.H. Emwas, R. Roy, R.T. McKay, L. Tenori, E. Saccenti, G.A.N. Gowda, D. Raftery, F. Alahmari, L. Jaremko, M. Jaremko, D.S. Wishart, NMR spectroscopy for metabolomics research, Metabolites 9 (2019).
[304] A.C. Dona, M. Kyriakides, F. Scott, E.A. Shephard, D. Varshavi, K. Veselkov, J.R. Everett, A guide to the identification of metabolites in NMR-based metabonomics/metabolomics experiments, Comput. Struct. Biotechnol. J. 14 (2016) 135–153.
[305] M. Pellecchia, I. Bertini, D. Cowburn, C. Dalvit, E. Giralt, W. Jahnke, T.L. James, S.W. Homans, H. Kessler, C. Luchinat, B. Meyer, H. Oschkinat, J. Peng, H. Schwalbe, G. Siegal, Perspectives on NMR in drug discovery: a technique comes of age, Nat Rev Drug Discov 7 (2008) 738–745.
[306] A.D. Gossert, W. Jahnke, NMR in drug discovery: a practical guide to identification and validation of ligands interacting with biological macromolecules, Prog. Nucl. Magn. Reson. Spectrosc. 97 (2016) 82–125.
[307] T. Sugiki, K. Furuita, T. Fujiwara, C. Kojima, Current NMR techniques for structure-based drug discovery, Molecules 23 (2018).
[308] W. Becker, K.C. Bhattiprolu, N. Gubensäk, K. Zangger, Investigating protein-ligand interactions by solution nuclear magnetic resonance spectroscopy, ChemPhysChem 19 (2018) 895–906.
[309] A. Dubey, K. Takeuchi, M. Reibarkh, H. Arthanari, The role of NMR in leveraging dynamics and entropy in drug design, J. Biomol. NMR 74 (2020) 479–498.
[310] L.D. Clark, I. Dikiy, K. Chapman, K.E. Rödström, J. Aramini, M.V. LeVine, G. Khelashvili, S.G. Rasmussen, K.H. Gardner, D.M. Rosenbaum, Ligand modulation of sidechain dynamics in a wild-type human GPCR, Elife 6 (2017).
[311] A.Z. Spitz, E. Zacharioudakis, D.E. Reyna, T.P. Garner, E. Gavathiotis, Eltrombopag directly inhibits BAX and prevents cell death, Nat. Commun. 12 (2021) 1134.